Master's thesis

NTNU
Norwegian University of Science and Technology
Faculty of Engineering
Department of Marine Technology

Aina Rindheim

Analysis of fire loading and buckling response of an aluminium structural member in a ferry hull

Master's thesis in Marine Technology
Supervisor: Bernt J. Leira and Multi Maritime AS
July 2020

NTNU
Norwegian University of
Science and Technology

Aina Rindheim

Analysis of fire loading and buckling response of an aluminium structural member in a ferry hull

Master's thesis in Marine Technology
Supervisor: Bernt J. Leira and Multi Maritime AS
July 2020

Norwegian University of Science and Technology
Faculty of Engineering
Department of Marine Technology

NTNU
Norwegian University of
Science and Technology

Master Thesis, Spring 2020
for
Master student Aina Rindheim

Analysis of fire loading and buckling response of an aluminium structural member in a ferry hull

Analyse av brannbelasting og respons for en aluminium konstruksjonskomponent i et fergeskrog

There is a continuous strive to reduce the weight of ferry hull structures by application of alternative materials to steel, with aluminium representing a prominent alternative. However, experience has shown that as a result of the parallell tendency to utilize electric propulsion systems based on application of batteries as a power source, there may an increasing risk that fire may occur. Accordingly, the resulting accidental temperature loading needs to be seriously considered for aluminium ferries at the design stage.

The purpose of the present master thesis is accordingly to consider fire in a passenger ferry in aluminium with particular focus on the requirements according to DNVGL (Det Norske Veritas Germanischer Lloyd), NMA (Norwegian Maritime Authority), SOLAS (Safety Of Life At Sea) and Eurocode rules. The following items are to be addressed:

1) Give a historical overview of the development of the present category of ships (i.e. ferries e.g. in terms of size, load-carrying capacity, architecture, type of materials, speed etc.)

2) Give a summary of the content of relevant design guidelines and rules for the present type of ships.

3) Give an overview of the main differences between steel and aluminium when applied as a ship hull material.

4) Give an overview of different categories of limit states that are relevant for design of ships and offshore structures (i.e. SLS, ULS, FLS and ALS (PLS)) and how design rules related to these limit states are implemented in the relevant rules.

5) It is subsequently focused upon analysis of fire scenarios for the present type of ship (which corresponds to the ALS (PLS) limit state. Relevant procedures for numerical analysis of structures subjected to thermal loads due to fire are first to be reviewed and summarized by the candidate. Subsequently, requirements in the applicable design documents related to fire protection systems and procedures are to be highlighted.

6) Based on particular drawings (or other sources), build a Finite Element model for a part of a ship hull and establish a relevant fire scenario to be analysed. A review is to be performed of computer software which is relevant for analysis of the established scenario and sub-model of the hull, and select the program that you find to be most suitable. Temperature and buckling analyses for this model based on application of the thermal loading corresponding to the selected scenario are then to be performed and the results are to be discussed.

7) Perform parametric studies to the extent that time allows based on discussion/agreement with the supervisor(s).

The work scope may prove to be larger than initially anticipated. Subject to approval from the supervisor, topics may be deleted from the list above or reduced in extent.

In the thesis, the candidate shall present his personal contribution to the resolution of problems within the scope of the thesis work. Theories and conclusions should be based on mathematical derivations and/or logic reasoning identifying the various steps in the deduction.

The candidate should utilise the existing possibilities for obtaining relevant literature.

The thesis should be organised in a rational manner to give a clear exposition of results, assessments, and conclusions. The text should be brief and to the point, with a clear language. Telegraphic language should be avoided.

The thesis shall contain the following elements: A text defining the scope, preface, list of contents, summary, main body of thesis, conclusions with recommendations for further work, list of symbols and acronyms, references and (optional) appendices. All figures, tables and equations shall be numbered.

The supervisor may require that the candidate, in an early stage of the work, presents a written plan for the completion of the work. The original contribution of the candidate and material taken from other sources shall be clearly defined. Work from other sources shall be properly referenced using an acknowledged referencing system.

Supervisor: Professor Bernt Johan Leira, NTNU

Sign:

Co-Supervisor:

Sign:

Start-up: January 15th, 2020

Deadline: June 28th, 2020

Summary

In this thesis a method for performing buckling analyses on hull structures under elevated temperatures was invented. The method is based on the idea that when a structure is heated, it will not have uniform temperature distribution throughout its cross-section. With the knowledge that the material properties change with the temperature, the structure was divided into little pieces and assigned the material properties according to their temperature. This gave the possibility to include the temperature distribution on advanced structures instead of analysing the model with constant temperature, and to perform buckling analyses with temperature effects.

The analyses will be performed in Abaqus on an aluminium stiffener which is a part of a bulkhead around the battery room of an aluminium passenger ferry. It will start with a heat transfer analysis which will give the temperature distribution of the structure. After this a linear buckling analysis will be performed with the model divided in to smaller pieces with the corresponding material properties, as found in the heat transfer analysis, and the eigenvalues and eigenmodes will be obtained. These are then used to analyse the nonlinear buckling shape and the critical buckling load for the structure.

A parametric study is to be performed for the following cases:

1. Aluminium stiffener in room temperature
2. Aluminium stiffener with fire on plate side without insulation, at around 500°C
3. Aluminium stiffener with fire on stiffener side without insulation, at around 500°C
4. Aluminium stiffener with fire on plate side with insulation after 60 minutes
5. Aluminium stiffener with fire on stiffener side with insulation after 60 minutes
6. Steel stiffener in room temperature
7. Steel stiffener with fire on plate side without insulation after 60 minutes
8. Plate consisting of multiple stiffeners in room temperature

It was found from the analyses that the insulated stiffeners with fire on the stiffener side were more fire resistant than the ones with the fire on the plate side. Also, the insulation had great effects on both the heat transfer and maintaining the structural integrity of the aluminium stiffeners. The steel showed greater resistance to fire than aluminium, and also stronger structural integrity. However, aluminium turned out to be a great replacement for hull design, if insulated correctly.

Sammendrag

I denne masteroppgaven har en metode for å analysere skrog konstruksjoner under forhøyet temperaturer blitt oppfunnet. Metoden baserer seg på ideen om at når en konstruksjon er oppvarmet, vil den ikke ha uniform temperaturfordeling gjennom tverrnittet. Med kunnskapen om at material egenskapene endrer seg ved temperatur, blir konstruksjonen delt inn i mindre deler og tildelt de materialegenskapene tilsvarende temperaturen i konstruksjonen. Dette gav muligheten til å inkludere temperaturfordeling i avanserte konstruksjoner istedenfor å analysere modellen ved en konstant temperatur, og muligheten til å utføre knekk-analyser med temperatur effekter.

Analysen vil bli gjort i Abaqus på en aluminium stiver som er en del av et skott rundt batterirommet på en aluminium passasjerferje. Den vil begynne med en varmeoverføringsanalyse som gir temperaturfordelingen i konstruksjonen. Etter dette vil en linær knekk analyse bli gjort med modelled delt inn i små deler med tilsvarende material egenskaper til temperaturen funnet i varmeoverføringsanalysen, og egenverdiene og egenmodene vil bli funnet. Disse er så brukt til å analysere den ikke-linære knekkformen og den kritiske knekklasten til strukturen.

En parameterstudie ble gjort for de følgende tilfellene:

1. Aluminium stiver i romtemperatur
2. Aluminium stiver med brann på platesiden uten isolasjon ved rundt 500°C
3. Aluminium stiver med brann på stiversiden uten isolasjon ved rundt 500°C
4. Aluminium stiver med brann på platesiden med isolasjon etter 60 minutter
5. Aluminium stiver med brann på stiversiden med isolasjon etter 60 minutter
6. Stål stiver i rom temperatur
7. Stål stiver med brann på platesiden uten isolasjon etter 60 minutter
8. Plate bestående av flere stivere i romtemperatur

Fra anlysene ble det konkludert med at en isolert stiver med brann på stiversiden ville tåle brann bedre enn den med brann på platesiden. Isolering hadde også god effekt på både varmeoverføringen og opprettholdingen av den strukturelle integriteten til aluminium stiverene. Stål stiverene tålte bedre å bli utsatt for varme enn aluminium, og hadde også noe sterkere struktur. Uansett, aluminium viste seg å være et godt materiale for å erstatte stål, dersom det er isolert riktig.

Table of Contents

List of Tables

List of Figures

Nomenclature

Abbreviations

ALS	Accidental Limit State
EES	Electrical Energy Storage
FDS	Fire Dynamics Simulator
FLS	Fatigue Limit State
FSS	Fire Safety Systems
$LRFD$	Loand and Resistance Factored Design
NMA	Norwegian Maritime Authority
$NPRA$	Norwegian Public Roads Administration's
PLS	Progressive Collapse Limit State
SLS	Serviceability Limit States
$SOLAS$	Safety Of Life At Sea
ULS	Ultimate Limit States

Symbols

$R_{fi,d,t}$	Design value of the resistance of the member in the fire situation at time t
β	Reliability index
Δl	Temperature induced elongation
Δl_{max}	Maximum arc length increment
Δl_{min}	Minimum arc length increment

$\Delta\lambda_{in}$	Initial load proportionality factor
Δ_{lin}	Initial arc length increment
γ_f	Load factor
γ_m	Material factor
λ	Load level parameter
λ_c	Thermal conductivity
λ_i	Eigenvalues
ν	Poisson ratio
ρ	Mass density in kg/m^3
ρ_a	Material density of aluminium
ρ_s	Material density of steel
σ_y	Yield strength in MPa
$\sigma_{ln(R/S)}$	Standard deviation of ln(R/S)
Θ_d	Design value of the temperature
θ_{al}	Aluminium temperature
$\Theta_{cr,d}$	Design value of the critical material temperature
c	Specific heat
E	Young's modulus in GPa
E_a	Young's modulus of aluminium
E_s	Young's modulus of steel
$E_{fi,d,t}$	Design value of the relevant effects of actions in the fire situation at time t
$E_{s,\theta}$	Slope of linear elastic range of steel at elevated temperatures
f_a	Eigenfrequency of aluminium
f_o	0.2 proos strength at room temperature
f_s	Eigenfrequency of steel
f_y	Yield strength of steel at 20°C
$f_{o,\theta}$	0.2 proof strength at elevated temperature

$f_{y,\theta}$	Effective yield strength of steel at elevated temperatures
$g(\lambda, r)$	Global equilibrium equation
K_0^{MN}	Tangent stiffness matrix
K_Δ^{NM}	Differential initial stress and load stiffness matrix
$k_{E,\theta}$	Reduction factor for the Young's modulus
$k_{y,\theta}$	Reduction factor for effective yield strength of steel
l	Length at 20°C
l_{period}	Total arc length scale factor
m_a	Mass of aluminium
m_s	Mass of steel
P^N	Preloads
P_0	Dead load
P_F	Limit state probability of failure
P_{ref}	Reference load vector defined in the Riks step
P_{total}	Current load magnitude
Q^N	Incremental loading pattern
R_d	Design resistance of a structure
R_k	Characteristic resistance
R_{int}	Internal load vector
R_{ref}	Fixed external load vector
S_d	Expected design load for a structure
S_k	Characteristic load effect
t_a	Thickness of aluminium plate
t_s	Thickness of steel plate
$t_{fi,d}$	Design value of the fire resistance
$t_{fi,requ}$	Required fire resistance time
v_i^M	Nontrivial displacement solutions

Chapter 1

Introduction

Ferries today have a higher demand for both size and load carrying capability. This demand leads to an increased amount of steel in the construction, thus increased weight. One way to decrease the weight of a ferry is to use lighter materials, like aluminium or sandwich structures. Multi Maritime AS have designed a new electric passenger ferry MM35PE EL, shown in Figure 1.1, that will operate in the Oslo fjord and have a complete hull of aluminium. The aluminium hull will give a significantly lighter ferry than if it was made of steel. On the other hand, the hull will be more prone to fire damage due to aluminium's low resistance to temperature, which will be discussed further in this thesis.

Figure 1.1: New design of the Oslo-ferries

In the project thesis from the previous semester, an aluminium redesign of the previous Multi Maritime design of the Oslo ferry, MS Kongen, was performed on the main deck (Rindheim, 2020). It was concluded that the aluminium deck had 63.7% weight saving when redesigning according to the rules and the original scantlings of the steel deck. However, the extra need for insulation when designing with aluminium was not taken into account. This means that even though aluminium is a lighter material than steel, the total weight savings might not be as large because of the insulation.

In light of the recent event of the electric steel ferry MF Ytterøyningen which had a fire in the battery room and in the switchboard room October 2019 (Lura & Anthun, 2019), the need for evaluating aluminium hull structure in fire is highly relevant. In the offshore sector in the marine industry, a lot of work has been done in accordance to rules and regulations when it comes to fire, mainly because the event of a fire on an oil platform is catastrophic. The ship industry, on the other hand, has not. The fire design on ships is based on classifications according to The Maritime Safety Committee (2010) on what fire divisions to use for bulkheads and decks, and how these should be insulated.

It would therefore be interesting to see how aluminium behaves during fire in an imagined situation of a battery-room fire. Especially important would it be to see when aluminium looses its strength and how it performs structurally under elevated temperatures.

1.1 Objective

The main objective of this thesis is to study the effects of fire in typical aluminium hull structures compared to steel in compression load. A parametric study on how insulation affects the heat transfer in the material and the strength will be performed as well.

Typically aluminium is used in superstructures and upper decks in ferries and cruise ships to decrease the weight. The bulkhead structures of aluminium will therefore be the components of the ships that are load bearing and holds up the decks in typical ferry and cruise ship designs. The main focus will therefore be on buckling of typical bulkhead stiffeners during elevated temperatures.

1.2 Design of the Oslo ferry

The ferry with the design designation MM35PE EL which will operate in the Oslo fjord is described as a modern, efficient and high quality hybrid/full-electric double ended passenger ferry according to the building specification (Multi Maritime, 2020). It will have automated high-power charging from shore to ensure enough battery capacity for fully electric operation on selected routes. In addition, the ferry will have two generators with the capacity to operate on bio diesel.

The battery energy storage system will have a total capacity of 1017 kWh divided in two battery rooms at each end of the ferry and will have insulation according to A-60 standard, which will be discussed further in Chapter 4. The battery room will be arranged according to the rule requirements with a water mist fire extinguishing system, detectors for gas, oxygen and fire, ventilation system for the rooms and battery racks. In addition, space has been reserved for 50% increase of battery capacity. The bio diesel generators will have a capacity of 2250 kW located in fwd and aft propulsion room.

The entire hull of the ferry shall be of aluminium construction. It should be built in seawater resistant aluminium construction with the qualities NV AW 5083-H321 for plates and NV AW 6082-T6 for profiles and extruded panels.

The scantlings for this ferry are listed in Table 1.1. The vessel is designed for passenger transport, but the design is inspired by conventional car ferries with its monohull structure.

Table 1.1: Main dimensions of the Oslo ferry

Main Dimensions	
Length over all	35.00 m
Breadth, moulded	8.00 m
Depth, moulded	3.80 m
Draught, scantling	2.20 m
Draught, summer	appr. 2.05 m
Gross tonnage	appr. 410 MT
Passengers and crew	354 pc

1.3 Historical fire accidents

The inspiration for this master thesis is the fire in MF ”Ytterøyningen”. MF ”Ytterøyningen” is an electric car ferry which had a fire the 10th of October 2019 that started in the batterypack. The cause was a leak in the water cooling system of the battery pack, which lead to an electric arc in the battery. This developed a lot of heat over time until the fire started. Saltwater was used to extinguish the fire, which lead to a short circuit in the battery which ended in an explosion (Lura & Anthun, 2019). This ferry was made of steel, but had it been in aluminium, the outcome would probably have been significantly worse.

17th of August 2018 there was a fire in the ferry ”Eid” in Lysefjorden, Rogaland. It was a tourist ferry with 49 passengers where the fire started as a consequence of engine heat. All passengers were evacuated (Vosgraff, 2018).

The most famous ship fire was the catastrophic fire of the cruise ship ”Scandinavian Star” in 1990 where 159 people lost their lives Sæther et al. (2013). The ship was set on fire, and it still remains a mystery what really happened that night.

1.4 Literature Review

In previous studies, structural tests have been performed to determine both the material properties of aluminium during elevated temperature and their deformation behaviour and failure modes. Analytical models have also been developed for prediction of the failure of simple components, with the downside that they can only be used for, as mentioned, simple components. In recent years several studies have focused more on numerical models, i.e. finite element models, to predict the performance of aluminium structures at elevated temperatures under compressive loading. With the strength of computer programs, more complex problems can be solved with little effort, however, in most cases the finite element and analytical models are verified using structural tests.

Hopperstad et al. (1997) did a study which used structural tests to validate a numerical model (Finite Element Analysis) for aluminium alloys AA6082 T4 and T6 with internal elements of 5083 M and 6082 TF alloys under in-plane compression. It was found that the correlation between the experimental and predicted ultimate compressive strengths were good and that the finite element model reproduced the main structural effects sufficiently.

Suzuki et al. (2005) used structural tests to validate analytical expressions based on lumped mass heat balance for estimating the temperature rise of unprotected and protected aluminium alloys and also the critical failure temperature of compression-loaded aluminium components in fire.

Also Amdahl et al. (2001) did a structural analysis focusing on the behaviour of aluminium plate girders, predominantly loaded in shear at elevated, but constant, temperatures. They compared the results with non-linear FE predictions and Eurocode 9 capacity formulas. The FE analysis showed good agreement with the tests at around 200°C but failed to capture the dramatic reduction at 225°C. The Eurocode 9 showed optimistic strength predictions at 200°C but were non-conservative at 225°C. Langhelle & Amdahl (2001) performed experiments to study the behaviour of AA 6082 aluminium alloy columns at elevated temperatures and applied finite element programs for a buckling test which was compared to numerical analyses and design rules. It was stated that there was still a need for more test on aluminium components due to lack of material data. They used the programs USFOS and Abaqus for the analyses and concluded they were well suited for column buckling tests at constant heating rates, but had a long way to go for modelling creep behaviour.

Maljaars et al. (2009) studied the buckling of fire exposed aluminium columns and developed a finite element model in DIANA 9.1 for this, which was verified with experiments. A parametric study with the finite element model concluded that the simple calculation model for flexural buckling of fire exposed aluminium columns in Eurocode 9 did not give accurate predictions of the buckling resistance in fire. It was then found an alternative design model taking into account the shape of the stress-strain relationships of aluminium alloys at elevated temperatures which agreed with the finite element model. So they used both structural tests, analytical models and finite element model in their study.

Feih et al. (2011) used a coupled thermal-mechanical finite element model to predict the deformation, softening and failure of a compression-loaded aluminium structure exposed to one-side heating by fire. They experienced that structural tests performed in previous literature was usually only valid for the specific geometry and loading condition of the test component, which made it difficult to use the information on other structures in different fire scenarios. Analytical and numerical models have also been developed in previous literature, but only for simple structural components, where the numerical models did not consider creep deformations. The limitations of the existing models were the reason Feih et al. (2011) wanted to create a finite element model which can take into account more advanced geometries and fire scenarios. The model is validated by comparing experimental data from fire structural tests performed on aluminium plate to assess the contributions the elastic creep and softening effects have on the failure and collapse of aluminium structures during fire exposure. The finite element analysis was done in the program ABAQUS in two steps:

- Analysis of the deformed specimen profile during initial compressive loading including geometry imperfection
- Fully-coupled thermo-mechanical analysis of the deformations of the structure due to the time-dependent 3D temperature profile and temperature dependent material properties.

The plate was modeled with reduced integration, 8-noded solid element with temperature degrees-of-freedom (C3D8RT).

Common for all the articles above are that they either use constant temperatures, or standard thermal profiles. Banerjee et al. (2009), however, simulated the start and development of fire in a room with the program Fire Dynamics Simulator (FDS), then a second program calculated the temperature distribution in a beam and finally, a third computer program was used to compute how the beam deformed over time due to combined effects of thermal and mechanical loads.

Arthur et al. (2011) looked at compression-controlled failures of aluminium plates subjected to an applied mechanical load and applied heat flux to simulate fire in a finite element analysis in Abaqus. The effects of creep were studied, but found that it was hard to find available data on the creep behaviour. Overall they experienced that the finite element model provided accurate predictions of the failure.

Tran et al. (2017) used Abaqus to assess the behaviour of a steel beam under and ISO-834 standard fire, which is considered as realistic fire action. They did a sequentially coupled thermal-stress analysis where they first did a heat transfer analysis and then a structural analysis. They included nonlinearities in the heat transfer analysis as variation in conductivity with temperature, and nonlinearities in yielding for the structural analysis. They considered a simply supported beam with a point load on the middle, i.e. they did a bending analysis. The conclusions were that the analyses were successfully performed

in Abaqus and the stresses increased with temperature, which makes understanding the response of the beam structure subjected to fire an ensurance of safety and serviceability states in design.

1.5 Limit states

A limit state is defined as a state where the structure or its elements is considered not to fulfil one of the criteria governing its performance or use it has been designed (Moan, 1994). This gives the foundation for the basic principles of design verification. The limit states are often categorized into two groups:

- Serviceability Limit States (SLS)
- Ultimate Limit States (ULS), including Accidental Limit State (ALS) and Fatigue Limit State (FLS)

Serviceability limit states specifies the serviceability or durability of structures. This limit state ensures the structure is functional and/or comfortable. Examples of these cases are vibrations, which are especially important for aluminium structures, corrosion, deflection, etc. The conditions are not strength-based but may render the structure unsuitable for its intended use (Gilbert, 2011). From Sapa Technology (2016) it is said that the serviceability limit state often is the critical design factor for aluminium because of the low modulus of elasticity.

Ultimate Limit State is the limit state where the structure is intended to withstand environmental loads with 100-year return period, i.e. 10^{-2} probability, and not have any damages. An example is offshore structures that under ULS are required to withstand the "100-year wave" (Moan, 1994).

Accidental Limit State, also called Progressive Collapse Limit State (PLS), is when the structure may have progressive failure due to accidental loss or overloading of single members (Moan, 1994). Accidental actions and abnormal environmental loads with 10.000-year return period, i.e. 10^{-4} probability, are considered in the ALS analysis, which can be fire, explosions, ship collisions or operational errors and technical faults (Moan, 2000; Amdahl, 2019).

Fatigue Limit State ensures crack propagation due to fatigue and cyclic loads are within acceptable limits. Where ULS considers large loads and different load combinations, FLS takes into account cyclic loads that can initiate crack growth in stress ranges below the yield limit.

1.6 Design check

Traditionally, the design criteria have been expressed as working stress design which uses only one safety factor to define the allowable limit. In recent years, however, the use of load and resistance factored design (LRFD) has been increasing. This method consists of several load and resistance factors, including uncertainties and safety requirements (Bia et al., 2016). The LRFD design check states that the expected design loads, S_d, for a structural component should not be larger than the structure's design resistance (Capacity), R_d, to be within the overall strength-requirement:

$$R_d \geq S_d \Rightarrow R_d - S_d \geq 0 \tag{1.1}$$

Taking into account the load factor γ_f and the material factor γ_m to account for uncertainty in load and flaws in material or fabrication errors, the dimensioning values for the design load and design resistance becomes:

$$S_d = \sum S_k \cdot \gamma_f \tag{1.2}$$

$$R_d = \sum \frac{R_k}{\gamma_m} \tag{1.3}$$

Where S_k is the characteristic load effect and R_k is the characteristic resistance.

Both the resistance and the load are random parameters and can be modelled by probability density functions since their actual values cannot be determined with certainty. This means the relationship between the load and the resistance of the structure can be shown by frequency distributions, where any overlap between S and R will give no safety margin above the limit state of the applied load (Manning, 1988).

Figure 1.2 shows the frequency distributions of the load S and resistance R. The overlap is shown by the shaded area and the safety margin against the load exceeding the relevant limit state becomes larger the smaller the area is. However, since S and R are random variables, there exists some probability that R may be less than S, which means the design criteria is broken (AISC, 1986). The probability density functions are based on a large amount of data gathered throughout the history of structural engineering.

Another way to display the same design criteria is to divide the expression in Equation 1.1 with S and express the results logarithmically. This will give a single-frequency distribution curve with combined uncertainties. The design requirement is then valid if:

$$\frac{R}{S} \geq 0 \tag{1.4}$$

Logarithmically, this gives a violated limit state if:

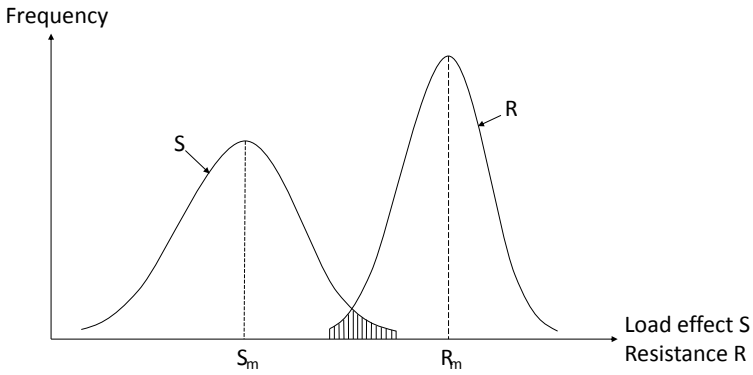

Figure 1.2: Frequency distribution of load effect S and resistance R, reproduced from AISC (1986)

$$ln(\frac{R}{S}) < 0 \tag{1.5}$$

The probability that the limit state is exceeded, P_F, is shown in Figure 1.3 as the shaded area. According to AISC (1986) the probability of failure can be reduced, with the consequence that the reliability increases, in two ways:

1. Shifting the mean of ln(R/S) to the right
2. Reducing the spread of the curve for a given position of the mean relative to the origin

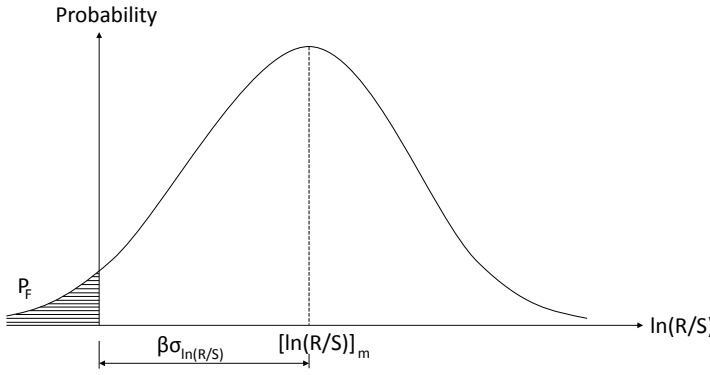

Figure 1.3: Definition of reliability index, reproduced from AISC (1986)

The distance from the origin to the mean is, as denoted in Figure 1.3, $\beta\sigma_{ln(R/S)}$. $\sigma_{ln(R/S)}$ is the standard deviation of ln(R/S) and β is called the reliability index. The two methods of decreasing the probability of failure can be combined by using this distance as the unit of measure. To conclude, β is directly related to the limit state probability of failure, P_F and is therefore used to make adjustments to the load and resistance factors to calibrate the LRFD specifications (Manning, 1988).

1.7 Report Structure

Chapter 2 is based on a literature review done in the project thesis during the fall semester 2019. It is a literature study on ferries and their historical development.

Chapter 3 gives the material properties for steel and aluminium in addition to the insulation used in the thesis.

Chapter 4 gives a summary of the relevant rules and regulations regarding structural fire design

Chapter 5 describes the finite element program used for the thesis, and also a description of the method invented to calculate buckling loads under elevated temperatures

Chapter 6 discusses the heat transfer analyses

Chapter 7 discusses the buckling analyses

Chapter 8 presents the results from the heat transfer analyses and the buckling analyses

Chapter 9 gives a discussion and concluding remarks regarding the method chosen and the results

Chapter 10 gives recommendations for further work.

Chapter 2

Ferries

With the coastline of Norway being 102.936 km in total (Kartverket, 2019), the Norwegian transportation system has always been dependent on ferries. According to Statens vegvesen (2019a), 20 million vehicles and 40 million passengers are transported yearly on Norwegian car ferries in about 130 ferry routes. Today it is The Norwegian Public Roads Administration's (NPRA) responsibility to operate the ferries, but already in 1274 a landlaw of Magnus Lagarbøtes stated that it was the landowners responsibility to provide bridges or fleets where rivers or streams were crossing the roads (Tjeltveit & Statens vegvesen, Rogaland, 1996). This shows how much the ferry industry has changed, and the main reason for the development is due to the increasing number of car owners

A revolution in the transportation methods was needed when cars made their arrival to Norway. Larger and more powerful ferries were the answer and made it possible to transport cars from one side of the fjord to another where bridges could not be built. A lot of people are dependent on the modern car ferry today, in which there are great expectations with regards to flexibility and effective traffic management (Tjeltveit & Statens vegvesen, Rogaland, 1996). Passenger ferries are also commonly used in coastal areas in which the development of these ferries moves towards greener and environmental friendly technology (LMG Marin et al., 2016). In the following sections a historical overview of the development of ferries will be given, as well as how ferries are designed today.

2.1 Historical development of ferries

Car ferries have been vital to the Norwegian transportation system, especially in the last hundred years. After 1968, a national regulation for ferry fares was introduced, where the NPRA gave stronger public control and and increase of economical support for the ferry

operations (Tjeltveit & Statens vegvesen, Rogaland, 1996). However, as mentioned, the ferries have been important for Norway's development of transportation systems already in 1274 when Magnus Lagarbøtes landlaw was introduced.

The first ferries that came in the 1890s (Tjeltveit & Statens vegvesen, Rogaland, 1996) were simple fleets and row-ferries made of wood used to transport people to the other side of rivers, today called passenger ferries. The bigger ferries could also transport horses and carriages. These had often small capacities and could only go on shorter distances. The row ferries had oars in each end and a big, open cargo area or a cargo deck midship, and were used into the 20^{th} century (Arisholm & Kolltveit, 2003).

What is considered the first modern ferry was a result of the *"railway boom"* and the first Norwegian steam ferry came in 1909 (Arisholm & Kolltveit, 2003). In the first decades of the century, the cars made their arrival to Norway. The number of cars at this point was very low, and when needed, the cars were transported onto the local row ferries by winches or platforms. This was a risky transportation method and the cars were in great danger of sliding into the sea. In 1912 the locals required a replacement of the row ferries with a steam or engine driven ferry large enough to load horses and carriages without unbuckling the carriages. The first automobile ferry was *Salhusfærgen* in 1918 which was an engine driven ferry in steel, 31 gross registertonns, 46 foot long and 15 foot wide, longitudinal ro/ro with a capacity of two to three cars or five horses (Arisholm & Kolltveit, 2003).

(a) "Lysefjord" eks. "Rennesøy", typical fjord ferry from 1969. *Photo: Jan B. Henriksen*

(b) "Hjelmeland", one of the early standarized pendel ferrys, built in 1969. *Photo: Johannes Østvold*

Figure 2.1: Pendel and fjord ferries (Tjeltveit & Statens vegvesen, Rogaland, 1996)

The increase of cars in the 1950-60's gave more focus on passenger comfort on board the ferries (Arisholm & Kolltveit, 2003). The saloons above deck were insulated, while the wheelhouse was lifted up to give the passengers better views through windows in the superstructure. The first hydraulic gates also came in the 60's which gave better control at sea and a hull shape reminding more of regular ships.

As mentioned, the NPRA introduced a national regulation for ferry fares in 1968. This regulation defined two standard models for the ferries. These were double ended ferries, called Pendel ferries (see Figure 2.1b), and ferries with conventional hulls, called Fjord ferries, see Figure 2.1a (Tjeltveit & Statens vegvesen, Rogaland, 1996). The double ended ferries were, as the name states, double ended with the wheelhouse in the middle. It had

propellers both forward and aft of the ferry, which made it easy to maneuver, especially since it did not require turning in the harbors. The fjord ferries were however built for longer distances with their often closed decks, depending on their trading areas (Arisholm & Kolltveit, 2003). With a conventional hull, the fjord ferries had to turn around in the harbors to load and unload the ferry, which meant each stop took longer time than the pendel ferries. The development of the architecture of ferries can be seen in Figure 2.2, which shows that the double ended ferries almost replaced the conventional ferries in the end of the 20^{th} century.

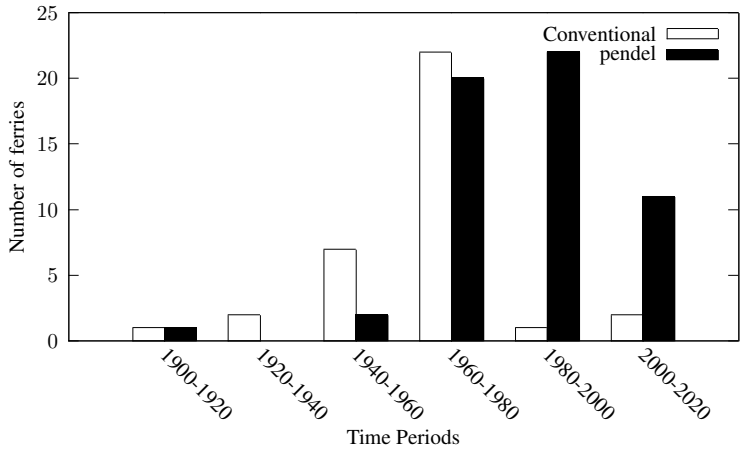

Figure 2.2: Comparison of architecture in different time periods for new builds, data from Hatteland (2019)

In the end of the 1970's the first hanging platform decks with ramps on each side were introduced to Norwegian ferries (Arisholm & Kolltveit, 2003). This increased the capacity of the ferries, and the decks were also installed on existing ferries. At this time also the trailer traffic increased, which gave a demand for designated space for large trucks. At this point the ferries were more or less standardized by the NPRA, and a lot of the standardized ferries were built in the 70s.

According to Arisholm & Kolltveit (2003) the main factors for the changes over time in the ferry fleet is capacity and safety. With changes in the capacity demand, the ferries had to be bigger, and with the increasing traffic, a short stopping time was preferred. This gave the pendel ferries great advantages to the fjord ferries. The safety factor played a role because old ferries with closed fronts could not transport dangerous goods. The high restriction regards dangerous goods made new ferries, built with this in mind, the favourable ferries. How the size of the ferries changed can be seen in Figure 2.3 and Figure 2.4. Both the average gross register tonnage and the average length of the ferries increased substantially throughout the years. The figures show well how the ferries had to increase their loading capacity according to the increasing amount of cars.

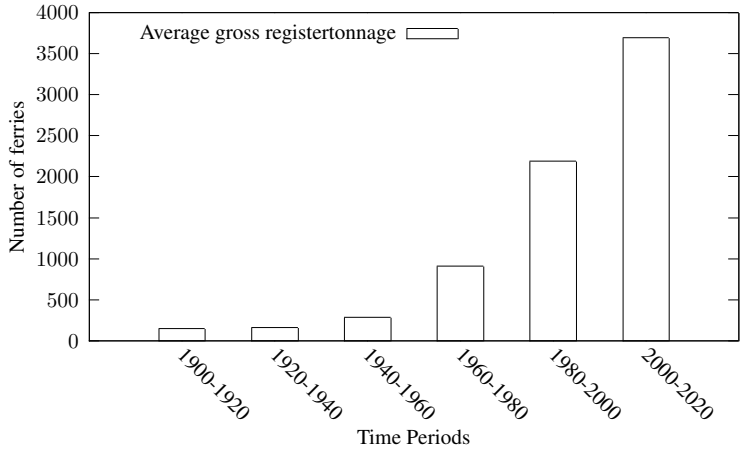

Figure 2.3: Average development of gross register tonnage in different time periods, data from Hatteland (2019)

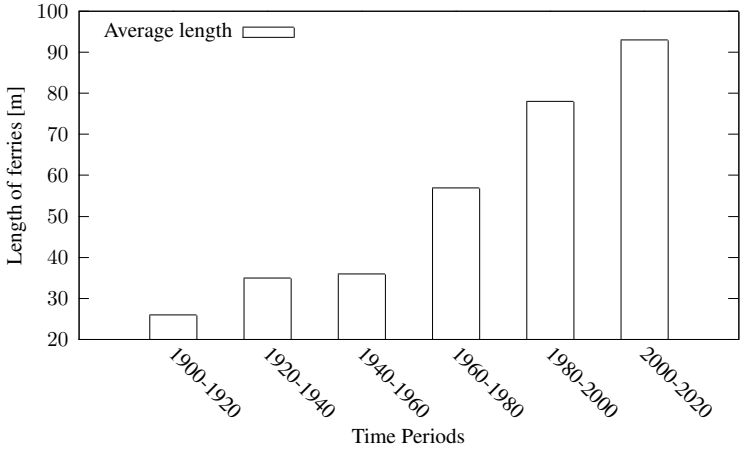

Figure 2.4: Average length of ships in different time periods, data from Hatteland (2019)

The figures are made from the archive of Hatteland (2019), where historical data from ferries in Rogaland shows the development of the ferries discussed above. The data from the archive is corresponding to that time the specific ferry was in operation, but in the figures, the ferries are compared by the year they were built. This means some of the ferries might have been rebuilt and will not give accurate numbers. The figures are therefore made just to show the main tendencies of the development of the ferries to confirm what is discussed in this section.

2.2 Current and future ferries

Today there is a big focus on green technology. Also the ferry industry is moving towards green technology and solutions to reduce emissions. The NPRA, which are responsible for operating the ferries, states that the reduction of emissions is very important for them and that *"in 2022 the emissions from ferries will be halved in Norwegian waters compared to 2015 level"* (Statens vegvesen, 2019b). They think that hydrogen driven ferries will lead to zero emission on longer distances, but that it is too expensive to be commercialised at the moment.

In Norway almost 80 ferries will be electric in 2022, where the first battery driven ferry, MF Ampere, came in 2015 (Statens vegvesen, 2019b; Gustavsen, 2019). Short ferry distances are well suited for electrically powered ferries and will reduce the emissions drastically and electricity is additionally a cheaper fuel in comparison with diesel.

The worlds first mono hull pendel ferry in aluminium is going to be built for Norled which is expected in operation 1^{st} of January 2020 (Markussen, 2018). With a lower weight with a hull in aluminium, there is a reduced need for power. If you combine both low weight with battery power, Markussen (2018) states that the ferry will be an *"environment lighthouse"*. The ferry will go on a short distance with the capacity of 16 cars, constructed for two trailers at 52 tons each.

The changes within the ferry industry is changing a lot these days, especially considering the environmental aspects of ferry designs. As seen above, Norway is very innovative and aim for new and better solutions in their ferry design and fuel. Battery ferries tends to get very heavy because of the battery packs, and it is desirable to keep the structural weight as low as possible for economical reasons. This is often done with superstructures or even the whole hull in aluminium instead of steel with a goal of not compromising the strength. Figure 2.5 shows the increase of both aluminium superstructures and hulls over the years.

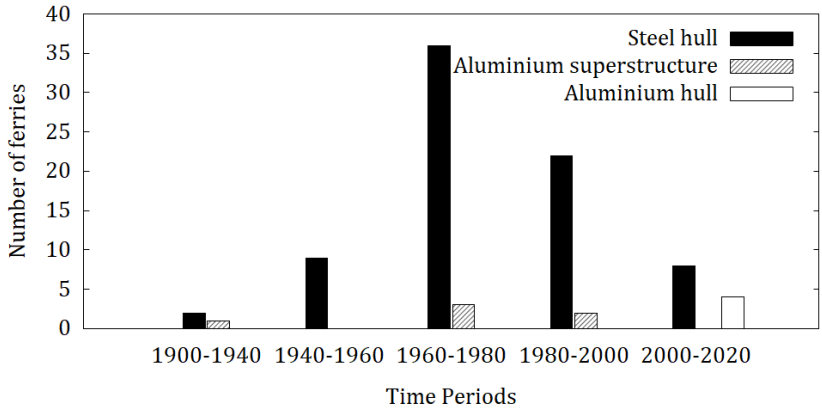

Figure 2.5: Building materials for ferries in different time periods, data from Hatteland (2019)

For high-speed low crafts there are several concepts to choose from when designing a passenger ferry, some of these are shown in Figure 2.6. The hydrofoil and air-pillow concepts needs high speed and light weight to be energy efficient. It is therefore challenging to incorporate heavier technology like batteries and hydrogen. Monohulls and catamarans are most used today and are also considered the most appropriate designs for the specific use of these passenger ships in Norway. The Trimaran is not especially used, but is assumed to not bring drastic changes in comparison to monohulls and catamarans.

Figure 2.6: Passenger ferry concepts (LMG Marin et al., 2016)

The choice of machinery for new ferries are important both for the performance of the ferries and the environmental aspect. Mostly used is the diesel mechanic propulsion, which produces emissions of NO_x, CO_2 and SO_x proportionally to the sulfur content in the fuel (LMG Marin et al., 2016). The emissions can however be reduced by using low-sulfide oil or motors designed to reduce NO_x emissions. The use of bio diesel can also reduce the emissions of CO_2.

Gas propulsion is another option, but it is not an easy solution to obtain good machinery on a high speed vessel. Today the use of an electric propulsion system is normal in combination with gas, this is however unnecessary and will give extra weight. The goal is to have a propulsion system using only gas, but this is per 2016 not available for maritime use (LMG Marin et al., 2016). An alternative for gas propulsion is fully electric ferries with battery propulsion system. The energy is taken from the power-network onshore and the battery packs on board stores the energy to operate until the next possibility for charging. The challenge with battery propulsion systems is that is is difficult to weight optimize battery-electric concepts, and the weight of the ferry could become a problem.

A combination of diesel and battery into a hybrid propulsion system the electric power could be used for operations in the basin. The power could also be shared between the main propulsion and the help-system in transit. However, in order for the system to give climate benefits, the need for larger capacities of diesel engine, electrical engine and battery size gives too large weight to give an effective ferry concept, which is not further recommended (LMG Marin et al., 2016).

From this chapter it is clear that newer technology gives larger weight for propulsion systems, and the need to reduce the weight of the hull is absolutely relevant for future ship

designs. The choice of material, hull shape and propulsion systems are all connected in order to design an environmental friendly, efficient and safe vessel. The ferries in the future will hopefully be even more environmental friendly, lighter and at the same time fulfill the demand.

Chapter 3

Steel and aluminium as hull material

Steel is the most common fabrication material for hull structures in the marine industry today. The strength and weldability of steel is the reason to choose this material above others. However, after the World War II, aluminium superstructures were being built in the US, and soon after aluminium superstructures of passenger ships became adopted for fabrication worldwide (Sielski, 2007b). In the 1990s hulls of high-speed merchant vessels were being built in aluminium, which needed more lightweight materials.

Aluminium has generally one-third of the Young's modulus and material density of steel. This gives aluminium alloys the characteristics of maintaining high strength with lower weight. Aluminium alloys are therefore used in ship constructions in order to save weight. Welding of aluminium alloys can however be a challenge. The low elastic modulus gives the material greater distortion and greater chances of buckling from residual stresses (Sielski, 2007b). This means the material gets weaker from the residual stresses obtained during welding. Even though aluminium alloys can have higher yield strength than steel, they often end up weaker because the material is welded. Steel however can be considered stronger after the welding, depending on the alloy, which makes the two materials very different from each other in a construction perspective.

3.1 Material properties

In the current ferry, the 5083-H321 and 6082-T6 aluminium alloys will be used. The 5083 alloy is often used in hull structures because of its corrosion resistance in salt-water

environment. It is also easier to weld than 6xxx-series alloys and more predictable in terms of post-weld strength. The 6082 alloy is often used for high-strength building and structural components (Norsk Hydro ASA, 2019). As mentioned, the plates will be of the aluminium alloy NV AW 5083-321, and the aluminium alloy NV AW 6082-T6 will be used for the profiles and extruded panels since stiffeners are high strength components of the deck structure. The chemical compositions of the alloys are shown in Table 3.1.

Table 3.1: Chemical composition of Aluminium Alloys in percentage by weight (Aluminum Association, 2015)

Alloy	Si	Fe	Cu	Mn	Mg	Cr	Zn	Ti
5083	0.40	0.40	0.10	0.40-1.0	4.0-4.9	0.05-0.25	0.25	0.15
6082	0.7-1.3	0.5	0.1	0.40-1.0	0.6-1.2	0.25	0.20	0.10

This thesis will compare aluminium structures to steel structures, and the most used steel alloy in hull structures is the NV-NS steel, i.e. normal strength steel. The general material properties of steel and the aluminium alloys are shown in Table 3.2.

Table 3.2: Material properties of steel NV-NS and aluminum alloys (ABS, 2019; DNV GL, 2015, 2018)

		Steel NV-NS	5083 Alloy	6082 Alloy
Young's modulus, E	GPa	210	71	69
Yield strength, σ_y	MPa	235	215	260
Mass density, ρ	$\frac{kg}{m^3}$	7800	2660	2700
Poisson ratio, ν	-	0.3	0.33	0.33
Melting point	°C	1480-1526	570	555
Thermal expansion	$\frac{1}{°C}$	$12{\cdot}10^{-6}$	$25{\cdot}10^{-6}$	$24{\cdot}10^{-6}$

The temperature dependent material properties of steel and aluminium are, however, found in EN 1999-1-2 (2007) and EN 1993-1-2 (2005) for aluminium and steel structural fire design and are summarised in Section 3.1.1 and 3.1.2 respectively. The proof strength and Young's modulus will be assessed, in addition to three thermal properties:

- Thermal elongation
- Specific heat
- Thermal conductivity

3.1.1 Aluminium

Proof strength and Young's modulus

Aluminium alloys at elevated temperatures with thermal exposure up to two hours will have the 0.2% proof strength of

$$f_{o,\theta} = k_{o,\theta} \cdot f_o \tag{3.1}$$

Where $f_{o,\theta}$ is the 0.2 proof strength at elevated temperature and f_o is the 0.2 proof strength at room temperature defined in EN 1999-1-1 (2007) to be 260 MPa for the 6082 alloy and 215 MPa for the 5083 alloy.

The change in proof strength at elevated temperatures for the relevant alloys is shown in Table 3.3 and the change in modulus of elasticity (Young's modulus) is shown in Table 3.4. A graph showing the relations between the proof strength and elastic modulus with elevated temperature is shown in Figure 3.1. For this thesis the strain is also needed, so the proof strength will not be used, but is gives a good representation of how the material behaves in temperature. The stress-strain used for this thesis is discussed in Section 3.3.1.

Table 3.3: 0.2% proof strength ratios $k_{p,\theta}$ for relevant aluminium alloys at elevated temperature for up to 2 hours thermal exposure period. (adapted from EN 1999-1-2 (2007) table 1a)

Alloy	Temper	Aluminium alloy temperature °C							
		20	100	150	200	250	300	350	550
EN AW-5083	H12[1)]	1.00	1.00	0.80	0.60	0.31	0.16	0.10	0
EN AW-6082	T6	1.00	0.90	0.79	0.65	0.38	0.20	0.11	0

1) The values may be applied also for temper H22/H32

Table 3.4: Modulus of elasticity of aluminium alloys at elevated temperature for a two hour thermal exposure period, $E_{al,\theta}$. (Adapted from EN 1999-1-2 (2007) table 2)

Aluminium alloy temperature, θ (°C)	Modulus of elasticity, $E_{al,\theta}$ (N/mm^2)
20	70.000
50	69.300
100	67.900
150	65.100
200	60.200
250	54.600
300	47.600
350	37.800
400	28.000
550	0

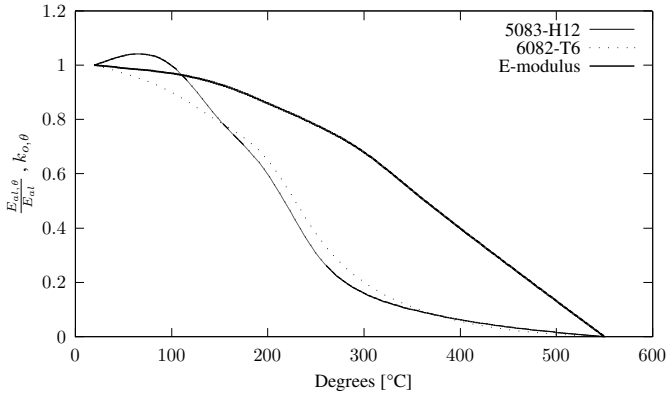

Figure 3.1: 0.2% proof strength ratios $k_{o,\theta}$ and ratio E=$E_{al,\theta}/E_{al}$ for aluminium alloys at elevated temperature for up to 2 hours thermal exposure period for 5083 and 6061 alloys. (Adapted from Table 3.3 and Table 3.4 based on EN 1999-1-2 (2007))

Thermal elongation

The thermal elongation $\Delta l/l$ is determined by the following formula, where l is the length at 20°C, Δl is the temperature induced elongation and θ_{al} represents the aluminium temperature:

$$\Delta l/l = 0.1 \cdot 10^{-7}\theta_{al}^2 + 22.5 \cdot 10^{-6}\theta_{al} - 4.5 \cdot 10^{-4} \tag{3.2}$$

The resulting curve is shown in Figure 3.2

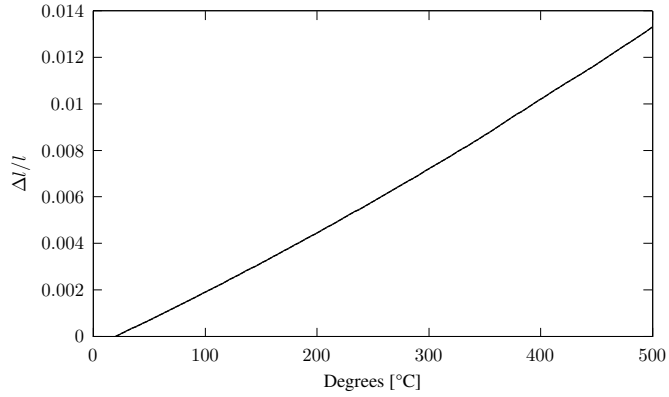

Figure 3.2: Relative thermal elongation of aluminium alloys as a function of the temperature. (Adapted from EN 1999-1-2 (2007), figure 3)

Specific heat

The specific heat, c, is according to Luscombe (2018) defined as the heat required to change the temperature of an object by one degree. In Eurocode the specific heat of aluminium should be determined from the following formula:

$$c_{al} = 0.41 \cdot \theta_{al} + 903 \quad (J/kg°C) \tag{3.3}$$

The specific heat with different temperatures is shown in Figure 3.3.

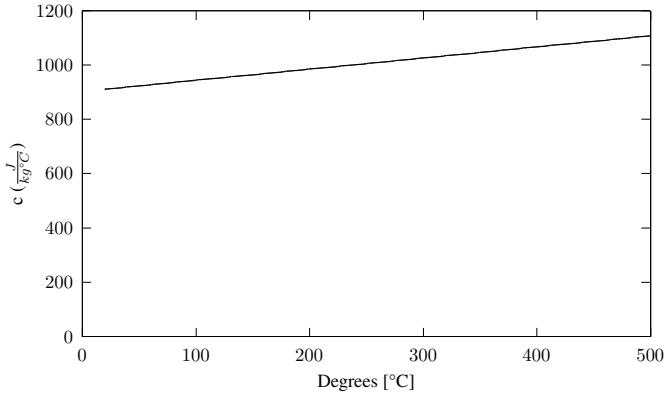

Figure 3.3: Specific heat of aluminium alloys as a function of the temperature (Adapted from EN 1999-1-2 (2007), figure 4)

Thermal conductivity

The thermal conductivity, λ_c, is according to Loeb (1954) defined as the amount of heat crossing a unit area of the material per unit time per unit temperature gradient. For aluminium alloys in Eurocode, the thermal conductivity is calculated in two different ways; one for alloys in 3xxx and 6xxx series, and one for alloys in 5xxx and 7xxx series. Since both 5xxx and 6xxx alloys are used, their respective formulas are:

$$\lambda_{al} = \begin{cases} 0.07 \cdot \theta_{al} + 190 \quad (W/m°C) & \textit{for 6xxx alloys} \\ 0.1 \cdot \theta_{al} + 140 \quad (W/m°C) & \textit{for 5xxx alloys} \end{cases} \tag{3.4}$$

The variation of the thermal conductivity is illustrated in Figure 3.4.

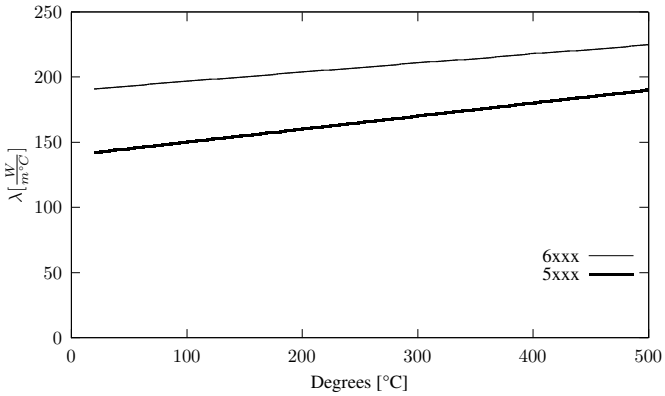

Figure 3.4: Thermal conductivity as a function of the temperature (Adapted from EN 1999-1-2 (2007), figure 5)

As shown in the figures, the material properties of the 6082 alloy and the 5083 alloy are quite similar. Therefore, for further work in this thesis, it will be assumed that the plate and stiffeners are of the same material, aluminium alloy 6082, in order to simplify calculations and finite element modelling.

3.1.2 Steel

Effective yield strength and Young's modulus

The effective yield strength for steel is the same as the 0.2% proof strength for aluminium. Both the effective yield strength and the Young's modulus are defined with reduction factors at elevated temperatures. The reduction factors are as follows:

- Effective yield strength, relative to yield strength at 20°C: $k_{y,\theta} = f_{y,\theta}/f_y$
- Slope of linear elastic range, relative to slope at 20°C: $k_{E,\theta} = E_{s,\theta}/E_s$

Where $f_{y,theta}$ is the effective yield strength at elevated temperatures, f_y is the yield strength of steel at 20°C, $E_{s,\theta}$ is the slope of linear elastic range at elevated temperatures and E_s is the modulus of elasticity at 20°C. The reduction factors are defined in Table 3.5 and shown in Figure 3.5

Table 3.5: Reduction factors for stress-strain relationship of carbon steel at elevated temperatures (Adapted from EN 1993-1-2 (2005) table 3.1)

Steel temperature θ_a	Yield strength $k_{y,\theta}$	Young's modulus $k_{E,\theta}$
20°C	1.000	1.000
100°C	1.000	1.000
200°C	1.000	0.900
300°C	1.000	0.800
400°C	1.000	0.700
500°C	0.780	0.600
600°C	0.470	0.310
700°C	0.230	0.130
800°C	0.110	0.090
900°C	0.060	0.0675
1000°C	0.040	0.0450
1100°C	0.020	0.0225
1200°C	0.000	0.000

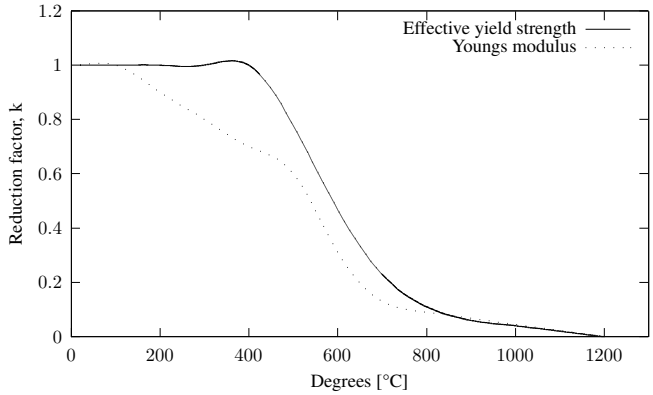

Figure 3.5: Reduction factors for the stress-strain relationship of steel at elevated temperatures (Adapted from Table 3.5 based on EN 1993-1-2 (2005))

Thermal elongation

The relative thermal elongation of steel $\Delta l/l$ is determined by the following equations and Figure 3.6:

$$\Delta l/l = \begin{cases} 1.2 \cdot 10^{-5}\theta_a + 0.4 \cdot 10^{-8}\theta_a^2 - 2.416 \cdot 10^{-4} & \textit{for } 20°C \leq \theta_a < 750°C \\ 1.1 \cdot 10^{-2} & \textit{for } 750°C \leq \theta_a \leq 860°C \\ 2 \cdot 10^{-5}\theta_a - 6.2 \cdot 10^{-3} & \textit{for } 860°C < \theta_a \leq 1200°C \end{cases} \tag{3.5}$$

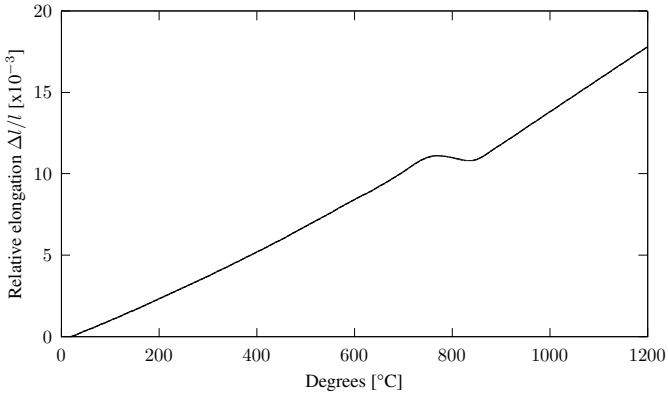

Figure 3.6: Relative thermal elongation of aluminium alloys as a function of the temperature. (Adapted from EN 1993-1-2 (2005), figure 3.3)

Specific heat

The specific heat, c, should be determined by the following equations which is also illustrated in Figure 3.7.

For 20°C $\leq \theta_a <$ 600°C:

$$c_a = 425 + 7.73 \cdot 10^{-1}\theta_a - 1.69 \cdot 10^{-3}\theta_a^2 + 2.22 \cdot 10^{-6}\theta_a^3 \quad (J/kg°C) \tag{3.6}$$

For 600°C $\leq \theta_a <$ 750°C:

$$c_a = 666 + \frac{13002}{738 - \theta_a} \quad (J/kg°C) \tag{3.7}$$

For 900°C $\leq \theta_a \leq$ 1200°C:

$$c_a = 650 \quad (J/kg°C) \tag{3.8}$$

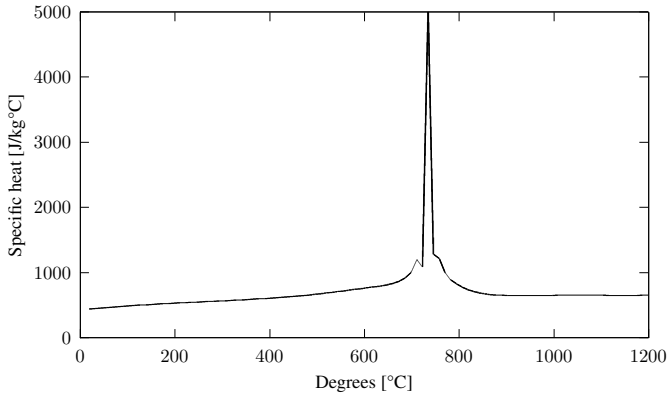

Figure 3.7: Specific heat of steel as a function of the temperature (Adapted from EN 1993-1-2 (2005), figure 3.4)

Thermal conductivity

The thermal conductivity, λ_c is determined by the following equations and illustrated in Figure 3.8

$$\lambda_c = \begin{cases} 54 - 3.33 \cdot 10^{-2}\theta_a \quad (W/mK) & \textit{for } 20°C \leq \theta_a < 800°C \\ 27.3 \quad (W/mK) & \textit{for } 800°C \leq \theta_a \leq 1200°C \end{cases} \tag{3.9}$$

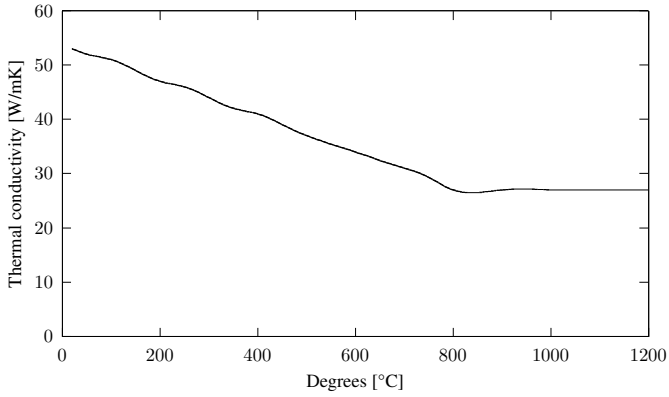

Figure 3.8: Thermal conductivity as a function of the temperature (Adapted from EN 1993-1-2 (2005), figure 3.5)

3.2 Special features of aluminium

3.2.1 Vibration

As mentioned, aluminium has about one-third the elastic modulus/Young's modulus and material density of steel. Because of this, the eigenfrequency of similar structures in steel and aluminium will be the same (Sielski, 2007b). This can be seen from Equation 3.10 which is the ratio of the eigenfrequencies for plates in steel and aluminium:

$$\frac{f_a}{f_s} = \sqrt{\frac{E_a t_a^3 m_s}{E_s t_s^3 m_a}} = \sqrt{\frac{E_a t_a^3 \rho_s t_s}{E_s t_s^3 \rho_a t_a}} \tag{3.10}$$

Since E_a/E_s is 1/3 and ρ_s/ρ_a is 3, the frequency relation becomes:

$$\frac{f_a}{f_s} = \frac{t_a}{t_s} \tag{3.11}$$

This means the ratios of the frequencies of the plates are proportional to the thickness of the plates, and with similar structures the frequencies would be the same. However, from Sielski (2007b) is was discussed that because of the reduced strength of aluminium, the structure will have greater stiffness, and the frequency vibrations will actually be higher even though the structure is designed for the same conditions. If the structure has a large mass, the increased frequency will be offset such that the aluminium structure may have to be made stiffer to prevent vibration problems.

Sielski (2007b) also stated that aluminium might be less tolerant of vibration if in the vibration structure might exist stress concentrations that could become points of fatigue crack initiation.

3.2.2 Corrosion

The corrosion resistance is also a factor that makes aluminium alloys a competitive material to steel. Generally the marine-grade aluminium alloys have good corrosion resistance, which makes them a good choice in corrosive environments like seawater. It is, however, the weight reduction aspect of the aluminium material that is the dominating characteristic for choosing aluminium over steel hulls.

3.3 Fire resistance

From Table 3.2 it is seen that aluminium has a relatively low melting point in comparison to steel. With a blue flame, the hottest one of all, being able to reach a temperature of 1400-1650°C (Helmenstine, 2020), it is understandable that an aluminium structure must be insulated in order to protect the structure from softening or melting in a shipboard fire with a melting point of around 550°C (Sielski, 2007a). If the aluminium needs to be insulated extensively, the weight advantage of aluminium over steel will be slightly reduced and also add on the price. There exist insulation methods for aluminium with spray-on techniques which are cheaper and lighter, but these methods have, however, issues with durability in marine constructions and are generally not used (Greene, 2005; Sielski, 2007a).

Aluminium does not have a brittle transition temperature like steel does. This means that when steel get brittle and prone to breaking at low temperatures, aluminium gets tougher, stiffer and stronger. In high temperatures, on the other hand, aluminium has a thermal expansion twice as large as of steel, as seen in Table 3.2. This means aluminium will expand twice as much as steel will with the same temperature increase. The stresses caused by restrained expansions are, however, moderate because of the low modulus of elasticity (Sapa Technology, 2016).

The yield strength is also temperature-dependent. Table 3.6 shows the yield strength of various aluminium alloys subjected to elevated temperature. With increasing temperature the strength decreases substantially. The values are gathered from Aluminum Association (2005); Sielski (2007a) and are not to be used for design purposes, just to prove a point. Figure 3.9 is a graphic representation of the information in Table 3.6 for °C and yield strength in MPa, and shows that at about 200-250°C the yield strength is about halved compared to room temperature. Aluminium is, however, very much weaker when welded compared to unwelded material, and this has to be taken into account when designing hull structures in aluminium since most hull structures are welded.

Table 3.6: Yield Strength of Some Aluminium Alloys at Elevated Temperatures (Sielski, 2007a; Aluminum Association, 2005)

Temperature		Yield strength (ksi/MPa)									
°F	°C	5083-0		5086-0		5454-H32		5456-0		6061-T6	
75	25	21	145	17	115	30	205	23	160	40	275
212	100	21	145	17	115	29	200	22	150	38	260
300	150	19	130	16	110	26	180	20	140	31	215
400	205	17	115	15	105	19	130	17	115	15	105
500	260	11	75	11	75	11	75	11	75	5	34
600	315	7.5	50	7.5	50	7.5	50	7.5	50	2.7	19
700	370	4.2	29	4.2	29	4.2	29	4.2	29	1.8	12

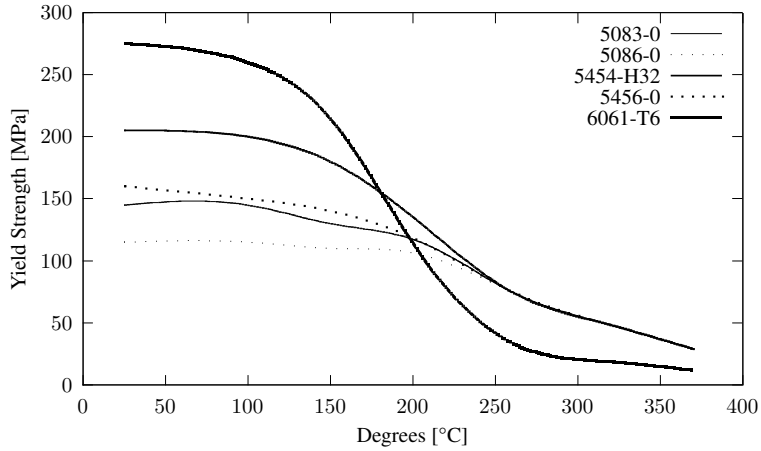

Figure 3.9: Yield strength at increasing temperatures for different aluminium alloys

3.3.1 Stress-strain conversion

Summers et al. (2015) has given the engineering stress and strain, also called nominal stress and strain, for aluminium alloy 6061-T651 at elevated temperatures, as shown in Figure 3.10. Since it is assumed that the plate and stiffeners are of the same material, i.e. the 6082 aluminium alloy, the stress-strain of the 5083 alloy will not be discussed. The material properties of the 6061-T651 alloy is the nearest equivalent grade to 6082-T6 alloy in material properties and composition according to 1st Choice Metals (n.d.), and it is therefore assumed that the stress-strain curves can be used for the 6082-T6 alloy as well.

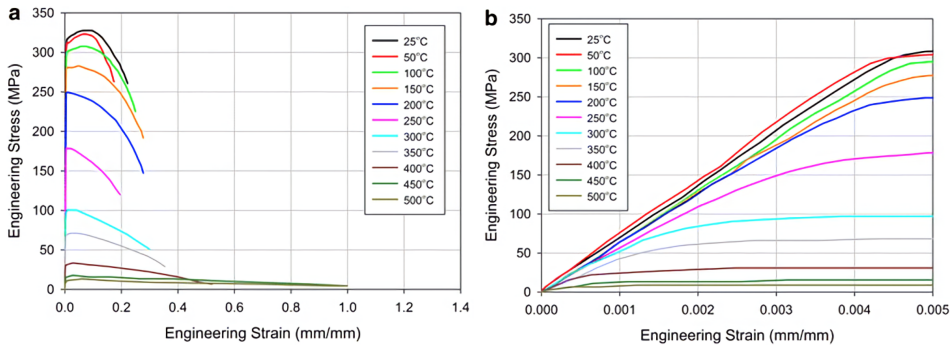

Figure 3.10: Engineering stress-strain for aluminium alloy 6061-T651 (Summers et al., 2015)

However, Abaqus uses true strain to define plasticity because materials that experience large inelastic strains yields at stress levels smaller than the magnitude of the elastic modulus of the materials, which implies true stress, or Cauchy stress and logarithmic strain (Abaqus, 2016a). This means the engineering stress-strain curve must be converted into a

true stress-strain curve. This is done by Equation 3.12 which finds the true stress (σ_t) and Equation 3.13 which finds the true logarithmic plastic strain (ε_{ln}):

$$\sigma_t = \sigma_n(1 + \varepsilon_n) \tag{3.12}$$

$$\varepsilon_{ln} = ln(1 + \varepsilon_n) - \frac{\sigma_t}{E} \tag{3.13}$$

where σ_n is the nominal or engineering stress, ε_n is the nominal or engineering strain and E is the Young's modulus. The conversion and the values for each temperatures are shown in Appendix B.

The stress-strain curves at elevated temperatures for steel are found from Ashkan (2020). He made a Matlab script which plotted the stress-strain curves at the different temperatures, based on EN 1993-1-2 (2005). He also made excel files where he had converted the nominal/engineering stress and strain values into Abaqus-friendly true stress and logarithmic plastic strain in the same way as discussed for aluminium. The excel spreadsheet from Ashkan (2020) is added in Appendix C. The nominal stress-strain curved from Matlab is shown in Figure 3.11

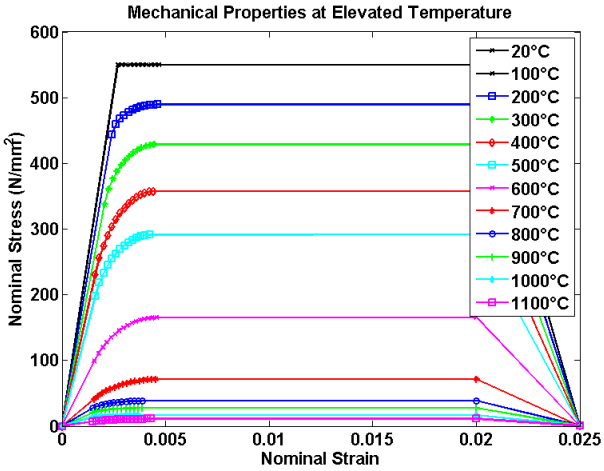

Figure 3.11: Engineering (nominal) stress-strain for steel (Ashkan, 2020)

Because the stress-strain properties are listed at intervals of 50°C for aluminium and 100°C for steel, the material properties will be assigned to the material with a temperature $\pm$ 25°C for aluminium and $\pm$ 50°C for steel. This means that if the stiffener is 67°C it should have the stress-strain properties of 50°C for aluminium and 100°C for steel.

3.3.2 Insulation

The chosen insulation material for the current ferry is the Rockwool SeaRox®FM 6000 range in the FM 6040 ALU version with A-60 standard insulation for bulkheads. This insulation is designed to optimize the speed of insulation because of its delivery on low weigh, flexible mats reinforced with alu foil on one side (Rockwool, 2017a). This type of insulation is suitable in areas where low weight is important, as it is on this aluminium passenger ferry. The material properties of the insulation is shown in Table 3.7 and the temperature dependent conductivity is shown in Table 3.8 obtained from Veillat (2018) using the low density value. It is used with 2x35mm thick plates all over the stiffener structure.

Table 3.7: Constant material properties of insulation

		SeaRox FM 6040 ALU
Density	kg/m^3	60
Specific heat	J/kg°C	840

Table 3.8: Conductivity properties of insulation

Temperature (°C)	Conductivity (W/m°C)
50	0.034
100	0.04
150	0.047
200	0.054
300	0.072
400	0.096
500	0.12
600	0.162

For standard insulation, the construction method is similar to Figure 3.12a, where the insulation comes in plate-form which is cut and placed in between the stiffener flange and the plate, while the lightweight version is placed more like Figure 3.12b since it comes on a roll. In this thesis the insulation will be modelled like Figure 3.12a to simplify the modelling

Due to the production method the insulation density may not be uniform, but since the insulation is classified, it will insulate sufficient even on the thinner parts of the material. It is also expected that large safety margins are included in the performance of the insulation.

For comparison reasons it is assumed that steel will have the Rockwool SeaRox®SL 620 A-60 bulkhead insulation (Rockwool, 2017b). It has a density of 100 kg/m^3 and is used with 60mm thick insulation on the plate structure and 25mm on the stiffener structure.

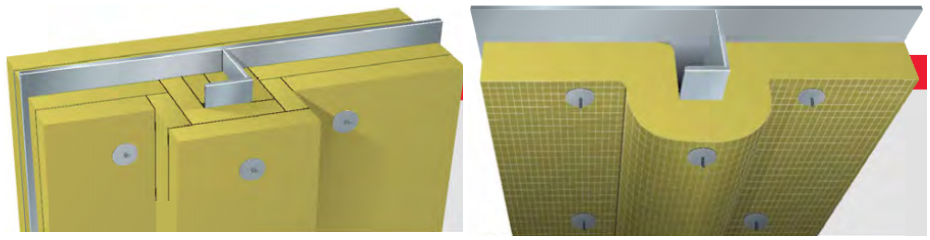

(a) Standard insulation

(b) Lightweight insulation

Figure 3.12: Construction methods for two types of insulation

Chapter 4

Rules and regulations

The ferry will be built according to DNV GL class rules and since it will fly the Norwegian Flag the relevant Norwegian Maritime Authority (NMA) regulations for passenger vessels operating in trade area 2 are to be fulfilled. Both of these regulations refer to the SOLAS regulation in their rules. Also Eurocode has some general verification methods with regards to fire resistance. A summary of the relevant rules for fire safety is discussed in the following sections.

4.1 DNV GL Rules for Classification

In DNV GL (2019) there are two definitions of battery class notations; Battery(Power) and Battery(Safety). The power notation is used where the electrical energy storage (EES) is used for electrical propulsion of the vessel, also including hybrid vessels with the main source of power based on EES. The Safety notation is for vessels where the aggregated EES installation in one EES space has a rated capacity of 20 kWh or above and not having the battery(Power) notation, i.e. where the EES power is not the main source of power. The Oslo ferries will have the battery(Power) notation, because their main propulsion systems are electric.

The fire safety for EES spaces are the same for both notations and is defined in section 2.4 of DNV GL (2019). With respect to fire integrity, the EES spaces shall be defined as a machinery space with reference to SOLAS Reg.II-2/3.30. For structural fire protection the EES spaces shall be defined as other machinery spaces, as given in SOLAS Reg.II-2/9.2.2.4 and 9.2.3 with the additional requirements that fire integrity of EES spaces shall be enclosed by A-0 fire integrity and have a A-60 fire integrity towards:

- Machinery spaces of category A as defined in SOLAS Reg.II-2/3
- Enclosed cargo areas for carriage of dangerous goods
- Muster and embarkation stations for passenger vessels.

The battery room is therefore protected against fire in hazardous spaced, and it is assumed that a fire in the battery room is unlikely. The access to the space shall be through normally closed doors with alarm or self-closing doors.

EES spaces should also have fire detection and fire extinguishing. The spaces shall be monitored by conventional smoke detection complying with the internal code for fire safety systems (FFS code). The alarm shall be given at the bridge, also complying with the FSS code. The extinguishing system shall be of a fixed total-flooding kind, approved for use in machinery spaces of category A as given in SOLAS Reg.II-2/10 and the FSS code.

4.2 Norwegian Maritime Authority

Under paragraph 4 of the Norwegian Maritime Authority (2014) regulations for passenger and cargo ships: fire protection on ships in domestic trade area, the rules from SOLAS Reg.II-2/5.3, 9.2.2 and 11 does not apply for domestic passenger ships which has:

1. Steel or equivalent material in bulkhead and deck dividing living areas from machine- and cargo rooms
2. Steel or equivalent material in bulkhead and decks in galley, painting room, lamp room, luggage-, mail- and storage room adjacent to the interior and doors to these rooms, except around galleys where hot food is not prepared
3. All stairs built on steel foundation
4. Class B division in bulkheads where there is no demand of steel or equivalent material
5. Exhaust and smoke outtake arranged such that the temperature does not cause any danger of ignition

And a ship with gross tonnage 300 or more should also have:

1. Closed stairwells of class A-30 from the deck the stair begins to the deck for embarkation of lifeboats
2. Non flammable corridor bulkheads which goes from deck to deck and all the way out to the ship-side

3. Roof plates with non flammable material in corridor and stairwells.

This means that the references made to SOLAS Reg.II-2/9.2.2.4 in the DNV GL rules can be ignored if the ship fulfils the requirements of the NMA above.

4.3 SOLAS

SOLAS Reg.II-2/3.30, (International Maritime Organization, 2014) states that machinery spaces are machinery spaces of category A and other spaces containing propulsion machinery, generators and major electrical machinery, oil filling stations etc., where machinery spaces of category A are those spaces and trunks to such spaces which contain:

1. Internal-combustion machinery used for main propulsion
2. Internal-combustion machinery used for purposes other than main propulsion where such machinery has in the aggregate a total power output of not less than 375 kW or
3. Any oil–fired boiler or fuel unit

The SOLAS Reg.II-2/9.2.2.4 determines the methods of protection in passenger ships, but is ignored due to the exception in Norwegian Maritime Authority (2014). The SOLAS Reg.II-2/9.2.3, however, is also ignored in this case because it determines the methods of protection in cargo ships. Cargo ships is not relevant for this thesis that focuses on a passenger ferry. Thus, the rules from DNV GL determines the fire integrity of the enclosed spaces around the battery room.

SOLAS Reg.II-2/10 has the purpose to suppress and swiftly extinguish a fire in the space of origin. This requirement assures that fixed fire-extinguishing systems shall be installed and having due regard to the fire growth potential of the protected spaces and that the fire-extinguishing appliances shall be readily available. The regulation specifies, inter alia, the water supply systems, fire pumps, portable and fixed fire extinguishers etc. The suppression of fire will, however, not be discussed further in this thesis.

As stated in the DNV GL rules, the battery room should be enclosed by either A-0 or A-60 fire integrity. The A-class divisions are defined in International Maritime Organization (2014) as divisions formed by bulkheads and decks which comply with the following criteria:

- They are constructed of steel or other equivalent material;
- They are suitably stiffened;

- They are insulated with approved non-combustible materials such that the average temperature of the unexposed side will not rise more than 140°C above the original temperature, nor will the temperature, at any one point, including a joint, rise more than 180°C above the original temperature within the time listed below:

Class "A-60"	60 min
Class "A-30"	30 min
Class "A-15"	15 min
Class "A-0"	0 min

- They are so constructed as to be capable of preventing the passage of smoke and flame to the end of one-hour standard fire test; and
- The Administration required a test of a prototype bulkhead in accordance with the Fire Test Procedures Code to ensure that it meets the above requirements for integrity and temperature rise.

Where steel or other equivalent material means any non-combustible material which, by itself or due to insulation provided, has structural and integrity properties equivalent to steel at the end of the applicable exposure to the standard fire test (e.g. aluminium alloy with appropriate insulation).

A standard fire test is a test in which specimens of the relevant bulkheads or decks are exposed in a test furnace to temperatures corresponding approximately to the standard time-temperature curve in accordance with the test method specified in the Fire Test Procedures Code. The Fire Test Procedures Code is the International Code for Application of Fire Test Procedures as adopted by the Maritime Safety Committee of the Organization by resolution MSC.307(8).

However, as mentioned in Section 1.2, the specification states that the entire battery room should be insulated with A-60 standard. It is therefore further assumed that this will overrule the regulations because it is a stricter requirement.

4.4 Eurocode

Eurocode has defined three domains of which a design check, as discussed in Section 1.6, should be performed to verify the fire resistance (EN 1991-1-2, 1995).

1. Time domain: $t_{fi,d} \geq t_{fi,requ}$ where $t_{fi,d}$ is the design value of the fire resistance and $t_{fi,requ}$ is the required fire resistance time
2. Strength domain: $R_{fi,d,t} \geq E_{fi,d,t}$ where $R_{fi,d,t}$ is the design value of the resistance of the member in the fire situation at time *t* and $E_{fi,d,t}$ is the design value of the relevant effects of actions in the fire situation at time *t*

3. Temperature domain: $\Theta_d \leq \Theta_{cr,d}$ where Θ_d is the design value of the temperature and $\Theta_{cr,d}$ is the design value of the critical material temperature

In this thesis all three of the domains will be checked. The time domain because of the A-60 requirements as discussed in Section 4.3, the strength domain because the critical buckling load must be found and the temperature domain because of the SOLAS regulations that the average temperature of the unexposed side will not rise more than 140°C above the original temperature.

Vassart et al. (2014) have stated that there are three design approaches for finding the mechanical response of structures in fire; global structure analysis, analysis of parts of the structure of member analysis. The global analysis considers the whole structure, the part analysis will have appropriate boundary conditions linking the part to the global structure, and a member analysis will assess a member separated from the rest of the structure, which will be replaced by the corresponding boundary conditions.

Depending on what approach is relevant, the mechanical response is calculated differently. For analyses with multiple members, i.e. the global or part analysis, interaction effects like load distribution from heated, weakened parts inside the fire compartment to stronger, cold parts outside must be taken into account. These approaches give more realistic mechanical response in fire, however, they require advanced calculation methods. The member analysis is applied to a single member isolated from the rest of the structure, which makes it easy to use with simplified calculation methods. The standard temperature-time curve is largely used for this method. There exists other temperature-time curves, for instance the hydro-carbon curve, but this is mostly relevant on oil platforms. Since this thesis will assess a single member, the standard temperature-time curve will be used as the fire-curve further in this thesis. The standard fire curve is described with Equation 4.1 and illustrated in Figure 4.1, where Θ_g is the gas temperature and t is the time in minutes (EN 1999-1-2, 2007).

$$\Theta_g = 20 + 345 \cdot log_{10}(8t + 1) \tag{4.1}$$

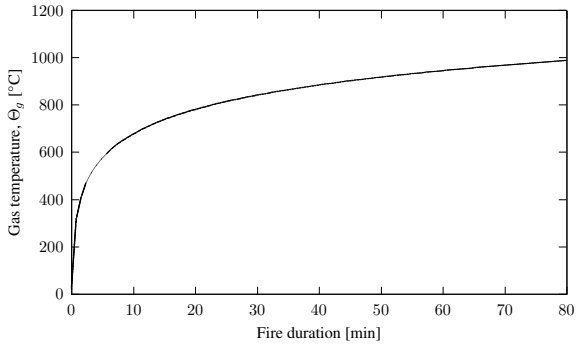

Figure 4.1: Standard fire curve

4.4.1 Heat transfer

The heat transfer is also defined in EN 1999-1-2 (2007), which must be calculated to find the capacity of members in a structure. This is defined for two cases; for unprotected internal aluminium members or internal aluminium structures insulated by fire protection material. The heat transfer with an increase of temperature $\Delta\theta_{al(t)}$ in a member during a time interval Δt is found with the heat transfer equations for the respective cases. For an unprotected internal aluminium member the heat transfer equation is:

$$\Delta\theta_{al(t)} = k_{sh}\frac{A_m/V}{c_{al}\rho_{al}}\dot{h}_{net}\Delta t \tag{4.2}$$

The section factor for unprotected aluminium members A_m/V [m^{-1}] is the ratio between "perimeter through which heat is transferred to aluminium and aluminium volume" (Bin, 2012). A_m is the surface area per unit length and V is the volume per unit length. $(\mathrm{A}_m/\mathrm{v})_b$ is the box value, a derivation of the section factor.

The correction factor for shadow effect k_{sh} takes into account the local shielding from radiative heat transfer due to the shape of a profile. Ignoring the shadow effect and setting the factor equal to one will give conservative solutions. The shadow correction factor is calculated with the following formulas:

$$k_{sh} = \begin{cases} 0.9\frac{(A_m/V)_b}{A_m/V} & \textit{for I-sections} \\ \frac{(A_m/V)_b}{A_m/V} \leq 1.0 & \textit{for all other cases} \end{cases} \tag{4.3}$$

The specific heat of aluminium c_{al} is as defined by Equation 3.3.

The aluminium density ρ_{al} is defined in Table 3.2 as 2660 kg/m^3 for the 5083 alloy and 2700 kg/m^3 for the 6082 alloy.

The net heat flux per unit area $\dot{h}_{net}$ is referenced to a different part of the Eurocode rules, EN 1991-1-2 (1995), and is defined as an iterative process as the sum of heat transfer by convection and radiation:

$$\dot{h}_{net} = \dot{h}_{net,c} + \dot{h}_{net,r} \quad (W/m^2) \tag{4.4}$$

.

The net convective heat flux component is determined by:

$$\dot{h}_{net,c} = \alpha_c \cdot (\Theta_g - \Theta_m) \quad (W/m^2) \tag{4.5}$$

where α_c [W/m^{2}K] is the coefficient of heat transfer by convection, Θ_g [°C] is the gas temperature in the vicinity of the fire exposed member and Θ_m [°C] is the surface temperature of the member. Since a standard temperature-time curve, which represents a model of a fully developed fire in a compartment, is assumed, the gas temperature of the fire exposed member Θ_g is given by Equation 4.1 and Figure 4.1

The net radiative heat flux component per unit surface area is determined by:

$$\dot{h}_{net,r} = \Phi \cdot \varepsilon_m \cdot \varepsilon_f \cdot \sigma \cdot [(\Theta_r + 273)^4 - (\Theta_m + 273)^4] \quad (W/m^2) \tag{4.6}$$

Where Φ is the configuration factor ε_m is the surface emissivity of the member, ε_f is the emissivity of the fire, σ is the Stephan Boltzmann constant equal to 5.67·10^{-8} (W/m^{2}K^4), Θ_r [°C] is the effective radiation temperature of the fire environment, and Θ_m [°C] is the surface temperature of the member. By assuming the member is fully fire engulfed, Θ_r is equal to the gas temperature Θ_g. From EN 1999-1-2 (2007), ε_f should be 1 and ε_m should be 0.7.

Chapter 5

Applied Software

5.1 Abaqus CAE

Abaqus is a finite element based program for computer-aided engineering. The program can be used for both modelling and analysis of mechanical components as well as visualisation. The program is, according to Abaqus (2016c), used to solve a wide range of engineering problems due to its capabilities for simulation of both linear and nonlinear problem. Its extensive element and material library gives Abaqus endless modelling possibilities. Three main analysis products make up the program - Abaqus/Standard, Abaqus/Explicit and Abaqus/CFD, where Abaqus/CAE is the interactive, graphical environment for Abaqus. Abaqus/Standard in version 2016 will be used in this thesis since it solves linear and nonlinear problems, including thermal response of components.

The program is divided into modules which gives the modelling process a logical aspect. A complete analysis consists of three distinct stages where the modules are involved: Pre-processing, simulation and post-processing. Figure 5.1 shows how the stages are linked together.

Pre-processing

In the pre-processing stage the model is defined of the physical problem and created in an Abaqus input file. The model is usually defined in Abaqus CAE, but for simple analyses the input file can be created in a text editor. In this stage the geometrical model and material model is created. Loads and boundary conditions are also applied to correctly represent the reality, and the model needs to be meshed.

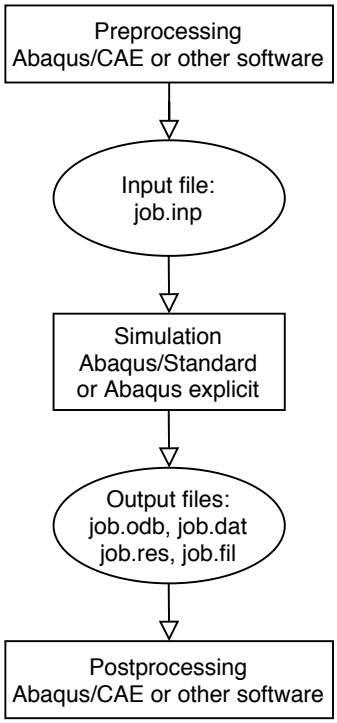

Figure 5.1: ABAQUS stages for simulation (Abaqus, 2016c)

Simulation

The simulation stage is where Abaqus/Standard or Abaqus/Explicit solves the defined numerical problem. Here the desired outputs are defined, where output variables like stresses and displacements and more can be chosen. This stage can take anywhere from seconds to days to complete, depending on the complexity, mesh and computer power.

Post-processing

The post-processing stage is where the results of the completed simulation stage with its calculated displacements, stresses or other variables, can be evaluated. The results can be displayed in the visualization module with a variety of possibilities to display the results like color contour plots, animations and deformed shape plots. The data can also be extracted with x-y data which can be transformed into excel spreadsheets for further calculation.

5.2 Analysis procedure

From the literature discussed in Section 1.4, it was clear that a sequentially coupled thermal-stress analysis was the most used method for calculating thermal response of structures. Most of the articles also used quite simple models, such as a plate or similar, and most only did static stress analyses. The goal of this thesis is to analyse the buckling behavior of hull structures subjected to fire. It is, however, not possible to perform a buckling analysis with a predefined field from a user-specified file in the available analysis program, Abaqus, according to Abaqus (2006a), and therefore a method of performing buckling analysis while including temperature effects has to be invented.

The method is based on the idea that when a structure is heated, it will not have uniform temperature distribution throughout its cross-section. With the knowledge that the material properties change with temperature, a method of dividing the structure into little pieces and assigning material properties corresponding to their temperature was created. This gives the possibility to include the temperature distribution in more advanced structures, and also to perform buckling analyses with temperature effects. The division of the aluminium stiffener is shown in Figure 7.6 and discussed further in Section 7.2.2.

The analysis will be done in three steps:

1. Heat transfer analysis
2. Linear buckling analysis
3. Nonlinear buckling analysis

The heat transfer analysis will give the temperature distributions of the structure. Then a linear buckling analysis will be performed with a model divided into smaller pieces and assigned the corresponding material properties to the temperatures found in the heat transfer analysis. The linear buckling analysis uses elastic material properties and will find eigenmodes and eigenvalues of the structure. The eigenmodes and eigenvalues are then used as a basis for imperfections and initial load for the nonlinear buckling analysis which uses both elastic and plastic material properties.

Since the objective is to see how load bearing structures behave during fire, especially focusing on the battery room, a typical stiffener of a bulkhead will be considered for the analyses. Analyses will be performed for both aluminium and steel for comparison reasons, but the main focus will be on the aluminium stiffener. A plate with multiple aluminium stiffeners will also be analysed to validate the response when the stiffeners are a part of the bulkhead. The dimensions of the stiffeners are shown in Figure 5.2 and Table 5.1. Typically aluminium bulkheads have a stiffener spacing of 0.25m and steel bulkheads have typically 0.5m stiffener spacing. With respect to design, the thickness of the plates in steel and aluminium usually are the same, but because aluminium is a weaker material due to its Young's modulus, the stiffeners have to be closer to maintain the same strength as for steel. This is the reason of the dimensions being different.

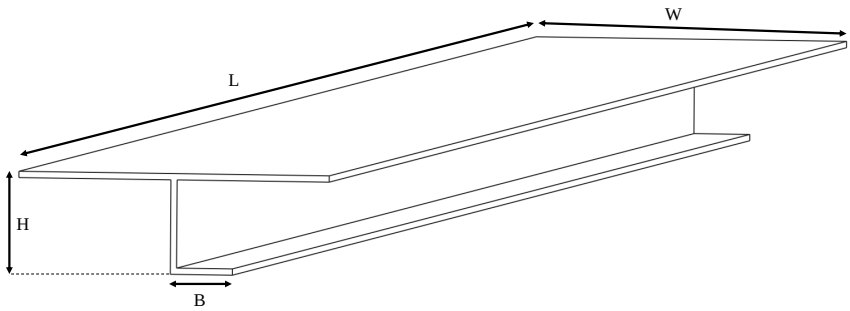

Figure 5.2: Stiffener dimension notations

Table 5.1: Stiffener dimensions

Material	L	W	H	B	t
Aluminium	2.4m	0.25m	0.075m	0.05m	0.005m
Steel	2.4m	0.5m	0.075m	0.05m	0.005m

As a parametric study the temperature will be added on different sides of the stiffener, either the stiffener side or the plate side. How the temperature will affect the stiffener is shown in Figure 5.3, where it is assumed that the underside of the stiffener flange is not affected by convection and radiation. This will be further discussed in Chapter 6. Analyses with insulation on different sides will also be performed to see how the insulation affects the heat transfer to the material and thereby the strength. The following cases will be considered:

1. Aluminium stiffener in room temperature
2. Aluminium stiffener with fire on plate side without insulation, at around 500°C
3. Aluminium stiffener with fire on stiffener side without insulation, at around 500°C
4. Aluminium stiffener with fire on plate side with insulation after 60 minutes
5. Aluminium stiffener with fire on stiffener side with insulation after 60 minutes
6. Steel stiffener in room temperature
7. Steel stiffener with fire on plate side without insulation
8. Plate consisting of multiple stiffeners in room temperature

The heat transfer analysis is discussed further in detail in Chapter 6 and the buckling analyses are discussed in Chapter 7. The next chapters will assess how the analysis procedure is performed in Abaqus and discuss the theory of the different type of analyses.

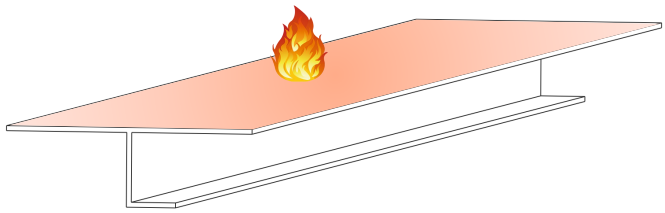

(a) Fire on plate side

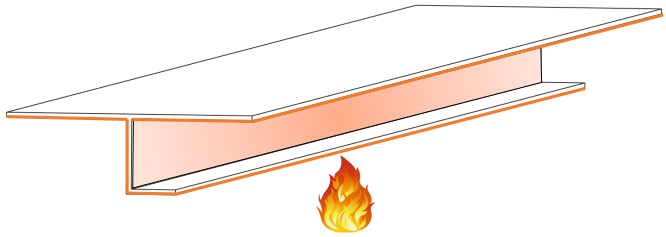

(b) Fire on stiffenerside

Figure 5.3: Fire scenarios

5.2.1 Assumptions

- The thickness is the same throughout the stiffener, i.e. 5mm
- The whole stiffener is assumed to be of the 6082 aluminium alloy, instead of separating the material between plate and stiffeners, as mentioned in Section 3.1.1 due to similar material properties and simplification of the model
- The underside of the flange is assumed not to be affected by fire on the stiffener side

5.3 Element formulation

Abaqus has, as mentioned, an extensive element library where each element has its own unique name. The behavior of the elements are characterized by five aspects: family, degrees of freedom, number of nodes, formulation and integration. In this thesis the element DC3D20, a 20-node quadratic heat transfer brick element will be used for the heat transfer analysis and the element S4R, a 4-node doubly curved thin or thick shell element with reduced integration, hourglass control and finite membrane strain will be used for the buckling analysis.

5.3.1 Brick element - DC3D20

The family of the DC3D20 element is the continuum (solid) element family and has only temperature as degrees of freedom. This 3D element is representing a 20-node quadratic brick with 3x3x3 integration points with full integration as shown in Figure 5.4. The element is well suited for heat transfer analysis which does not take stresses into account, and at the same time it gives accurate results due to the number of nodes and the full integration method.

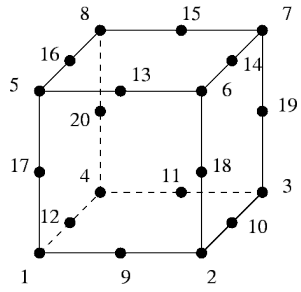

Figure 5.4: Twenty-node brick element (Abaqus, 2016c)

5.3.2 Shell element - S4R

The S4R element belongs to the shell element family and has six degrees of freedom at each of the four nodes, x-, y-, and z translation and rotation about the x-, y- and z-axis as shown in Figure 5.5. It is a general-purpose conventional shell element which allows transverse shear deformation. This means it will use thick shell theory as the shell thickness increases and become discrete Kirchoff thin shell elements as the thickness decreases, i.e. the transverse shear deformation decreases with the shell thickness. The element uses reduced integration which will reduce calculation time. It is suitable for buckling behavior because of its many degrees of freedom, its double-curve properties and since is allows for transverse shear deformation (Ellobody, 2014).

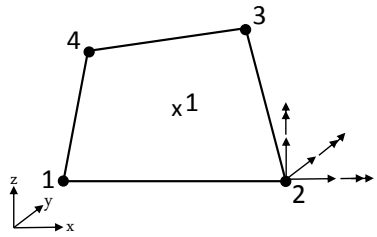

Figure 5.5: Four-node shell element with 6 DOF

Chapter 6

Heat Transfer Analysis

A heat transfer analysis calculates the temperature of the nodes after heating in the form of temperature-dependent conductivity, convection and radiation. In this thesis the nodal temperatures are calculated after being exposed to one-sided heating by fire on either the plate-side or the stiffener-side, with and without insulation. As discussed, most previous articles performed a sequentially coupled thermal analysis, but in Abaqus temperatures and field variables cannot be read from a user-specified file in a modified Riks static analysis step, i.e. the buckling step (Abaqus, 2006b). Because of this, a new method was conducted and the heat transfer analysis was uncoupled in order to get the temperature distribution in the material, and a separate buckling analysis was done with the material properties according to the corresponding temperature in different parts of the stiffener. The temperature was modelled with convection and radiation with an amplitude equal to the ISO fire curve in Figure 4.1, and the heat flow between the stiffener and the insulation was modelled with conduction. This will be discussed further below.

6.1 Modelling

6.1.1 Mesh

For the heat transfer analysis solid brick elements of the type DC3D20 was used, as discussed in Section 5.3.1, because of their heat transfer capabilities and the accurate results. It was found easier to use solid elements rather than shell elements because they had more points to interpolate the temperature and thus get more accurate results. The stiffener was meshed with a seed size of 0.005, i.e. the thickness of the stiffener, while the insulation was modelled with a coarser mesh, firstly to decrease calculation time and secondly because

the temperature distribution of the stiffener was more important than in the insulation. A summary of the meshes used is shown in Table 6.1 and Figure 6.1 shows the mesh of the stiffener with insulation on the plate side and the stiffener side. As seen from the figures, the mesh on the insulation on the stiffener side might not be optimal due to the distortion of the elements. This could have been fixed with smaller mesh size, but that would lead to long computational time, and again, the temperature distribution in the stiffener was the most important.

Table 6.1: Mesh sizes in the heat transfer analysis

Part	Mesh size [mm]
Stiffener	0.005
Insulation	0.03

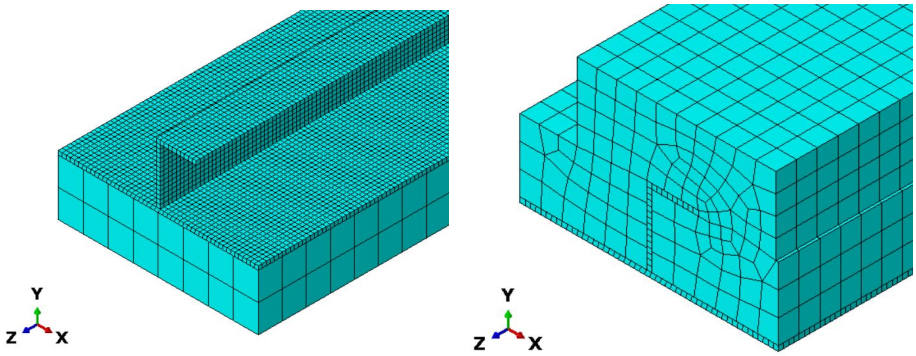

(a) Mesh on plateside

(b) Mesh on stiffenerside

Figure 6.1: Mesh for insulated stiffener in heat transfer analysis

6.1.2 Heat transfer step

For the analysis, a heat transfer step was created for a time period of 3600 seconds, or 60 minutes, which is the requirement for an A-60 classed bulkhead as discussed in Chapter 4. The maximum number of increments was increased so that the analysis would find a solution in each time step. The increment sizes was set to begin with 0.01 with a minimum of $1{\cdot}10^{-6}$ and the maximum of 3600. This means that if the analysis did not find any change in temperature during the 3600 seconds, it would stop. A predefined field was also added in the initial step to be 20°C.

6.1.3 Material model

For the heat transfer analysis conductivity, expansion coefficient, specific heat and density had to be defined. Because an uncoupled heat transfer analysis is used, no elastic

or plastic properties are defined because the analysis does not consider mechanical response. The conductivity and specific heat are used according to Eurocode, as discussed in Section 3.1.1 and Section 3.1.2. The densities, defined in Table 3.2 as 2700 kg/m^3 for aluminium and 7800 kg/m^3 for steel, are included because the specific heat is dependent on the density. The expansion coefficient is found in the same table to be $24{\cdot}10^{-6}$ for aluminium and $12{\cdot}10^{-6}$.

6.2 Convection

Convection is a type of heat transfer in which a heated fluid, such as air or liquid carries the thermal energy when it travels away from the source (Machine Design, 2015). This means the air around a fire can be heated and move the heat from one place to another, from the air around a fire source to the stiffeners in a battery room of a ferry.

In Abaqus convection is defined by a surface film coefficient and a sink temperature. These are defined as interactions and placed where it is assumed the model will experience convection. The film coefficient, also called heat transfer coefficient, is assumed to be 25 for both materials, which is in the same order of magnitude as the research done by Khalif & Mousawi (2016). The coefficient is based on assumptions due to the lack of data. The sink temperature is set to one because it is multiplied with the amplitude of the ISO fire curve. Figure 6.2 shows the placement of the convection and radiation on uninsulated and insulated stiffeners.

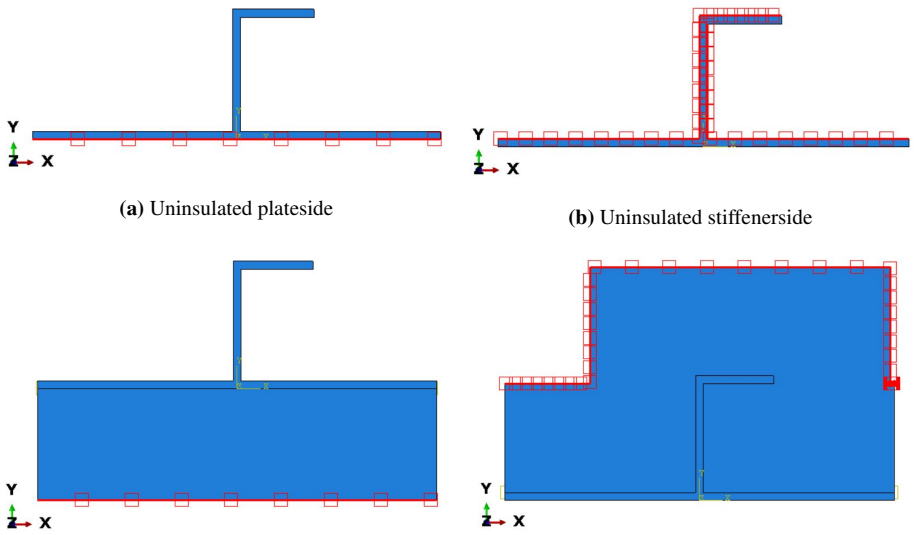

(a) Uninsulated plateside

(b) Uninsulated stiffenerside

(c) Insulated plateside

(d) Insulated stiffenerside

Figure 6.2: Radiation and convection placements in Abaqus

6.3 Radiation

Thermal radiation is heat moving away from an object due to the emission of electromagnetic waves. It is the direct result of random movements of atoms and molecules in matter. The radiation will increase with how hot an object is (Machine Design, 2015). The thermal radiation is calculated using the Stefan-Boltzmanns constant which is $5.67{\cdot}10^{-8}$ and it is therefore important to define this constant in the attributes of Abaqus.

For the interaction of radiation in Abaqus the emissivity and ambient temperature must be defined in addition to the ambient temperature amplitude. According to EN 1999-1-2 (2007) the emissivity of aluminium is to be taken as 0.7 and the ambient temperature is set to 1 because this is multiplied with the amplitude, which is the amplitude of the fire curve also in this case. The same values are used for steel, according to EN 1993-1-2 (2005). The radiation is placed on the model at the same surfaces as the convection, this is shown in Figure 6.2 for the different cases.

6.4 Conduction

Conduction is the most common form of heat transfer which transfers via direct molecular collision, or on other words, physical contact between objects of different temperature (Machine Design, 2015). Warmer surfaces has higher kinetic energy and will transfer the thermal energy with colder, lower kinetic energy surfaces.

The conduction is defined as a contact property between the insulation and the stiffener in Abaqus. The interaction property between the insulation and the stiffener use a surface-to-surface contact property where the master and slave surfaces must be defined. For a hard contact, the nodes are constrained to not penetrate the other surface. In master-slave contact, nodes on the slave surface cannot penetrate the segments on the master surface (Abaqus, 2016b). The following guidelines are generally used for determining master and slave surfaces:

- The larger of the two surfaces should act as the master surface
- If the surfaces are of comparable size, the surface on the stiffer body should act as the master surface
- If the surfaces are of comparable size and stiffness, the surface with the coarser mesh should act as the master surface

The insulation is therefore set to be the master surface since the insulation has coarser mesh than the stiffener and the surfaces are of similar size. The thermal conductance is set as 1000 when the clearance is zero and zero when the clearance is larger than 0.001.

This assures that the conduction will only happen between surfaces in contact, defined in Abaqus.

Chapter 7

Buckling Analysis

There are two types of buckling analysis, a linear eigenvalue buckling and a nonlinear unstable collapse/postbuckling analysis. Buckling analyses are done to find the critical buckling load, and when that happens the structure looses the ability to carry loads and collapses. This is usually shown in a load-displacement curve as in Figure 7.1, where the critical load is on the top of the curve and the rest is unstable response after buckling. It is usually considered buckling when stiff structures carries the load through axial actions rather than bending actions, like a vertical stiffener in a bulkhead as in this case.

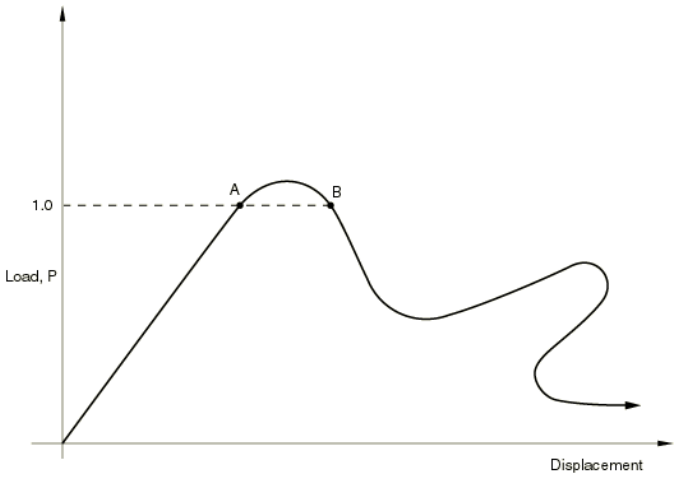

Figure 7.1: Proportional loading with unstable response (Abaqus, 2006a)

First a linear eigenvalue buckling will be performed which obtains the eigenmodes and

eigenvalues. The eigenmodes are then saved to a file which will be uploaded as imperfections in the nonlinear buckling analysis. The nonlinear buckling analysis uses the eigenvalues as loads to be sure the buckling will occur since the linear buckling analysis in most cases overpredicts the critical buckling load. The linear buckling analysis uses elastic material properties, while the nonlinear buckling considers plasticity in addition to the elastic properties. A flow chart of the buckling analysis is shown in Figure 7.2

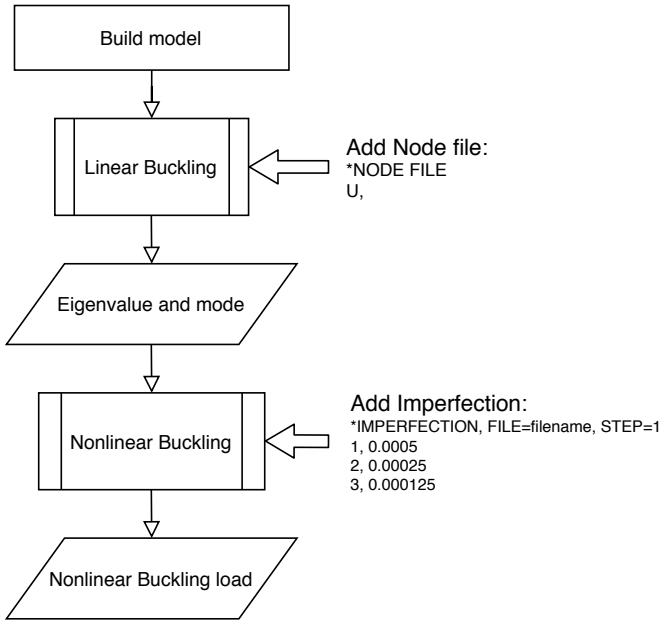

Figure 7.2: Flow chart of buckling analysis

7.1 Stiffener tripping

A type of buckling is when plate-stiffener combinations are subjected to torsional instability of the stiffener, and the stiffeners twist along heir length between the support. This is called stiffener stripping. Because of asymmetric sections such as angles are more susceptible to this type of failure because the shear center is offset from the centroid of the section, causing rotation under load. Bulb flats and flat bar stiffeners with little or no flange are also prone to tripping because of their little lateral stability (Sielski, 2007b).

Figure 7.3 shows typical shapes for plate buckling and plate buckling for weak stiffeners in addition to the local buckling of the web of the stiffener. The local buckling of the web and flange is usually not a problem for standard profiles, since they will have sufficiently large thickness-width ratio to prevent local buckling, according to Leira (2018). It is also discussed that torsion buckling of stiffeners together with associated plate flange can be

critical. The stiffener and plate induced buckling is shown in Figure 7.4. The stiffener induced buckling is where the stiffener fails on the compressive side while the displacement direction is to the tensile side of the stiffener. The plate-induced buckling implies a shift of the elastic neutral axis of the cross-section, where the plate is weaker than the stiffener.

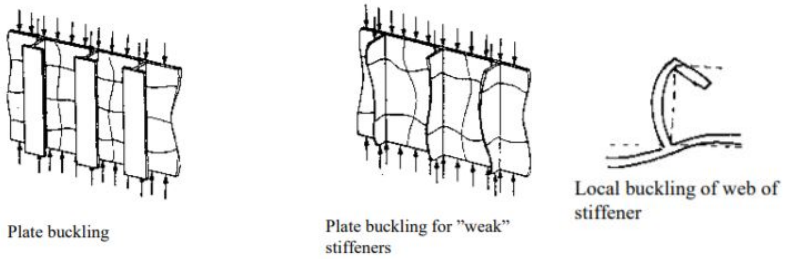

Figure 7.3: Failure modes for stiffener plate

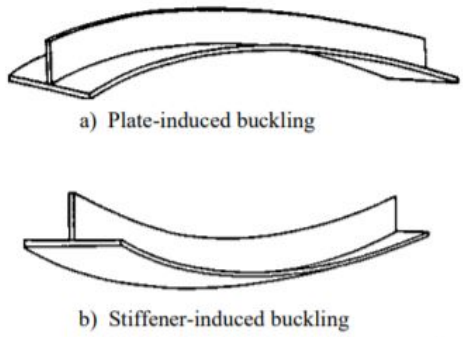

Figure 7.4: Plate induced and stiffener induced buckling

7.2 Modelling

7.2.1 Mesh

The shell element S4R was used for both of the buckling analyses. Shell elements were used due to the large deformations expected, especially for the nonlinear analysis. The mesh size was chosen to be 0.01, which was a fine enough mesh to give accurate enough results and not distortions which coarser meshes can, with relatively low computational time. The mesh of the stiffener is shown in Figure 7.5, and is the same for both aluminium and steel.

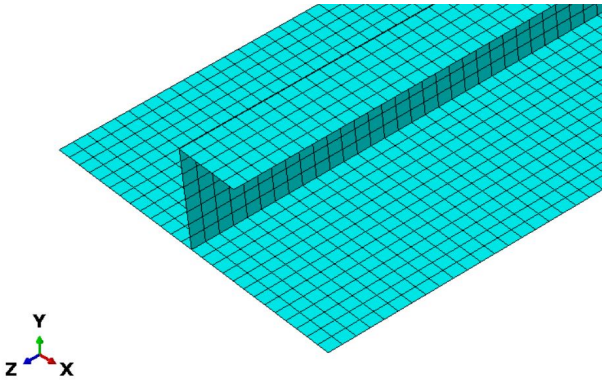

Figure 7.5: Mesh on shell buckling model

7.2.2 Material model

For the material model, the cross-section of the stiffener was divided into smaller pieces and assigned material properties corresponding to what was found in the heat transfer analysis. In this way the different material properties would simulate the temperature distribution in the material and the response. How the model is divided is shown in Figure 7.6 with the correct dimensions. The steel stiffener, however, is divided in smaller parts, which is shown in Figure 7.7. The temperatures were obtained by plotting the temperature at each node in the different parts of the structure from the heat transfer analysis. They were then noted in a spreadsheet and the corresponding material properties were calculated to the different parts. The spreadsheets are added in Appendix A.

The linear buckling analysis uses an elastic material model, while the nonlinear buckling analysis includes plasticity as well. This is discussed in detail in their respective sections.

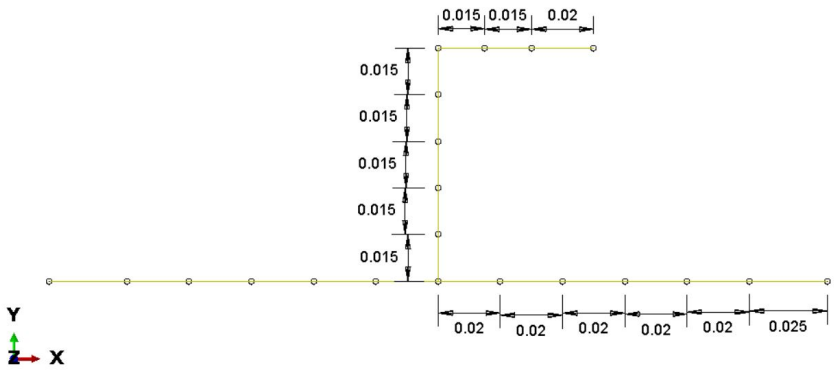

Figure 7.6: Divided model for buckling analyses in aluminium

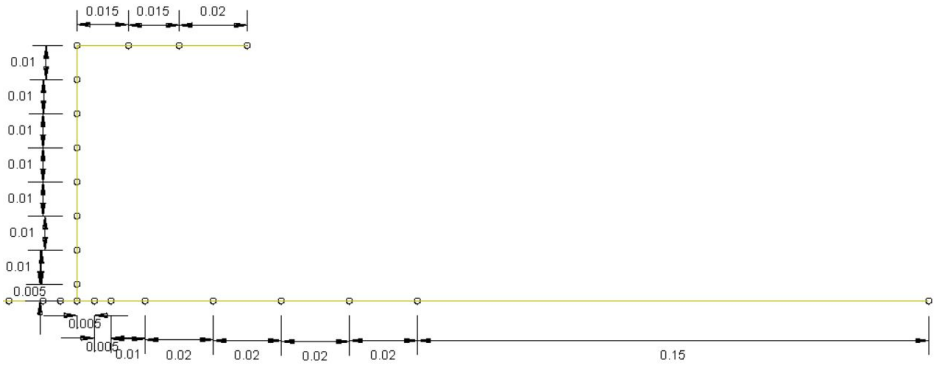

Figure 7.7: Divided model for buckling analyses in steel, showing half of the stiffener

7.2.3 Boundary conditions

In both the buckling analysis boundary conditions had to be defined. Since the model consists of a stiffener in a bulkhead, it is assumed that the bottom of the stiffener is fully clamped since the deck connected to the stiffener is stiffer than the bulkhead itself. The bottom of the stiffener is therefore held against translation and rotation in x-, y- and z direction. The top of the stiffener is also connected to the deck above, but to initiate buckling, the translation in z direction is free to move. This means the top of the stiffener is held against translation in x- and y direction and rotation in x-, y- and z direction. The boundary conditions are summarized in Table 7.1. Figure 7.8 shows the boundary conditions and the orientation of the stiffener in Abaqus, where the top-right part of the image is the bottom and the bottom-left part of the image is the top.

Table 7.1: Boundary conditions of the stiffener in the buckling analyses

	Translation	Rotation
Top	x, y	x, y, z
Bottom	x, y, z	x, y, z

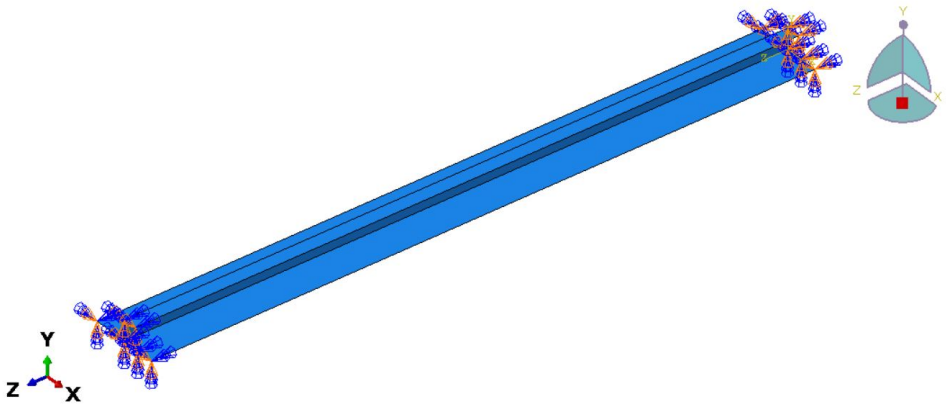

Figure 7.8: Boundary conditions of the stiffener

7.2.4 Load condition

The load condition is different in the linear and nonlinear buckling analysis, but the placement and load type is the same. The differences will be discussed further in the next sections. The load used in Abaqus is a shell edge load with the unit FL^{-1}, corresponding to N/m, placed on all edges at the top of the stiffener in the negative z direction. Figure 7.9 shows the load applied in Abaqus with the same orientation as Figure 7.8.

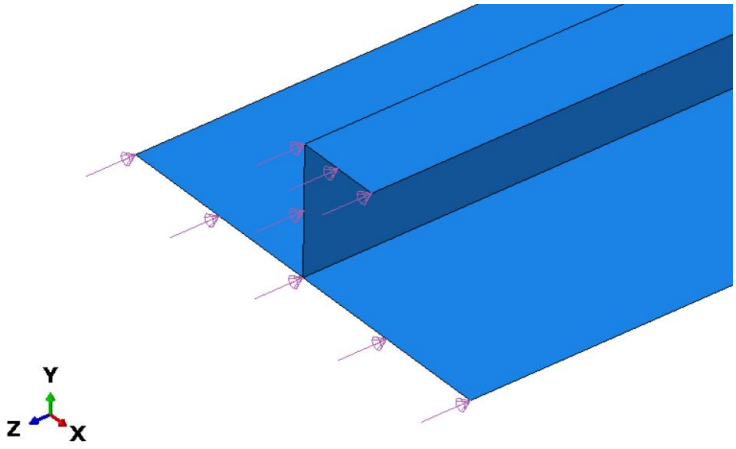

Figure 7.9: Loads on the top of the stiffener

7.3 Linear Buckling Analysis

A linear buckling analysis, or eigenvalue buckling analysis is based on the elastic and stress stiffness matrices which provides the buckling loads and buckling modes. The buckling loads are the basis for the applied load in the nonlinear buckling analysis and the buckling modes are the basis for the nonlinear imperfections. Linear analysis assumes small displacements, however, in reality, most structures will not reach the predicted critical buckling load due to imperfections and nonlinearities. This means linear buckling will over-predict the expected buckling loads and is not recommended for accurate buckling predictions (University of Alberta, 2003). The linear buckling analysis uses incremental loading to find the critical load. The load applied is therefore a unit load which means the eigenvalues obtained after the analysis are corresponding to the critical buckling load in linear theory.

7.3.1 Eigenvalue buckling problem

The eigenvalue buckling problem will in Abaqus look for loads where the model stiffness matrix becomes singular, so that the Equation 7.1 has nontrivial solutions (Abaqus, 2006a). The buckling problem is formulated as an eigenvalue problem:

$$(K_0^{MN} + \lambda_i K_\Delta^{NM}) v_i^M = 0 \tag{7.1}$$

where K_0^{MN} is the tangent stiffness matrix corresponding to the base state, which includes the effect of the preloads P^N (if any), K_Δ^{NM} is the differential initial stress and load stiffness matrix due to the incremental loading pattern Q^N, λ_i are the eigenvalues and v_i^M are the nontrivial displacement solutions. M and N refer to the degrees of freedom for the whole model and i refers to the ith buckling mode.

7.3.2 Buckling step

The linear perturbation procedure with the buckling step is where the eigenvalue problem is solved, and also where the unit load is added. There are two iteration eigenvalue extraction methods in that step, the Lanczos and the subspace. The Lanczos method is usually used when a large number of eigenmodes is required for a system with many degrees of freedom and the subspace iteration method may be faster with less than 20 eigenmodes needed. In this thesis only three eigenmodes are requested, both due to computational time and the low probabilities that the higher eigenmodes will affect the buckling shape, therefore the subspace iteration is chosen.

7.3.3 Material model

The response of an eigenvalue buckling analysis is defined by the linear elastic stiffness in the base state of the model. This means that nonlinear or inelastic material properties are ignored. The defined material model for this buckling analysis only includes the elastic properties, i.e. the Young's modulus and the Poisson ratio. The model in the buckling analyses are, as mentioned, divided into parts, and the material properties are defined according to the heat transfer analysis and the corresponding temperatures.

7.3.4 Node file

An important notice when doing a linear buckling analysis in Abaqus is to change the keywords with the following line:

**NODE FILE*
U,

This line creates a file with the eigenmodes which can be loaded in the nonlinear buckling analysis as imperfections, right where the modes on the linear model were.

7.4 Nonlinear Buckling Analysis

The nonlinear buckling analysis can analyse nonlinear geometrical problems and nonlinear material behaviour (Moan, 2003). Due to this nonlinear buckling analyses will generally provide more accurate solutions than a linear approach, which considers only small displacements and linear elastic material behavior (e.g. $\sigma = E\varepsilon$). Geometrically nonlinear static problems, which involves buckling, the load-displacement response shows a negative stiffness and in order to remain in equilibrium, the structure must release strain energy (Abaqus, 2006a). In Abaqus there are several methods for modelling static equilibrium states during the unstable phase, but in this thesis the modified Riks method will be used. This method can be used for cases where the loading is proportional, i.e. the load magnitudes are governed by a single scalar parameter

7.4.1 Riks method

The Riks method is based on the arc length method originally introduced in 1972 by Riks and Wempner. The arc length method uses a global equilibrium equation as in Equation 7.2

to define a state of proportional loading, where the loading pattern is fixed (Moan, 2003). The Riks method solves simultaneously for loads and displacements, and another quantity must be used to measure the progress of the solution; the arc length l is used along the static equilibrium path.

$$g(\lambda, r) = R_{int} - \lambda R_{ref} = 0 \tag{7.2}$$

Where R_{ref} is a fixed external load vector, R_{int} is the internal load vector and the scalar λ is a load level parameter. Abaqus uses different notation which is summarized in Table 7.2.

Table 7.2: Abaqus notation of the Riks method

Symbol	Abaqus symbol	Describtion
$g(\lambda, r)$	P_{total}	Current load magnitude
R_{int}	P_0	Dead load, any loads existing at the beginning of the step
λ	λ	Load proportionality factor
R_{ref}	P_{ref}	Reference load vector defined in the Riks step

The increments are solved by the Newton's method in Abaqus. An initial increment in arc length along the static equilibrium path Δl_{in} is defined when the step is defined. The initial load proportionality factor $\Delta\lambda_{in}$ is computed by Equation 7.3. l_{period} is a user-specified total arc length scale factor typically set to 1, and minimum and maximum arc length increments can be used to control the automatic incrementation. Table 7.3 shows the values chosen for the buckling analyses for this thesis.

$$\Delta\lambda_{in} = \frac{\Delta l_{in}}{l_{period}} \tag{7.3}$$

Table 7.3: Arc length increments

Parameter	Definition	Value
Δl_{in}	Initial arc length increment	0.01
l_{period}	Total arc length scale factor	1
Δl_{min}	Minimum arc length increment	$1{\cdot}10^{-6}$
Δl_{max}	Maximum arc length increment	$1{\cdot}10^{36}$

7.4.2 Geometric imperfections

In the Riks step it is important to include nonlinear geometry for the nonlinear buckling analysis. It is in this step the load is defined, which is the same as the eigenvalue found in the linear buckling analysis. It is also important to include geometric imperfections in a nonlinear buckling analysis. This is done by superimposing buckling modes from

the eigenvalue buckling analysis. This can be done by adding the following line to the keywords above the step-section:

**IMPERFECTION, FILE=filename, STEP=1*
1,0.0005
2,0.00025
3,0.000125

Where the filename is the name of the linear buckling analysis job. The first numbers correspond to the eigenmodes while the second numbers are scale factors and are 10% of the thickness of the structure and decreasing 50% for each mode since it is assumed that the first mode is dominating. The scale factors are of small magnitude so they do not affect the analysis

7.4.3 Material model

The material model for the nonlinear buckling analysis includes plastic properties in addition to the elastic. The plastic material model includes yield stress and plastic strain. The values used are the true stress and true logarithmic strains as discussed in Section 3.3.1 where Figure 3.10 was converted from engineering stress-strain. The values were digitized using WebPlotDigitizer as an app from google chrome. An overview of the stress-strain values for the different temperatures are shown in the spreadsheet in Appendix B. The values for steel were obtained from Ashkan (2020) as discussed in Section 3.3.1, and the values are found in Appendix C

Chapter 8

Results

In this section the results are presented. Only the most relevant cases will be discussed and a summary of the critical buckling load for all cases is shown in Table 8.1. Larger and the rest of the figures and excel sheets are added in the appendix, while program files and excel files are included in the submission of the thesis.

8.1 Heat transfer analysis

The temperature distribution for aluminium without insulation with fire on the plate side is shown in Figure 8.1 after 512 seconds, or 8.5 minutes, at about 500°C. It is seen that the stiffener and the plate has a temperature difference of more than 100°C, which will give significant differences in material properties. At 400 degrees the Young's modulus is 26 GPa, while the Young's modulus is 3.6 GPa at 500 degrees. This means the stiffener section is seven times stronger than the plate section. The temperature distribution with its corresponding Young's modulus is added in Appendix A.1.

On the other hand, the stiffener with fire on the stiffener side reaches about 500°C after only 356 seconds, or 6 minutes, i.e. 2.5 minutes earlier than when the fire is on the plate side, as shown in Figure 8.2. This is because a fire on the stiffener side will give heat transfer on both the plate, web and flange, as discussed in Section 5.2 and 6 and shown in Figure 5.3 and 6.2, while a fire on the plate side will only affect the plate. The difference in temperature is also lower, because of the more evenly distributed heat transfer. The maximum temperature is 493°C in the intersection of the web and flange, with an E-modulus of 9.3 GPa. The minimum temperature is 465°C on the plate with an E-modulus of 14.7 GPa. The stiffener section then has 63% the strength of the plate section. The temperature distribution with the corresponding Young's modulus is added in Appendix A.2

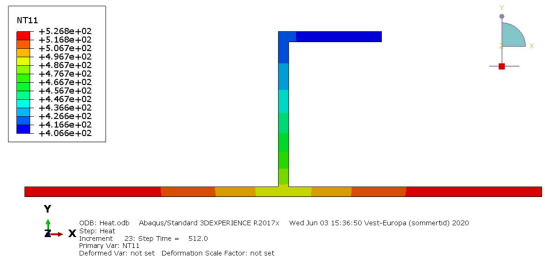

Figure 8.1: Temperature distribution for aluminium stiffener without insulation at about 500 °C with fire on plate side

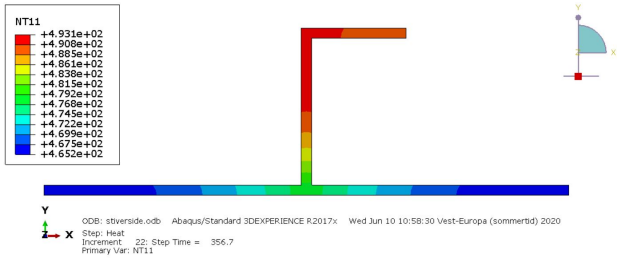

Figure 8.2: Temperature distribution for aluminium stiffener without insulation at about 500 °C with fire on stiffener side

By insulating the stiffeners the temperature in the aluminium material is reduced, and it has a more uniform temperature than without protection. Figure 8.3 shows the stiffener insulated on the plate side after 60 minutes of the standard fire. It is clear that the insulation absorbs quite a lot of the heat and slows down the process of heating the aluminium. From Appendix A.3 the temperature distribution of the stiffener is shown with the corresponding Young's modulus, where the highest temperature of the stiffener is 190°C and the lowest is 181°C. This is a difference of nine degrees and the young's modulus have a difference of 0.835 GPa. In comparison to the uninsulated stiffeners, the insulated stiffener is close to uniform heating, and will probably behave as if it was.

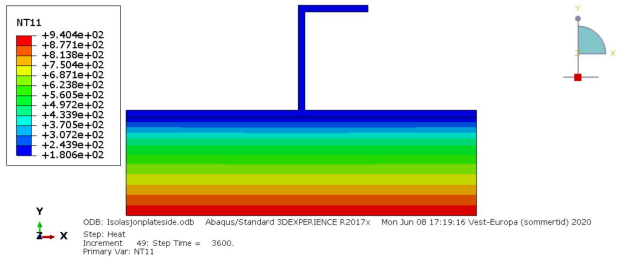

Figure 8.3: Temperature distribution for aluminium stiffener with insulation and heat on plate side after 60 minutes

The same goes for when insulating the stiffener side, as shown in Figure 8.4. The temperature difference in this case is 14°C with the maximum temperature of 194°C. This gives a difference in Young's modulus of 1.312 GPa, and like the insulation on the plate side, this is not considered a significantly different material property as of structural response.

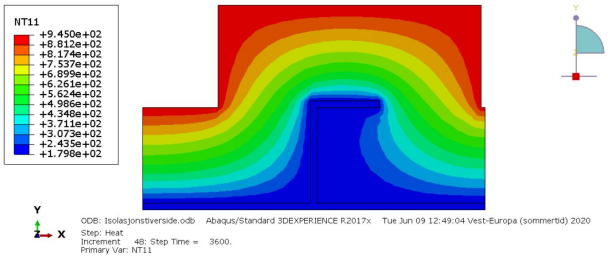

Figure 8.4: Temperature distribution for aluminium stiffener with insulation and fire on stiffener side

Steel will, however, show a much larger span of temperatures due to its low thermal conductivity and specific heat. At around 735°C the specific heat is, on the other hand, very high. The temperature varies drastically at this temperature, which is why the steel stiffener for the buckling analyses had to be divided into smaller pieces than the aluminium stiffener had. The temperature distribution is shown in Figure 8.5 and Appendix A.5 shows the distribution with the corresponding Young's modulus. The uninsulated steel stiffener shows the results after 60 minutes because it has a higher melting point, which is above the added heat, while aluminium melted at 550°C. The highest temperature of the steel stiffener is 941°C while the lowest is 700°C, a difference of 241°C. The highest Young's modulus is 43.8 GPa and the lowest is 6.54 GPa. This gives a difference in the Young's modulus of 37.27 GPa, with the plate being the weak part. Even though the steel stiffener was analysed until 60 minutes, and the uninsulated aluminium stiffener was stopped after 8.5 minutes, it is still stronger than the aluminium, where the lowest Young's modulus was 3.6 GPa. This indicates that steel has a much greater fire resistance than aluminium.

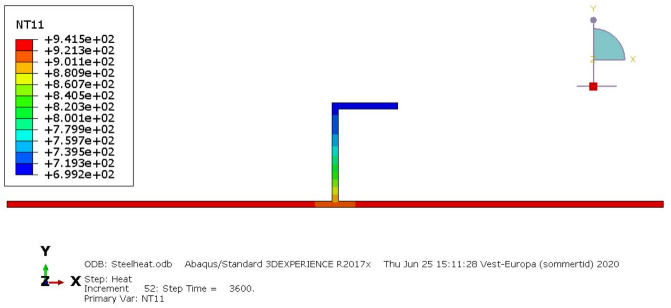

Figure 8.5: Temperature distribution for steel stiffener without insulation and fire on stiffener side after 60 minutes

8.2 Linear Buckling

8.2.1 Room temperature, steel VS aluminium

The linear buckling analysis gives the eigenmodes and eigenvalues of the stiffener, which are based on the geometry of the models. This is why a big difference in eigenmodes is seen in the aluminium stiffener in Figure 8.6 and the steel stiffener in Figure 8.7. The plate is wider on the steel model than for aluminium, but still the same thickness, which makes the plate a more vulnerable part of the structure.

Even though both stiffeners are analysed in room temperature, they obtain different eigenvalues. For mode 1 the aluminium stiffener had an eigenvalue of 304,402, while the steel stiffener in mode 1 had an eigenvalue of 253,731. This means according to linear theory that the buckling load for aluminium is higher than the buckling load for steel. Even though aluminium has a lower Young's modulus than steel, the change in plate width might have affected the strength of the steel stiffener.

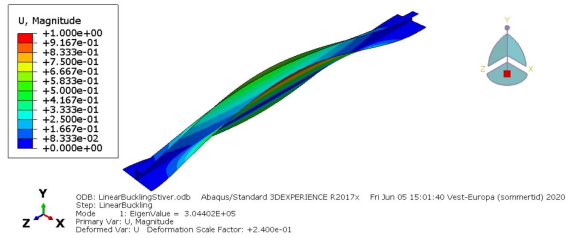

(a) Mode 1

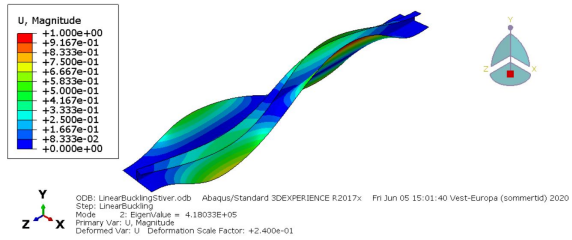

(b) Mode 2

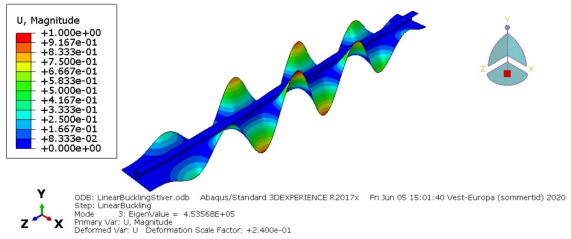

(c) Mode 3

Figure 8.6: Eigenmodes for unprotected aluminium stiffener at 20 °C

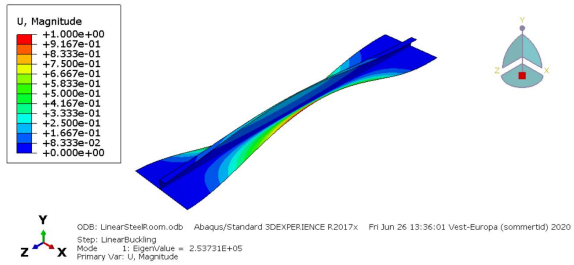

(a) Mode 1

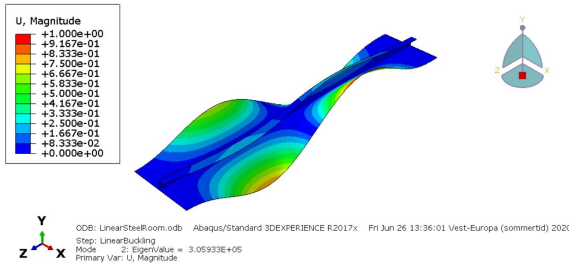

(b) Mode 2

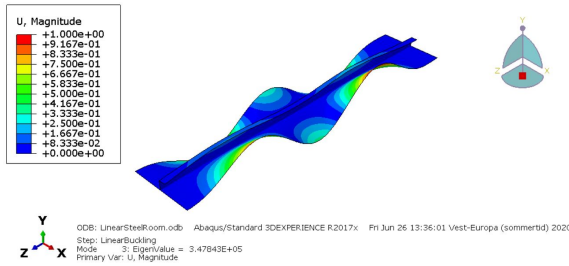

(c) Mode 3

Figure 8.7: Eigenmodes for steel stiffener in room temperature

8.2.2 Stiffeners with insulation VS room temperature

Both the stiffener with insulation on the plate side and the one on the stiffener side have the same eigenmodes as the stiffener in room temperature. Their eigenmodes can be seen in Appendix E. The stiffeners with insulation had a relative stable temperature distribution throughout the cross section, and thereby little difference in the material properties, as discussed in Section 8.1. This is why the stiffeners with insulation has the same eigenmodes as the stiffener in room temperature. The stiffeners with insulation had the eigenvalues 284,984 on the plate side and 272,412 on the stiffener side. This means the stiffener with insulated plate side is 4.6% higher critical buckling load according to linear theory. They are also between 6-11% weaker than the stiffener in room temperature, which is not a lot considering it has been exposed to fire in 60 minutes. Their critical buckling loads according to linear theory are also 7-11% stronger than the stiffener of steel in room temperature.

8.2.3 Stiffeners without insulation, plate side VS stiffener side

The aluminium stiffeners without insulation at 500°C have the most significantly different eigenmodes. The stiffener with insulation on the plate side is shown in Figure 8.8 and on the stiffener side is shown in Figure 8.9. The first modes are similar to the stiffeners in room temperature and with insulation, but at mode 2 and 3 they start getting different. This can come of two things:

1. The material is weaker in some places than others.
2. Bad discretisation of the divided stiffener and its materials, i.e. large jumps of material properties from one part to another.

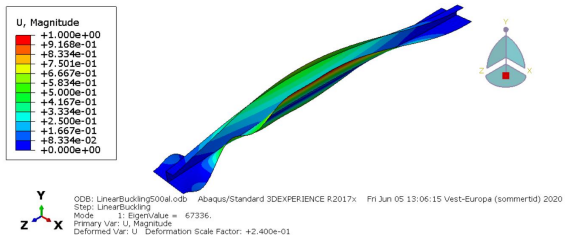

(a) Mode 1

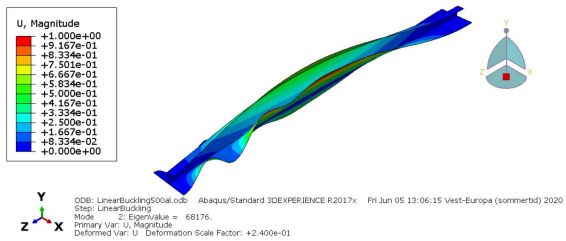

(b) Mode 2

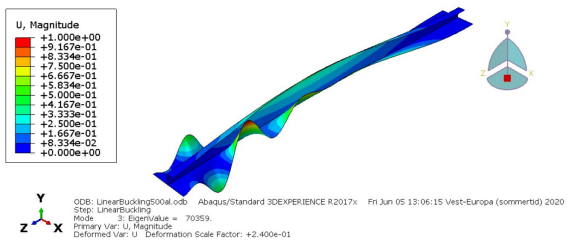

(c) Mode 3

Figure 8.8: Eigenmodes for unprotected aluminium stiffener at 500 °C on plate side

The difference from fire on the stiffener side and the plate side with respect to the 2^{nd} and 3^{rd} eigenmodes can come from that either the plate is more weak or the stiffener is more weak. The fact that the stiffener with fire on the plate side shows eigenmodes at the

top of the stiffener, while the stiffener with fire on the stiffener on the plate side, shows the stiffeners will respond differently to loads. Also, as mentioned, the stiffener with fire on the stiffener side is evaluated at an earlier time than the other stiffener. The stiffener with fire on the stiffener side therefore has a bit lower average value, and the two stiffeners might not be 100% comparable.

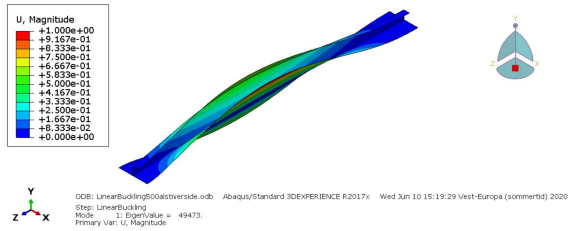

(a) Mode 1

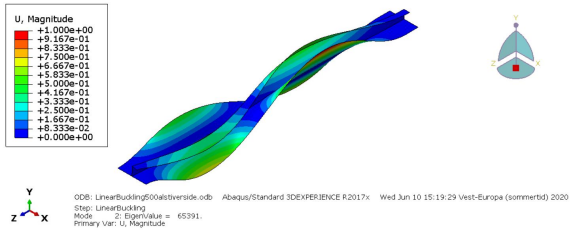

(b) Mode 2

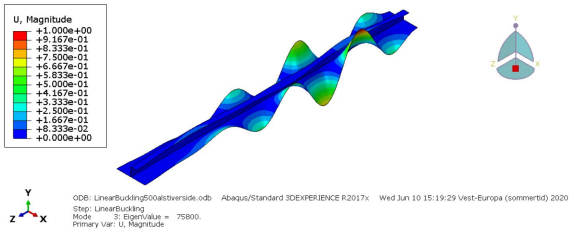

(c) Mode 3

Figure 8.9: Eigenmodes for unprotected aluminium stiffener at 500 °C stiffener side

The eigenvalues for the stiffeners with fire on the plate side and on the stiffener side are 67.336 and 49.473 respectively. This means the stiffener with the fire on the stiffener side is the weakest stiffener according to the linear theory. This makes sense because the stiffener strength is reduced substantially due to the fire, in comparison to the plate. A weakened stiffener will loose the global strength of a stiffener panel more than a weakened plate.

8.2.4 Steel stiffener with fire on plate side

The steel stiffener subjected to fire on the plate side has also some special eigenmodes, as seen in Figure 8.10. As mentioned, the temperature difference in this stiffener was 241°C, which will give a much weaker plate than stiffener. This is probably why the eigenmodes are so large on the edges of the plate and does not affect the stiffener as much. The steel stiffener after 60 minutes of fire exposure has an eigenvalue of 19,075, which is about 30% of the eigenvalue of aluminium at 500°C with fire on the plate side. This means the stiffener is weaker in terms of linear theory after 60 minutes, than the aluminium stiffener after 8.5 minutes. If compared at the same time, the steel stiffener would be considered stronger.

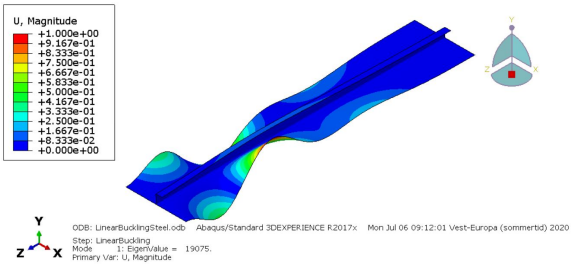

(a) Mode 1

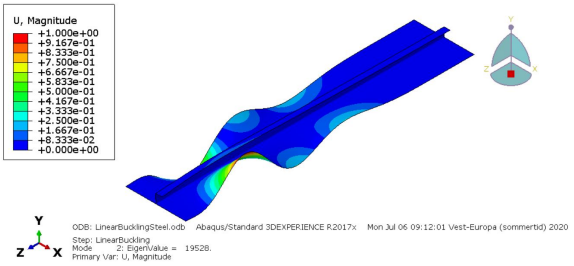

(b) Mode 2

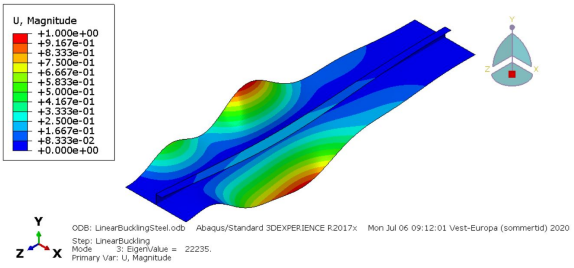

(c) Mode 3

Figure 8.10: Eigenmodes for steel stiffener in fire on plate side

8.2.5 Plate field

The plate field consisting of five stiffeners of aluminium in room temperature was evaluated for validation reasons. Since the stiffeners were only constrained on the top and bottom, it was important to check whether the responses on the plate section of the stiffeners were realistic when combined in a plate field. The eigenmodes for the plate field with stiffeners on the edges are seen in Figure 8.11. From the figure it is seen that the eigenmodes are quite similar to mode 3 of aluminium in room temperature, which might indicate that the realistic eigenvalues for the single stiffeners are the eigenvalues obtained from mode 3, and not mode 1 as assumed in this thesis. The plate field has an eigenvalue in mode 1 of 678,968, which is more than twice as large as one single aluminium stiffener in room temperature. This means that a stiffener panel is stronger than if evaluating one single stiffener. This can be because of either the geometry of the single stiffener, or the boundary conditions. Had the sides of the single stiffener been constrained such that it would simulate it being a part of a larger plate field, the stiffener might have behaved differently.

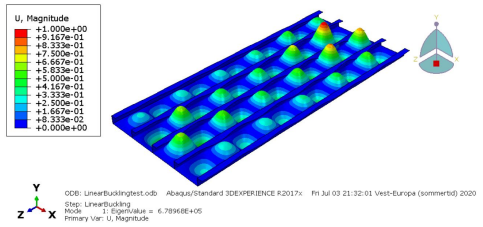

(a) Mode 1

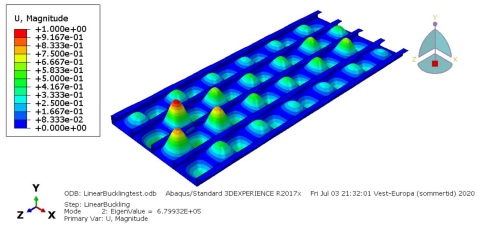

(b) Mode 2

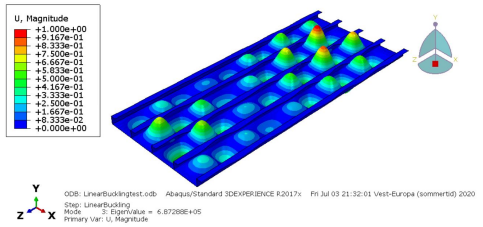

(c) Mode 3

Figure 8.11: Eigenmodes for aluminium plate field in room temperature

8.3 Nonlinear Buckling

The nonlinear buckling analysis gives the critical buckling loads, according to nonlinear theory, and shows the buckling shape of the structures. The buckling shape for an aluminium stiffener in room temperature is shown in Figure 8.12. It is seen that the stiffener buckles out in the y-direction, which indicates plate-induced buckling, i.e. the plate is weaker than the stiffener. In room temperature the eigenvalue was 304,4402 and the critical buckling load from the nonlinear analysis is 600,810. This means the linear buckling load underestimates the critical buckling load, or in other words, is very conservative.

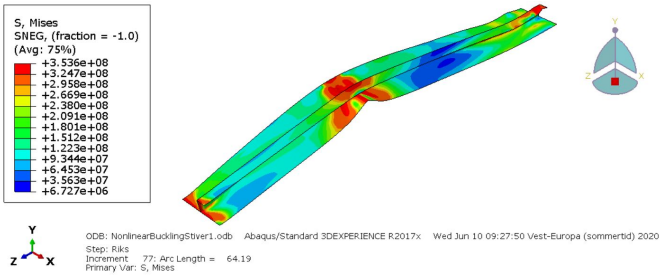

Figure 8.12: Buckling shape after critical load - aluminium room temperature

The buckling shape of the aluminium stiffener with fire on the stiffener side, however, buckled out in the negative y-direction, as seen in Figure 8.13. This indicates stiffener-induced buckling, i.e. that the stiffener is weaker than the plate. This makes sense, because the stiffener had the highest temperature in the heat transfer analysis and therefore also the lowest material properties.

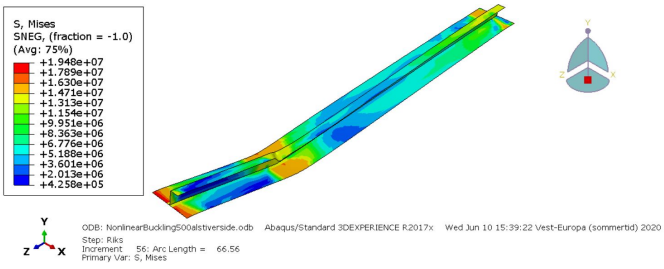

Figure 8.13: Buckling shape after critical load - uninsulated aluminium with fire on stiffener side

The stiffener with fire on the plate side is the only stiffener which has a higher eigenvalue, of 67,336, than the nonlinear critical buckling load of 47,013 N/m. This might indicate that the nonlinear properties have had a negative effect for the strength of this stiffener. The stiffener is, by all means, very weakened due to the fire and the temperature being very close to the melting point.

The steel buckling shape is quite different from the aluminium buckling shapes. While the aluminium stiffener is almost crushed and showing large displacements, the steel stiffener only contracts on the middle with a slightly case of stiffener tripping, where the stiffener bends over. This can be seen in Figure 8.14 for room temperature and in Figure 8.15 in fire on plate side.

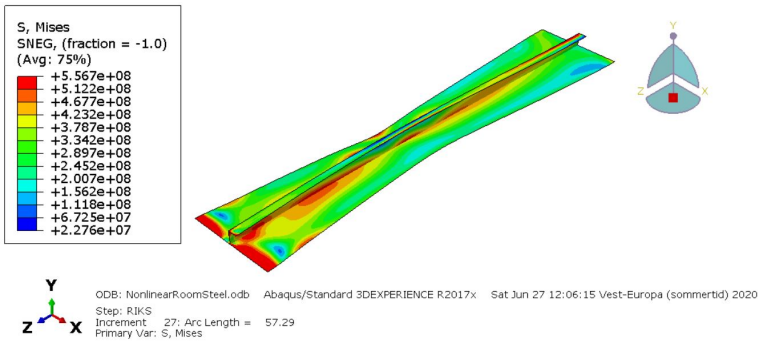

Figure 8.14: Buckling shape after critical load - Steel room temperature

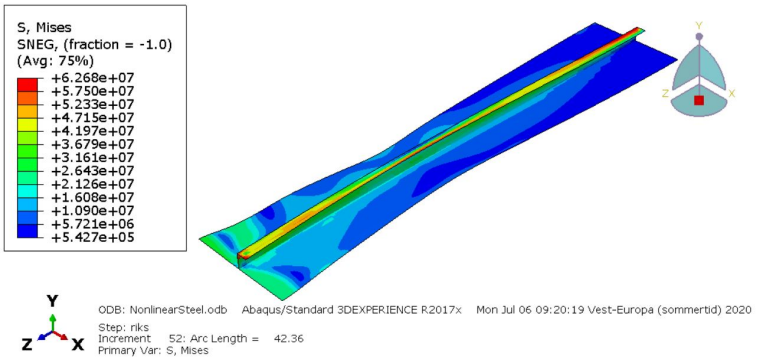

Figure 8.15: Buckling shape after critical load - Steel with fire on plate side

For validation, the nonlinear buckling shape for the aluminium plate field is shown in Figure 8.16. By comparing the plate to the aluminium stiffener in Figure 8.12 it is seen that the shape is very much alike. This means that the stiffeners are correctly modelled and display the reality. The plate has a critical buckling load of 757,178 N/m, i.e. 156,368 N/m or 26% above the single stiffener.

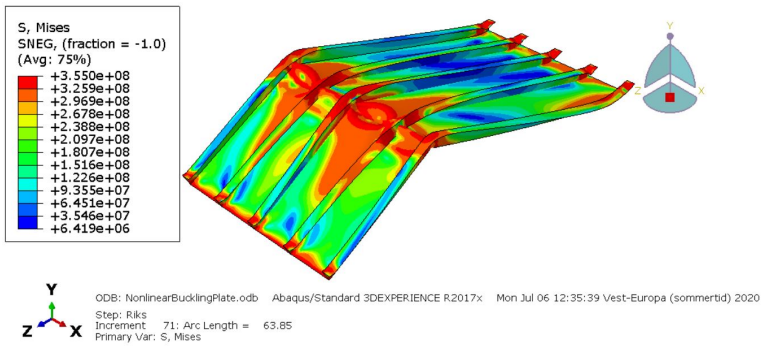

Figure 8.16: Buckling shape after critical load

All the eigenvalues and critical buckling loads are summarized in Table 8.1. The cases are numbered to match with the load-arclength curves in Figure 8.17, where the critical buckling length is found at the top of the curves. The curves are the same as the load proportionality factor in Abaqus, only the loads are scaled to the real loads.

Table 8.1: Critical buckling load and eigenvalues for the different fire scenarios

Case	Fire scenario	Eigenvalue	Critical buckling load
1	Room temperature	304402	600810 [N/m]
2	Fire on plateside: Uninsulated at 500 °C	67336	47014 [N/m]
3	Fire of stiffenerside: Uninsulated at 500 °C	49473	51381 [N/m]
4	Fire on plateside: Insulated	284984	513307 [N/m]
5	Fire on stiffenerside: Insulated	272412	512118 [N/m]
6	Steel room temperature	253731	1007023 [N/m]
7	Steel fire on plate side	19075	47130[N/m]
8	Plate field in room temperature	678968	757178 [N/m]

The table and figure shows clearly that the steel stiffener in room temperature is the structure that can withstand the most loading with a critical buckling load of 1,007,024 N/m. That is 406,213 N/m more than the aluminium stiffener in room temperature. Case 2, 3 and 7, i.e. the uninsulated aluminium stiffeners with fire on the plate side and the stiffener side in addition to the steel stiffener with fire on the plate side, also stands out by having a very low critical buckling load in comparison to the other cases. This is to be expected since they all are uninsulated and directly affected by the fire. The insulated cases, however, show no significant difference in the figure. This means the insulation not only helps with the heat transfer, but it also maintains the structural integrity of the stiffener by not allowing the heat to weaken the material.

The rest of the buckling shapes are added in Appendix F. The load-arclength curves for each case is also added in Appendix G. In addition to this, load-displacement curves has been made in the negative z-direction, to see how much the stiffener is pressed together in the load direction. These are shown in Appendix H.

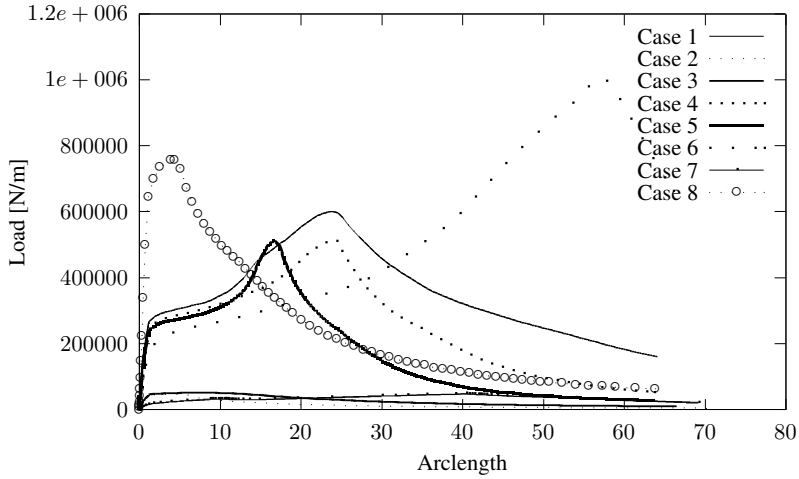

Figure 8.17: Load-arclength curve

The load-displacement curves of the steel stiffeners, however, stands out when comparing to the ones for aluminium. The load displacement curve for aluminium in room temperature is shown in Figure 8.18 and for steel in room temperature is shown in Figure 8.19.

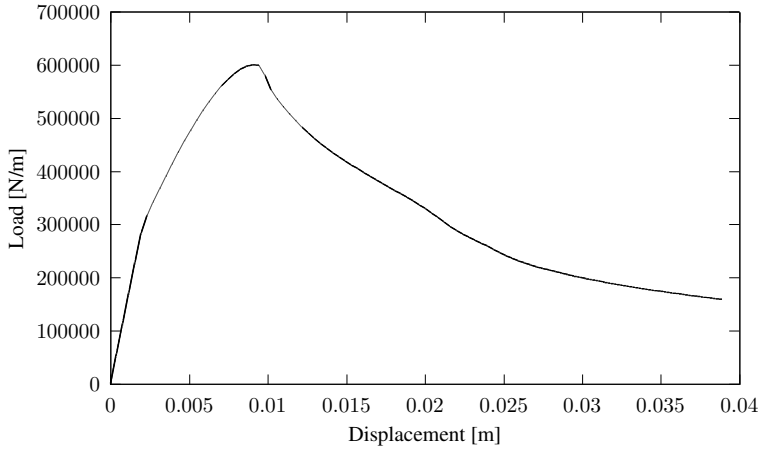

Figure 8.18: Load-displacement curve for aluminium stiffener in room temperature

The load-displacement curve for aluminium in room temperature has a top point, like the load-arclength curves does, which gives the critical buckling load. The load-displacement curve for steel, on the other hand, shows unstable response after a while, but always increasing so it is impossible to find the critical buckling load. Since the displacement is considered to be only in the negative z-direction, it will not catch up buckling in other directions. From the load-arclength curves the critical load for the steel stiffeners are found,

which then indicates that the critical buckling for the steel stiffeners does not occur in the negative z-direction.

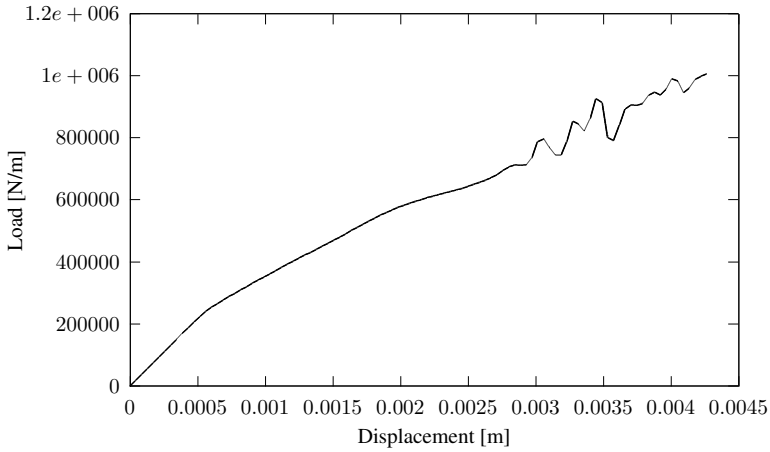

Figure 8.19: Load-displacement curve for steel stiffener in room temperature

8.4 Weight comparison

The weight for 1 meter width of aluminium and steel stiffeners with insulation on stiffener side and plate side is shown in Table 8.2. The aluminium is still lighter than steel, even with the insulation. The total weight savings for aluminium comparing to steel are 44-50% depending on where the stiffener is insulated.

Table 8.2: Weight comparison on one meter wide stiffener combinations

	Uninsulated	Insulation on plate side	Insulation on stiffener side
Aluminium	48.6 kg	58.68 kg	66.672 kg
Steel	117 kg	131.4 kg	133.14 kg

Chapter 9

Discussion and concluding remarks

Table 8.1 summarizes the most important results obtained in this thesis, namely the critical buckling loads for the different cases. From this table the following conclusions can be made:

1. Steel is more fire resistant than aluminium, and can tackle higher temperatures without insulation
2. Insulation helps on the heat transfer on the stiffener and also maintains the structural integrity despite some elevation in the temperature of the stiffener
3. If a choice had to be made whether to insulate the stiffener side or the plate side, it would be best to insulate the plate side because it has the lowest critical buckling load
4. Aluminium is a great replacement for hull design, if insulated correctly

These results amplifies the level of catastrophe if a fire were to arise in a battery room of a ferry in aluminium without proper insulation. According to the rules, the battery room should be insulated from possible fire development other places in the ship, but as seen on MF "Ytterøyningen" it is possible to have heat generation and fire, also in the battery room. Extensive risk assessments should therefore be performed when considering designing an entire hull in aluminium, and as mentioned, it only takes 8.5 minutes before the aluminium will have a temperature above 500°C, which is very close to the melting temperature.

It is, however, important to note that the critical buckling loads in this thesis represent the maximum capacity for the structure. In design there would have to be included safety factors like for example the f_1 factors of DNV GL for calculating the yield stress. It is the

total capacity of the stiffener with regards to geometry and also material properties that is calculated.

How the stiffeners are modelled might be questionable. The boundary conditions imply that they are columns or beams, as there are no constraints on the sides of the stiffener. To validate the modelling, a plate field with multiple stiffener was modelled to show the effect of a bulkhead construction, rather than columns. As discussed in the results, the buckling shapes ended up being quite similar. It would, however, be a need for further investigation on how to constrain such stiffeners when only looking at one stiffener as a part of a bulkhead.

The fire scenario chosen in this thesis was the standard temperature-time fire curve from EN 1999-1-2 (2007). This is typically used when assessing single members in fire tests. Comparing to a natural fire, however, the standard fire curve might not be the most realistic representation of a fire. The natural fire is often shown with Figure 9.1. The natural fires decrease in temperature after reaching its maximum temperature, often due to fire extinguishing, while the standard fire curve increases in temperature until it flattens out at a constant temperature. This means that under a natural fire the structure can experience a cool-down phase, while it with the standard fire curve will be exposed to high temperatures over a longer period of time. The standard fire curve therefore gives conservative results of fire resistance of structures compared to the natural fire curve.

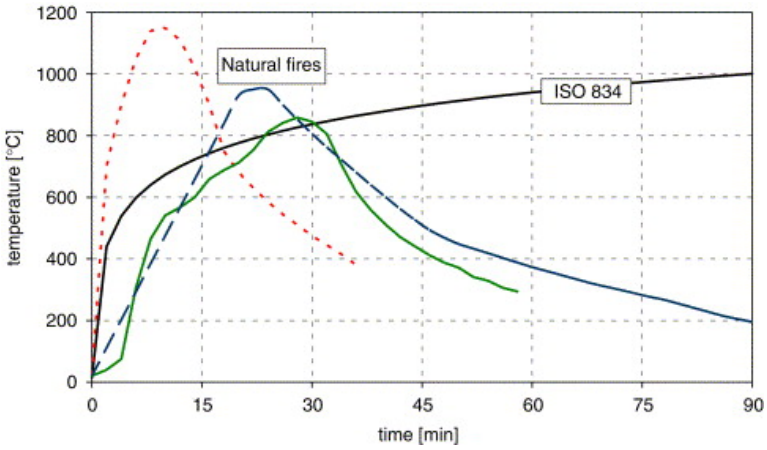

Figure 9.1: Natural fire curve VS standard fire curve (Zehfuss & Hosser, 2007)

For the design checks as discussed in Section 4.4, the time and temperature domain is held for all the cases except the aluminium and steel stiffeners without insulation. All the stiffeners obtain a temperature below 200 degrees (or 180°C above the original temperature) when insulated after 60 minutes. The buckling analyses finds the design value of the relevant effects of actions in the fire situation, which can be used against design rules to find whether the structure is within the structural requirements or not.

The weight comparison of the two materials shows that even though aluminium needs

thicker insulation than steel, it is still lighter than steel by 44-50% depending on where the stiffener is insulated. If the aluminium stiffener then is insulated properly against fire so it will not loose its strength if heated, it is a great alternative to steel if the goal is to make the ship lighter.

The material models used in this thesis are, however, somewhat questionable. Finding material properties was not an easy task, and it was therefore impossible to get accurate values at specific temperatures. The stress and strain curves were found for temperatures every 50 and 100°C for aluminium and steel, respectively. This means the model in aluminium would be given the material properties at temperatures $\pm$ 25 of the given stress-strain curves, and the model in steel would be given the material properties $\pm$ 50 of the given stress-strain curves. This will give sudden jumps in material properties when the structure is divided into smaller pieces for the buckling analysis, and might affect the results.

The fact that the stiffener is divided into smaller pieces and not have continuous material properties is also important to discuss. This is the reason for the material experiencing jumps in material properties. To account for this, the stiffener was divided in extra small pieces where the changes in temperature were large. It would still, however, have the large jumps in the stress-strain properties due to lack of data.

This method of performing a heat transfer analysis and collecting the corresponding material properties to perform buckling analyses does, however, not take into account the expansion of the material. This could be included in the heat transfer analysis, but the material properties are not dependent on the expansion of the material. Therefore, the models does not show this effect of temperature on materials. Further analyses and preferably material tests could have been performed to validate the method and to see whether the expansion would affect the analysis or not.

All in all, a functioning method has been developed for investigating how hull structures behaves under the influence of fire. It includes the effects of different temperature distribution, depending on where the fire is, and how the structures looses strength under axial loading condition and buckling, instead of using constant temperatures like previous studies. What can be done for further work is discussed in Chapter 10

Chapter 10

Further work

For further work the first priority would be to perform material tests to see how the material behaves under relevant temperatures in order to get more accurate results with regards to the buckling and the division of the structure. Just by increasing the number of temperatures evaluated in a stress-strain relationship would help a lot by increasing the accuracy of the study. This will also give a more realistic image of the temperature distribution and the material properties.

Another test that should be prioritised is model testing. By performing model test the constraints on the stiffener could be validated or changed according to the test. Model tests including fire would put the method of calculating the buckling loads to the test and to see if the buckling shape corresponds to the finite element buckling shape. A model test would verify the method, and highlight weaknesses and strength with it. It would also see whether expansion affects the result, or if it is fine to ignore the expansion effects.

A goal would also be to find a method to do a fully coupled thermal-buckling analysis so the change in time and temperature in relation to buckling would be analysed. For a fully coupled analysis the temperatures would have accurate distributions in the material and not be discretised and get jumps in material values. To create a model including all thermal effects including the thermal expansion would be the goal for further development of a thermal buckling model.

References

1st Choice Metals. (n.d.). *Aluminium 6000 series.* Retrieved 09.06.2020, from https://www.1stchoicemetals.co.uk/aluminium/grades-guide/6000-series/

Abaqus. (2006a). Abaqus analysis user's manual [Computer software manual]. (6.2.4 Unstable collapse and postbuckling analysis)

Abaqus. (2006b). Abaqus analysis user's manual [Computer software manual]. (27.6.1 Predefined fields)

Abaqus. (2016a). Abaqus analysis user's guide [Computer software manual]. (23.1.1 Inelastic behavior)

Abaqus. (2016b). Abaqus analysis user's guide [Computer software manual]. (36.3.1 Defining contact pairs in Abaqus/Standard)

Abaqus. (2016c). Getting started with abaqus/cae [Computer software manual].

ABS. (2019). *Materials and welding, part 2, chapter 5, section 5.* Spring, Texas: American Bureau of Shipping.

AISC. (1986). *Load and resistance factor design specification for structural steel buildings* (1st ed.). Chicago, Illinois: American Institute of Steel Construction, INC.

Aluminum Association. (2005). *Aluminium design manual*. Arlington, Virginia: The Aluminum Association.

Aluminum Association. (2015). *International alloy designations and chemical composition limits for wrought aluminum and wrought aluminum alloys.* Arlington, Virgina: The Aluminum Association.

Amdahl, J. (2019). General principles. *TMR4195 Design of offshore structures*. Retrieved 27.02.2020, from https://ntnu.blackboard.com

Amdahl, J., Langhelle, N. K., & Lundberg, S. (2001). Aluminium plated structures at elevated temperatures. *Proceedings of OMAE*, *20*.

Arisholm, T., & Kolltveit, B. (2003). 85 år med norske bilferjer: Historie med utfordrende kulturminner. *Årbok (Norsk Sjøfartsmuseum)*, *2002*, 11-56.

Arthur, K. M., Case, S. W., Lattimer, B. Y., & Dowling, N. E. (2011). *Predicting the failure of aluminum exposed to simulated fire and mechanical loading using finite element modeling* (Unpublished master's thesis). Virgina Polytechnic Insitute and State University, Blacksburg, VA.

Ashkan. (2020). *Stress-strain curve for thin-walled steel structures at elevated temperatures.* Matlab Central File Exchange. Retrieved 04.07.2020, from `https://se.mathworks.com/matlabcentral/fileexchange/41127-stress-strain-curve-for-thin-walled-steel-structures-at-elevated-temperatures?s_tid=FX_rc2_behav`

Banerjee, D., Gross, J., Hess, W., Olano, M., & Terrill, J. (2009). Visualization of structural behavior under fire. *U.S. department of Commerce*.

Bia, Y., Jin, W., Bolger, C., & Limbers, M. (2016). *Marine structural design* (2nd ed.). Amsterdam, Netherlands: Butterworth-Heinemann.

Bin, Z. (2012). Fire resistance assessment of steel structures. *Workshop 'Structural Fire Design of Buildings according to the Eurocodes'*. Retrieved 02.04.2020, from `https://eurocodes.jrc.ec.europa.eu/doc/2012_11_WS_fire/presentations/04-ZHAO-EC-FireDesign-WS.pdf`

DNV GL. (2015). *Rules for classification DNVGL-RU-HSLC-Pt3 - high speed and light craft, chapter 2: Hull structural design, steel.* DNV GL.

DNV GL. (2018). *Rules for classification DNVGL-RU-HSLC-Pt3 - high speed and light craft, chapter 3: Hull structural design, aluminium.* DNV GL.

DNV GL. (2019). *Rules for classification DNVGL-RU-SHIP-Pt6 - additional class notations, chapter 2: Propulsion, power generation and auxilary systems.* DNV GL.

Ellobody, E. (2014). *Finite element analysis and design of steel and stee-concrete composite bridges* (1st ed.). USA: Butterworth-Heinemann.

EN 1991-1-2. (1995). *Eurocode 1: Actions on structures - part 1-2: General actions - actions on structures exposed to fire.* CEN.

EN 1993-1-2. (2005). *Eurocode 3: Design of steel structures - part 1-2: General rules - structural fire design.* CEN.

EN 1999-1-1. (2007). *Eurocode 9: Design of aluminium structures - part 1-1: General structural rules.* CEN.

EN 1999-1-2. (2007). *Eurocode 9: Design of aluminium structures - part 1.2: Structural fire design.* CEN.

Feih, S., Mouritz, A., Kandare, E., & Lattimer, B. (2011). Structural analysis of compression deformation and failure of aluminium in fire. *Journal of Structural Engineering*.

Gilbert, R. (2011, 12). The serviceability limit states in reinforced concrete design. *Procedia Engineering*, *14*, 385-395.

Greene, E. (2005). Labor-saving passive fire protection systems for aluminum and composite construction. *Ship Structure Committee*(SSC-442).

Gustavsen, T. M. (2019). Ferjesektoren - status og videre utvikling. *Statens vegvesen: Ferjekonferansen 2019*. Retrieved 09.12.2019, from `https://www.vegvesen.no/fag/trafikk/ferje/ferjekonferansen`

Hatteland, S. (2019). *Skipsarkiv rogaland: En teknisk og historisk presentasjon av sjøverts rutetrafikk i rogaland.* Retrieved 27.11.2019, from `http://www.skipsarkiv-rogaland.net/fartoey%20-%20bilferger.htm`

Helmenstine, A. M. (2020). *Why is fire hot? how hot is it? understanding the temperature of a flame.* ThoughtCo. Retrieved 05.03.2020, from `https://www.thoughtco.com/why-is-fire-hot-607320`

Hopperstad, O., Langseth, M., & Hanssen, L. (1997). Ultimate compressive strength of plate elements in aluminium: Correlation of finite element analyses and tests. *Thin Walled Structures*, *29*, 31-46.

International Maritime Organization. (2014). *SOLAS consolidated edition* (6th ed.). London: International Maritime Organization.

Kartverket. (2019). *Norges kystlinje.* Retrieved 25.03.2020, from `https://www.kartverket.no/kunnskap/Fakta-om-Norge/norges-kystlinje/kystlinjen-i-kilometer/`

Khalif, D. A. J. N., & Mousawi, I. R. A. A. (2016). Comparison of heat transfer coefficients in free and forced convection using circular annular finned tubes. *International Journal of Application or Innovation in Engineering & Management (IJAIEM)*, *5*(4). Retrieved from `https://www.ijaiem.org/Volume5Issue4/IJAIEM-2016-04-24-37.pdf`

Langhelle, N. K., & Amdahl, J. (2001). Experimental and numerical analysis of aluminium columns subjected to fire. *Proceedings of the Eleventh International Offshore and Polar Engineering Conference*, *4*, 711-717.

Leira, B. J. (2018). *Marine structures, basic course.*

LMG Marin, CMR Prototech, & Norsk Energi. (2016). *Potensialstudie - energieffektiv og klimavennlig passasjerbåtdrift* (No. 359012-R-001).

Loeb, A. L. (1954). Thermal conductivity: VIII, A Theory of Thermal Conductivity of Porous Materials. *Journal of the American Ceramic Society*, *37*, 96-99. doi: https://doi.org/10.1111/j.1551-2916.1954.tb20107.x

Lura, C., & Anthun, M. (2019). *Har funne årsaka til brannen og eksplosjonen på mf "ytterøyningen"*. Retrieved 25.06.2020, from https://www.nrk.no/vestland/har-funne-arsaka-til-brannen-pa-ferja-mf-_ytteroyningen_-i-kvinnherad-1.14817180

Luscombe, J. H. (2018). *Thermodynamics*. Boca Raton: CRC Press, Taylor Francis Group.

Machine Design. (2015). *What's the difference between conduction, convection and radiation?* Retrieved 17.06.2019, from https://www.machinedesign.com/learning-resources/whats-the-difference-between/document/21834474/whats-the-difference-between-conduction-convection-and-radiation

Maljaars, J., Twilt, L., & Soetens, F. (2009). Flexural buckling of fire exposed aluminium columns. *Fire Safety Journal*, *44*(5), 711-717. doi: 10.1016/j.firesaf.2009.02.002

Manning, S. O. (1988). *A study of the load and resistance factor design methodology* (Unpublished master's thesis). University of Cincinnati, Ohio.

Markussen, H. M. (2018). *Norled bestiller verdens første enskrogs pendelferge i aluminium.* Retrieved 09.12.2019, from https://www.skipsrevyen.no/article/norled-bestiller-verdens-foerste-enskrogs-pendelferje-i-aluminium/

Moan, T. (1994). *Design of marine structures*. Trondheim: NTNU.

Moan, T. (2000). *Accidental actions background to norsok n-003*. Trondheim: Norwegian University of Science and Technology.

Moan, T. (2003). *Finite element modelling and analysis of marine structures*. Trondheim: Norwegian University of Science and Technology. (Chapter 12)

Multi Maritime. (2020). Building Specification: Electric Double ended Passenger Ferry, Design MM35PE EL (327-101-R01).

Norsk Hydro ASA. (2019). *5083 alloy.* Retrieved 05.12.2019, from https://www.hydro.com/en-NO/products-and-services/extruded-profiles/alloys-for-extruded-profiles/5083-alloy/

Norwegian Maritime Authority. (2014). *Forskrift om brannsikring på skip (for-2014-07-01-1099).* Retrieved 30.06.2020, from https://lovdata.no/dokument/LTI/forskrift/2014-07-01-1099

Rindheim, A. (2020). *Redesign of a steel ferry deck in aluminium* (Unpublished master's thesis). NTNU, Trondheim.

Rockwool. (2017a). *Searox fm 6000 range.* Retrieved 19.06.2019, from https://cdn01-rti.rockwool.com/siteassets/tools--documentation/documentation/marine--offshore-global/datasheets/rw-ti-searox-fm-6000-range_int_en.pdf?f=20190513060225

Rockwool. (2017b). *Searox sl 620.* Retrieved 06.07.2019, from https://cdn01-rti.rockwool.com/siteassets/marine--offshore/drawings/rti_drawing_steel_bulkhead_a-60_searox_sl_620-60_25mm_details.pdf?f=20181107033526

Sapa Technology. (2016). *Design manual, success with aluminium profiles*. Sapa: Innovative aluminium solutions.

Sielski, R. A. (2007a). Aluminum structure design and fabrication guide. *Ship Structure Committee*(SSC-452).

Sielski, R. A. (2007b). *Aluminum structure design and fabrication guide* (No. SSC-452). Ship Structure Committee.

Statens vegvesen. (2019a). *Ferjesambandene er en del av vegnettet.* Retrieved 04.12.2019, from https://www.vegvesen.no/fag/trafikk/ferje

Statens vegvesen. (2019b). *Vegvesenet bidrar til grønn revolusjon i ferjedriften.* Retrieved 09.12.2019, from https://www.vegvesen.no/om+statens+vegvesen/presse/nyheter/nasjonalt/vegvevesenet-bidrar-til-gronn-revolusjonen-i-ferjedriften

Summers, P. T., Chen, Y., Rippe, C. M., Allen, B., Mouritz, A. P., Case, S. W., & Lattimer, B. Y. (2015). Overview of aluminum alloy mechanical properties during and after fires. *Fire Science reviews*, *4*(3).

Suzuki, J. I., Ohmiya, Y., Wakamatsu, T., Harada, K., Yusa, S., & Kohno, M. (2005). Evaluation of fire resistance of aluminum alloye members. *Fire Science and Technology*, *24*, 237-255.

Sæther, A. S., Øystein Larsen-Vonstett, Svendsen, S. H., Peters, T., Ege, R. T., & Flågen, K. T. (2013). *Mysteriet "scandinavian star.* Retrieved 07.07.2020, from https://scandinavian-star.vg.no/

The Maritime Safety Committee. (2010). International code for application of fire test procedures. *Resolution MSC*, *307*(88).

Tjeltveit, N., & Statens vegvesen, Rogaland. (1996). *Ferje-rogaland*. Stavanger: Statens vegvesen, Rogaland.

Tran, V.-L., Thai, D.-K., Nguyen, D.-D., Phan, H.-T., & Nguyen, V.-Q. (2017). Finite element simulation of steel beam under fire. Vietnam: Vinh University Conference.

University of Alberta. (2003). *Buckling.* Retrieved 19.06.2019, from https://sites.ualberta.ca/~wmoussa/AnsysTutorial/IT/Buckling/Print.pdf

Vassart, O., Zhao, B., Cajot, L., Robert, F., Meyer, U., & Frangi, A. (2014). Eurocodes: Background applications structural fire design. *JRC Science and Policy reports*. Retrieved 21.04.2020, from https://eurocodes.jrc.ec.europa.eu/doc/2012_11_WS_fire/report/2012_11_WS_fire.pdf

Veillat, R. (2018). *Insulation density and thermal conductivity.* Retrieved 16.06.2019, from https://www.isover.co.uk/news/insulation-density-and-thermal-conductivity

Vosgraff, S. K. (2018). *Brann i turistferje under preikestolen slukket.* Retrieved 07.07.2020, from https://finansavisen.no/nyheter/naeringsliv/2018/08/brann-i-turistferje-under-preikestolen-slukket

Zehfuss, J., & Hosser, D. (2007). A parametric natural fire model for the structural fire design of multi-storey buildings. *Fire Safety Journal*, *42*(2), 115-126. doi: https://doi.org/10.1016/j.firesaf.2006.08.004

Appendix

A Temperature and material distribution (temperature-distribution.xlsx)

In order to obtain exact Young's modulus values, the values according to EN 1999-1-2 (2007) for aluminium and EN 1993-1-2 (2005) for steel as listed in Table 3.4 and Table 3.5, were plotted in Geogebra and a polynomial regression was done to find the graph fitting the data points. The following 4^{th} order polynomial function was used for the aluminium Young's modulus:

$$f(x) = 1.37x^4 - 1181.28x^3 + 39366.29x^2 - 20394133.33x + 70419022099.65 \quad (1)$$

And for steel the following function was used:

$$f(x) = -0.49x^4 + 1572.31x^3 - 1503234.32x^2 + 224512015.6x + 2020848 \quad (2)$$

A.1 Aluminium without insulation, fire on plate side

Aluminium without insulation at 512s about 500 degrees

Flange temp:	Node	Sorting	Distance	Average	Young's modulus
406,58	251356	1	0,05		
406,736	251354	2	0,045	**407**	2,6606E+10
407,178	251346	3	0,04		
407,914	251348	4	0,035		
408,944	251340	5	0,03		
410,267	251332	6	0,025	**410**	2,5989E+10
411,884	251334	7	0,02		
413,787	251324	8	0,015		
416,01	251326	9	0,01	**417**	2,4545E+10
418,39	251319	10	0,005		
419,382	251321	11	0		

Web temp:	Node	Sorting	Distance	Average	Young's modulus
419,983	251315	1	0,075		
422,944	251310	2	0,07	**423**	2,3308E+10
426,319	251305	3	0,065		
429,949	251299	4	0,06		
433,868	251284	5	0,055	**434**	2,1042E+10
438,065	251286	6	0,05		
442,541	251293	7	0,045		
447,291	251276	8	0,04	**447**	1,8381E+10
452,314	251274	9	0,035		
457,61	251266	10	0,03		
463,174	251264	11	0,025	**463**	1,5153E+10
469,01	251256	12	0,02		
475,091	251254	13	0,015		
481,519	251140	14	0,01	**481**	1,1622E+10
487,819	251142	15	0,005		

Plate Temp	Node	Sorting	Distance	Average	Young's modulus
526,625	251247	1	0,125		
526,571	251245	2	0,12		
526,408	251239	3	0,115	**526**	3,5853E+09
526,135	251237	4	0,11		
525,752	251231	5	0,105		
525,259	251229	6	0,1		
524,654	251223	7	0,095	**524**	3,9104E+09
523,936	251221	8	0,09		
523,105	251215	9	0,085		
522,157	251213	10	0,08		
521,092	251207	11	0,075	**520**	4,5710E+09
519,908	251205	12	0,07		
518,602	251371	13	0,065		
517,171	251199	14	0,06		
515,614	251197	15	0,055	**515**	5,4156E+09
513,927	251191	16	0,05		
512,107	251189	17	0,045		
510,15	251183	18	0,04		
508,053	251181	19	0,035	**507**	6,8076E+09
505,813	251175	20	0,03		
503,425	251173	21	0,025		
500,886	251169	22	0,02		
498,186	251163	23	0,015		
495,338	251159	24	0,01	**495**	8,9796E+09
492,272	251153	25	0,005		
489,645	251148	26	0		

A.2 Aluminium without insulation, fire on stiffener side

Aluminium without insulation fire on stiffenerside at 356s about 500 degrees

Flange temp:	Node	Sorting	Distance	Average	Young's modulus
489,448	251356	1	0,05		
489,483	251354	2	0,045	**490**	9,9111E+09
489,589	251346	3	0,04		
489,765	251348	4	0,035		
490,012	251340	5	0,03		
490,33	251332	6	0,025	**490**	9,9111E+09
490,719	251334	7	0,02		
491,179	251324	8	0,015		
491,717	251326	9	0,01	**492**	9,5368E+09
492,3	251319	10	0,005		
492,676	251321	11	0		

Web temp:	Node	Sorting	Distance	Average	Young's modulus
492,587	251315	1	0,075		
492,898	251310	2	0,07	**493**	9,3505E+09
493,046	251305	3	0,065		
492,987	251299	4	0,06		
492,73	251284	5	0,055	**493**	9,3505E+09
492,273	251286	6	0,05		
491,613	251293	7	0,045		
490,748	251276	8	0,04	**491**	9,7237E+09
489,676	251274	9	0,035		
488,392	251266	10	0,03		
486,892	251264	11	0,025	**487**	1,0477E+10
485,168	251256	12	0,02		
483,225	251254	13	0,015		
481,013	251140	14	0,01	**481**	1,1622E+10
478,709	251142	15	0,005		

Plate Temp	Node	Sorting	Distance	Average	Young's modulus
465,254	251247	1	0,125		
465,273	251245	2	0,12		
465,332	251239	3	0,115	**465**	1,4754E+10
465,43	251237	4	0,11		
465,567	251231	5	0,105		
465,744	251229	6	0,1		
465,96	251223	7	0,095	**466**	1,4556E+10
466,216	251221	8	0,09		
466,512	251215	9	0,085		
466,849	251213	10	0,08		
467,227	251207	11	0,075	**467**	1,4357E+10
467,646	251205	12	0,07		
468,107	251371	13	0,065		
468,611	251199	14	0,06		
469,157	251197	15	0,055	**469**	1,3962E+10
469,747	251191	16	0,05		
470,381	251189	17	0,045		
471,061	251183	18	0,04		
471,785	251181	19	0,035	**472**	1,3371E+10
472,557	251175	20	0,03		
473,376	251173	21	0,025		
474,243	251169	22	0,02		
475,16	251163	23	0,015		
476,122	251159	24	0,01	**476**	1,2589E+10
477,153	251153	25	0,005		
478,027	251148	26	0		

A.3 Aluminium with insulation, fire on plate side

Aluminium WITH insulation fire on plateside after 60 minutes

Flange temp:	Node	Sorting	Distance	Average	Young's modulus
180,579	251356	1	0,05		
180,59	251354	2	0,045	**181**	6,2484E+10
180,621	251346	3	0,04		
180,675	251348	4	0,035		
180,749	251340	5	0,03		
180,844	251332	6	0,025	**181**	6,2484E+10
180,961	251334	7	0,02		
181,099	251324	8	0,015		
181,26	251326	9	0,01	**181**	6,2484E+10
181,432	251319	10	0,005		
181,504	251321	11	0		

Web temp:	Node	Sorting	Distance	Average	Young's modulus
181,548	251315	1	0,075		
181,763	251310	2	0,07	**182**	6,2394E+10
182,009	251305	3	0,065		
182,274	251299	4	0,06		
182,561	251284	5	0,055	**183**	6,2303E+10
182,869	251286	6	0,05		
183,198	251293	7	0,045		
183,548	251276	8	0,04	**184**	6,2211E+10
183,919	251274	9	0,035		
184,312	251266	10	0,03		
184,726	251264	11	0,025	**185**	6,2119E+10
185,161	251256	12	0,02		
185,616	251254	13	0,015		
186,099	251140	14	0,01	**186**	6,2027E+10
186,574	251142	15	0,005		

Plate Temp	Node	Sorting	Distance	Average	Young's modulus
189,779	251247	1	0,125		
189,774	251245	2	0,12		
189,76	251239	3	0,115	**190**	6,1649E+10
189,735	251237	4	0,11		
189,7	251231	5	0,105		
189,655	251229	6	0,1		
189,601	251223	7	0,095	**190**	6,1649E+10
189,536	251221	8	0,09		
189,462	251215	9	0,085		
189,377	251213	10	0,08		
189,283	251207	11	0,075	**189**	6,1744E+10
189,179	251205	12	0,07		
189,064	251371	13	0,065		
188,94	251199	14	0,06		
188,806	251197	15	0,055	**189**	6,1744E+10
188,662	251191	16	0,05		
188,508	251189	17	0,045		
188,344	251183	18	0,04		
188,17	251181	19	0,035	**188**	6,1839E+10
187,985	251175	20	0,03		
187,791	251173	21	0,025		
187,587	251169	22	0,02		
187,373	251163	23	0,015		
187,15	251159	24	0,01	**187**	6,1933E+10
186,913	251153	25	0,005		
186,712	251148	26	0		

A.4 Aluminium with insulation, fire on stiffener side

Aluminium WITH insulation fire on stiffenerside after 60 minutes

Flange temp:	Node	Sorting	Distance	Average	Young's modulus
193,893	251356	1	0,05		
193,74	251354	2	0,045	**194**	6,1261E+10
193,491	251346	3	0,04		
193,233	251348	4	0,035		
192,965	251340	5	0,03		
192,669	251332	6	0,025	**193**	6,1359E+10
192,348	251334	7	0,02		
192,002	251324	8	0,015		
191,632	251326	9	0,01	**192**	6,1456E+10
191,28	251319	10	0,005		
191,199	251321	11	0		

Web temp:	Node	Sorting	Distance	Average	Young's modulus
191,008	251315	1	0,075		
190,446	251310	2	0,07	**190**	6,1649E+10
189,864	251305	3	0,065		
189,288	251299	4	0,06		
188,699	251284	5	0,055	**189**	6,1744E+10
188,107	251286	6	0,05		
187,521	251293	7	0,045		
186,941	251276	8	0,04	**187**	6,1933E+10
186,368	251274	9	0,035		
185,805	251266	10	0,03		
185,256	251264	11	0,025	**185**	6,2119E+10
184,722	251256	12	0,02		
184,206	251254	13	0,015		
183,704	251140	14	0,01	**184**	6,2211E+10
183,251	251142	15	0,005		

Plate Temp	Node	Sorting	Distance	Average	Young's modulus
179,756	251247	1	0,125		
179,758	251245	2	0,12		
179,766	251239	3	0,115	**180**	6,2573E+10
179,779	251237	4	0,11		
179,797	251231	5	0,105		
179,822	251229	6	0,1		
179,855	251223	7	0,095	**180**	6,2573E+10
179,895	251221	8	0,09		
179,944	251215	9	0,085		
180,003	251213	10	0,08		
180,074	251207	11	0,075	**180**	6,2573E+10
180,156	251205	12	0,07		
180,252	251371	13	0,065		
180,363	251199	14	0,06		
180,489	251197	15	0,055	**181**	6,2484E+10
180,631	251191	16	0,05		
180,791	251189	17	0,045		
180,97	251183	18	0,04		
181,168	251181	19	0,035	**181**	6,2484E+10
181,387	251175	20	0,03		
181,626	251173	21	0,025		
181,886	251169	22	0,02		
182,168	251163	23	0,015		
182,471	251159	24	0,01	**182**	6,2394E+10
182,801	251153	25	0,005		
183,102	251148	26	0		

A.5 Steel without insulation, fire on plate side

Steel without insulation after 60 minutes

Flange temp:	Node	Sorting	Distance	Average	Young's modulus
699,153	419548	1	0,05		
699,308	419546	2	0,045	**700**	4,3811E+10
699,774	419539	3	0,04		
700,547	419537	4	0,035		
701,639	419532	5	0,03		
703,075	419524	6	0,025	**703**	4,3082E+10
704,893	419526	7	0,02		
707,127	419516	8	0,015		
709,896	419518	9	0,01	**711**	4,1171E+10
713,046	419511	10	0,005		
714,395	419513	11	0		

Web temp:	Node	Sorting	Distance	Average	Young's modulus
715,328	419507	1	0,075	**718**	3,9536E+10
719,937	419502	2	0,07		
725,694	419497	3	0,065	**729**	3,7039E+10
732,656	419491	4	0,06		
741,26	419485	5	0,055	**746**	3,3354E+10
751,732	419478	6	0,05		
764,083	419476	7	0,045	**771**	2,8327E+10
778,196	419468	8	0,04		
793,811	419466	9	0,035	**802**	2,2751E+10
810,453	419458	10	0,03		
827,561	419456	11	0,025	**836**	1,7475E+10
845,079	419452	12	0,02		
862,91	419235	13	0,015	**872**	1,2835E+10
881,303	419237	14	0,01		
898,969	419245	15	0,005	**899**	9,9776E+09

Plate Temp	Node	Sorting	Distance	Average	Young's modulus
941,419	419444	1	0,25		
941,419	419442	2	0,245		
941,419	419436	3	0,24		
941,419	419434	4	0,235		
941,419	419428	5	0,23		
941,418	419426	6	0,225		
941,418	419420	7	0,22		
941,418	419418	8	0,215		
941,417	419412	9	0,21		
941,416	419410	10	0,205		
941,416	419561	11	0,2		
941,415	419402	12	0,195		
941,413	419404	13	0,19		
941,412	419394	14	0,185		
941,409	419396	15	0,18	**941**	6,5393E+09
941,407	419386	16	0,175		
941,404	419388	17	0,17		
941,399	419380	18	0,165		
941,394	419378	19	0,16		
941,388	419372	20	0,155		
941,38	419370	21	0,15		
941,369	419364	22	0,145		
941,357	419362	23	0,14		
941,34	419356	24	0,135		
941,32	419354	25	0,13		
941,295	419348	26	0,125		
941,263	419346	27	0,12		
941,223	419340	28	0,115		
941,172	419338	29	0,11		
941,109	419332	30	0,105		
941,029	419330	31	0,1		
940,928	419324	32	0,095	**941**	6,5393E+09
940,802	419322	33	0,09		
940,642	419316	34	0,085		
940,442	419314	35	0,08		
940,19	419308	36	0,075	**940**	6,6076E+09
939,872	419306	37	0,07		
939,472	419590	38	0,065		
938,968	419300	39	0,06		
938,334	419298	40	0,055	**938**	6,7460E+09
937,534	419292	41	0,05		
936,528	419290	42	0,045		
935,26	419284	43	0,04		
933,663	419282	44	0,035	**932**	6,7460E+09
931,652	419276	45	0,03		
929,12	419274	46	0,025		
925,934	419270	47	0,02	**924**	7,7882E+09
921,917	419264	48	0,015		
916,908	419260	49	0,01	**914**	8,6126E+09
910,469	419254	50	0,005		
904,125	419249	51	0	**904**	9,5052E+09

B Stress-strain conversion (temperaturedistribution.xlsx)

Engineering stress/strain

500 degrees:		450 degrees:		400 degrees:		350 degrees:		300 degrees:		250 degrees:		200 degrees:	
Stress [PA]	Strain	Stress[Pa]	Strain	Stress[Pa]	Strain	Stress[Pa]	Strain	Stress[Pa]	Strain	Stress[Pa]	Strain	Stress[Pa]	Strain
1,40E+07	0	1,50E+07	0	3,18E+07	0	6,87E+07	0	1,00E+08	0	1,78E+08	0	2,50E+08	0
1,15E+07	0,16	1,90E+07	0,026	3,37E+07	0,02	7,20E+07	0,02	1,01E+08	0,028	1,79E+08	0,02	2,41E+08	0,07
1,02E+07	0,28	1,59E+07	0,07	3,05E+07	0,09	7,00E+07	0,069	8,90E+07	0,11	1,72E+08	0,05	2,24E+08	0,15
9,50E+06	0,407	1,46E+07	0,25	2,23E+07	0,31	5,80E+07	0,18	7,40E+07	0,2	1,59E+08	0,1	1,96E+08	0,2
8,90E+06	0,54	1,27E+07	0,5	1,08E+07	0,47	4,30E+07	0,3	5,20E+07	0,3	1,40E+08	0,15	1,47E+08	0,3
8,90E+06	0,7	1,20E+07	0,6	9,54E+06	0,69	3,00E+07	0,34			1,20E+08	0,2		
7,63E+06	0,84	9,50E+06	0,7	7,00E+06	0,88								
5,00E+06	1	7,00E+06	0,89	5,00E+06	1								
		5,00E+06	1										
E-Modul [Pa]:	1,00E+10	E-modul [Pa:]	2,10E+10	E-modul [Pa:]	2,80E+10	E-modul [Pa:]	3,78E+10	E-modul [Pa:]	4,76E+10	E-modul [Pa:]	5,46E+10	E-modul [Pa:]	6,93E+10

True stress/strain

500 degrees:		450 degrees:		400 degrees:		350 degrees:		300 degrees:		250 degrees:		200 degrees:	
Stress [PA]	Log Strain	Stress[Pa]	Log Strain	Stress[Pa]	Log Strain	Stress[Pa]	Log Strain	Stress[Pa]	Log Strain	Stress[Pa]	Log Strain	Stress[Pa]	Log Strain
14000000	0,000	15000000	0,000	31800000	0,000	68700000	0,000	100000000	0,000	178000000	0,000	250000000	0,000
13340000	0,147	19494000	0,025	34374000	0,019	73440000	0,018	103828000	0,025	182376000	0,016	257870000	0,064
13056000	0,246	17013000	0,067	33245000	0,085	74830000	0,065	98790000	0,102	180390000	0,045	257600000	0,136
13366500	0,340	18250000	0,222	29213000	0,269	68440000	0,164	88800000	0,180	174900000	0,092	235200000	0,179
13706000	0,430	19050000	0,405	15876000	0,385	55900000	0,261	67600000	0,261	161000000	0,137	191100000	0,266
15130000	0,529	19200000	0,469	16122600	0,524	40200000	0,292			144000000	0,180		
14039200	0,608	16150000	0,530	13160000	0,631								
10000000	0,692	13230000	0,636	10000000	0,693								
		10000000	0,693										

C Steel stress-strain properties (StressStrainSteel.xlsx)

True Stress [MPa]	Plastic Strain	Temperature
0	0	20
0	0	20
551,4756098	0	20
551,5856098	0,000188118	20
551,6956098	0,000386986	20
551,8056098	0,000585815	20
551,9156098	0,000784604	20
552,0256098	0,000983354	20
552,1356098	0,001182063	20
552,2456098	0,001380733	20
552,3556098	0,001579364	20
552,4656098	0,001777954	20
552,5756098	0,001976505	20
561	0,017066042	20
0,1025	0,024692113	20

True Stress [MPa]	Plastic Strain	Temperature
0	0	100
0	0	100
551,4756098	0	100
551,5856098	0,000188118	100
551,6956098	0,000386986	100
551,8056098	0,000585815	100
551,9156098	0,000784604	100
552,0256098	0,000983354	100
552,1356098	0,001182063	100
552,2456098	0,001380733	100
552,3556098	0,001579364	100
552,4656098	0,001777954	100
552,5756098	0,001976505	100
561	0,017066042	100
0,1025	0,024692113	100

True Stress [MPa]	Plastic Strain	Temperature
0	0	200
0	0	200
444,917766	0	200
460,8739889	0,00010434	200
468,8522412	0,000260558	200
474,5756996	0,000428957	200
479,0036223	0,000604338	200
482,5238107	0,0007846	200
485,337812	0,000968649	200
487,5643593	0,001155842	200
489,2782145	0,001345775	200
490,5276818	0,001538185	200
491,343405	0,001732907	200
491,7430105	0,001929844	200
499,29	0,017096448	200
0,1025	0,024692057	200

True Stress [MPa]	Plastic Strain	Temperature
0	0	300
0	0	300
337,8431105	0	300
361,6383566	4,81403E-05	300
377,1635139	0,000153005	300
388,9599217	0,000280565	300
398,4021453	0,000422441	300
406,1295448	0,000574734	300
412,4999733	0,00073526	300
417,7355438	0,000902667	300
421,9829239	0,00107606	300
425,3423773	0,001254827	300
427,8832171	0,001438546	300
429,6525723	0,00162693	300
430,6805083	0,001819794	300
437,58	0,017134457	300
0,1025	0,024691988	300

True Stress [MPa]	Plastic Strain	Temperature
0	0	400
0	0	400
231,3718537	0	400
256,1181455	2,3325E-05	400
275,3489302	8,89314E-05	400
291,0678246	0,000178971	400
304,2338953	0,00028676	400
315,3942983	0,000408487	400
324,8948188	0,000541741	400
332,9688038	0,000684896	400
339,7807041	0,000836806	400
345,4496589	0,000996641	400
350,0632245	0,001163792	400
353,6857908	0,001337808	400
356,3639147	0,001518366	400
358,1297466	0,001705242	400
359,0031959	0,001898297	400
364,65	0,017261512	400
0,1025	0,024691898	400

True Stress [MPa]	Plastic Strain	Temperature
0	0	500
0	0	500
198,3187317	0	500
218,5577066	3,12285E-05	500
233,4374895	0,000109873	500
245,2721961	0,000213235	500
255,01082	0,000333599	500
263,1534275	0,000466898	500
270,0007591	0,000610688	500
275,7488369	0,000763375	500
280,5321539	0,000923867	500
284,4459316	0,001091388	500
287,5585933	0,001265382	500
289,9191705	0,001445451	500
291,5618572	0,001631317	500
292,5088323	0,001822799	500
297,33	0,01738531	500
0,1025	0,024691779	500

True Stress [MPa]	Plastic Strain	Temperature
0	0	600
0	0	600
99,15422502	0	600
110,5770125	1,62851E-05	600
119,966726	6,81611E-05	600
127,8959121	0,00014298	600
134,689115	0,000235634	600
140,5510058	0,000342903	600
145,6199138	0,00046261	600
149,9938603	0,000593213	600
153,7446081	0,000733583	600
156,9258398	0,000882875	600
159,5781929	0,001040449	600
161,7324936	0,001205821	600
163,4118923	0,001378626	600
164,6332963	0,001558598	600
165,4083264	0,001745555	600
165,7439338	0,001939386	600
168,3	0,017154319	600
0,1025	0,024691	600

True Stress [MPa]	Plastic Strain	Temperature
0	0	700
0	0	700
41,3138485	0	700
46,19282886	1,30023E-05	700
50,31501577	5,79547E-05	700
53,85932228	0,000124551	700
56,93650597	0,000208636	700
59,620593	0,000307432	700
61,96373014	0,000418981	700
64,00404288	0,000541853	700
65,77014607	0,000674975	700
67,28389668	0,000817527	700
68,56215413	0,000968875	700
69,61794633	0,001128531	700
70,46126153	0,00129612	700
71,0995936	0,001471362	700
71,53831705	0,001654053	700
71,78093899	0,001844064	700
72,93	0,017066042	700
0,1025	0,024688766	700

True Stress [MPa]	Plastic Strain	Temperature
0	0	800
0	0	800
27,54098916	0	800
30,29387993	4,71429E-05	800
32,13380682	0,00014706	800
33,54276959	0,000270297	800
34,67558874	0,00040846	800
35,60582824	0,000557564	800
36,37515056	0,000715349	800
37,00962159	0,000880404	800
37,52656344	0,001051789	800
37,93789075	0,001228859	800
38,25190102	0,001411163	800
38,47429799	0,001598394	800
38,60879553	0,001790349	800
39,27	0,017674172	800
0,1025	0,024687057	800

True Stress [MPa]	Plastic Strain	Temperature
0	0	900
0	0	900
20,65574187	0	900
22,54248311	6,00012E-05	900
23,71752534	0,000174726	900
24,59771716	0,00031072	900
25,29623952	0,000459802	900
25,86391047	0,000618301	900
26,32863402	0,0007842	900
26,7075068	0,000956264	900
27,01169912	0,001133684	900
27,24876577	0,001315916	900
27,42385905	0,001502586	900
27,54040775	0,001693448	900
27,60050645	0,00188835	900
28,05	0,017775527	900
0,1025	0,024685205	900

True Stress [MPa]	Plastic Strain	Temperature
0	0	1000
0	0	1000
13,77049458	0	1000
14,68309518	9,74242E-05	1000
15,16172893	0,000245182	1000
15,50706625	0,00040735	1000
15,77503933	0,000577864	1000
15,98862683	0,000754234	1000
16,15987237	0,000935154	1000
16,29591756	0,00111985	1000
16,4012914	0,001307831	1000
16,47895036	0,001498777	1000
16,53080511	0,00169248	1000
16,55800241	0,001888816	1000
16,83	0,017978237	1000
0,1025	0,024681501	1000

True Stress [MPa]	Plastic Strain	Temperature
0	0	1100
0	0	1100
6,88524729	0	1100
7,68370265	2,32442E-05	1100
8,307396009	8,76687E-05	1100
8,818593917	0,000176443	1100
9,247552606	0,000283006	1100
9,611677878	0,000403586	1100
9,922028986	0,000535785	1100
10,18609773	0,000677977	1100
10,40917965	0,000829016	1100
10,59512079	0,000988068	1100
10,74675439	0,001154518	1100
10,86616947	0,001327913	1100
10,95488157	0,001507924	1100
11,01394293	0,001694325	1100
11,04401237	0,001886971	1100
11,22	0,017370107	1100
0,1025	0,02467039	1100

D Heat transfer results

D.1 Uninsulated aluminium stiffener with fire on plate side at 500°C

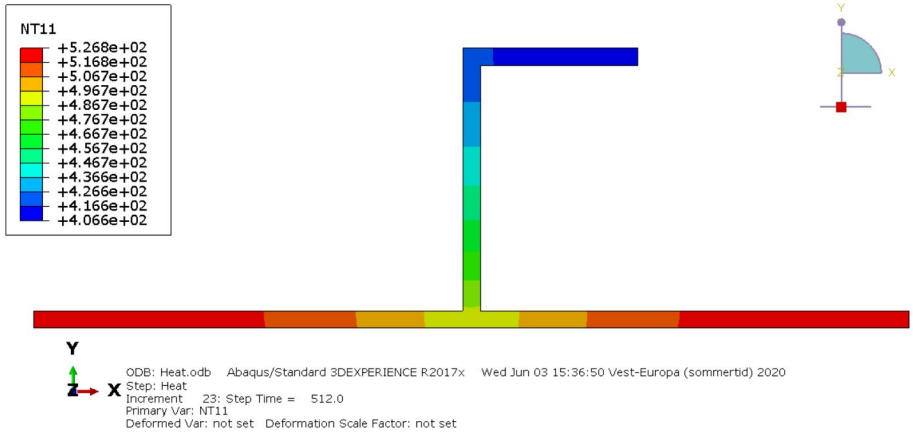

D.2 Uninsulated aluminium stiffener with fire on stiffener side at 500°C

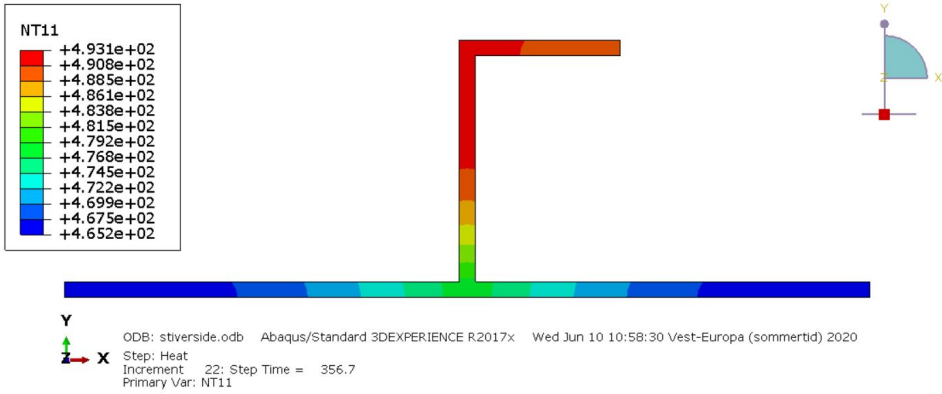

D.3 Insulated aluminium stiffener with fire on plate side after 60 minutes

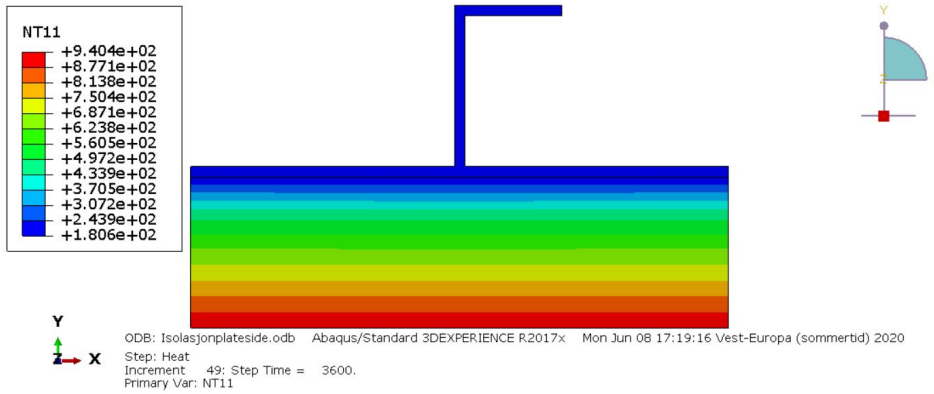

D.4 Insulated aluminium stiffener with fire on stiffener side after 60 minutes

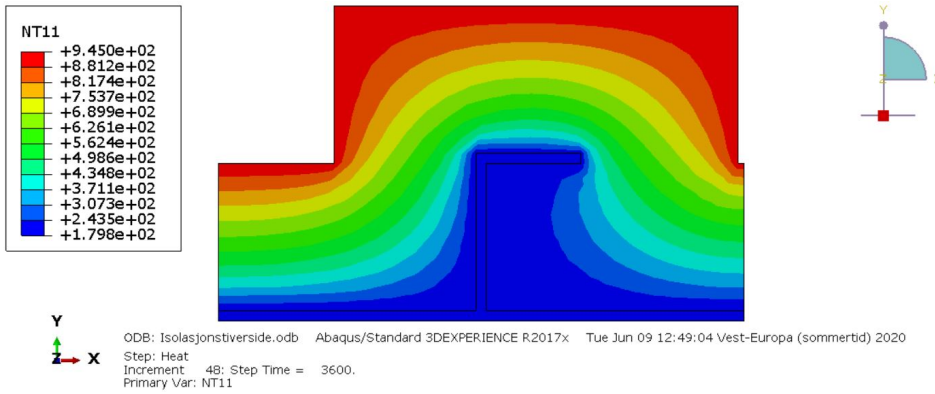

D.5 Uninsulated steel stiffener with fire on plate side after 60 minutes

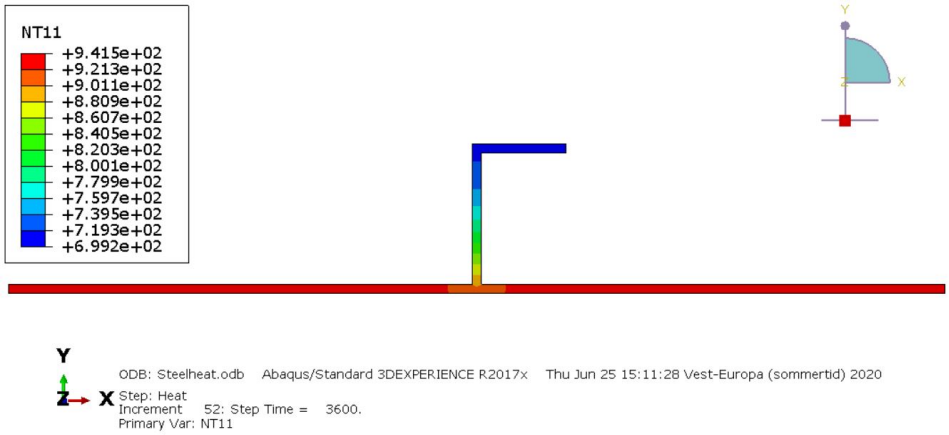

E Linear Buckling - Eigenmodes

E.1 Aluminium stiffener in room temperature

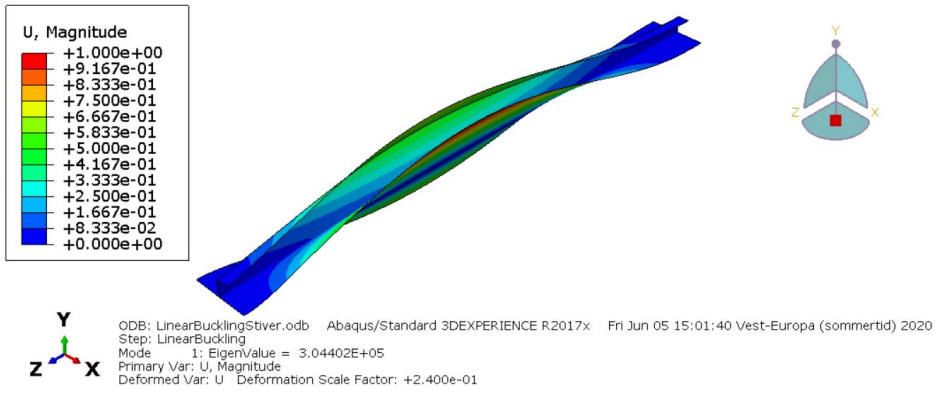

(a) Mode 1

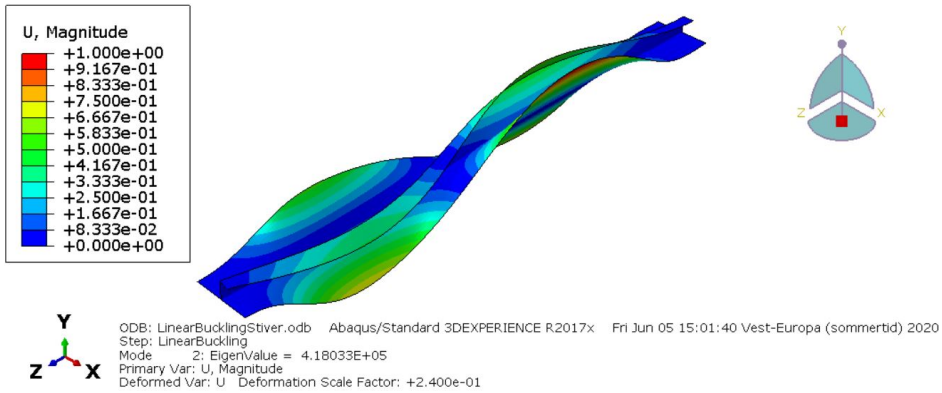

(b) Mode 2

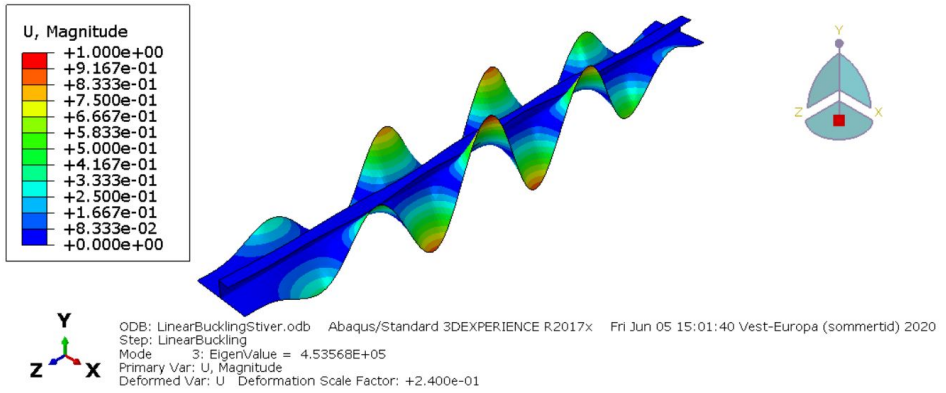

(c) Mode 3

E.2 Uninsulated aluminium stiffener with fire on plate side at 500°C

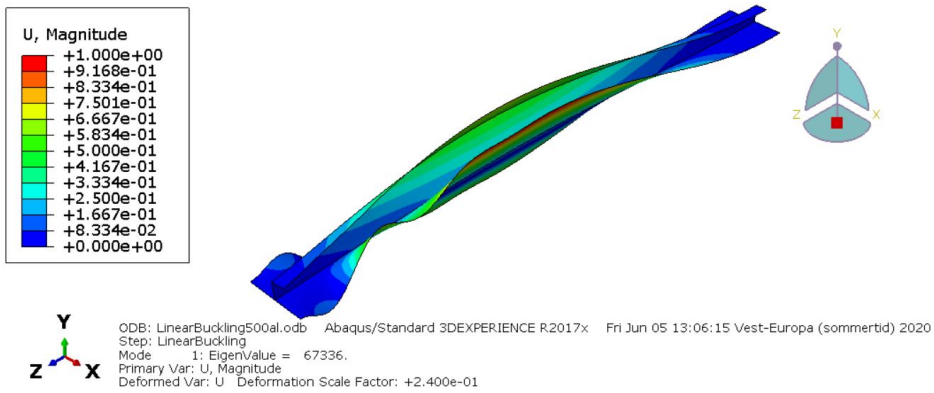

(a) Mode 1

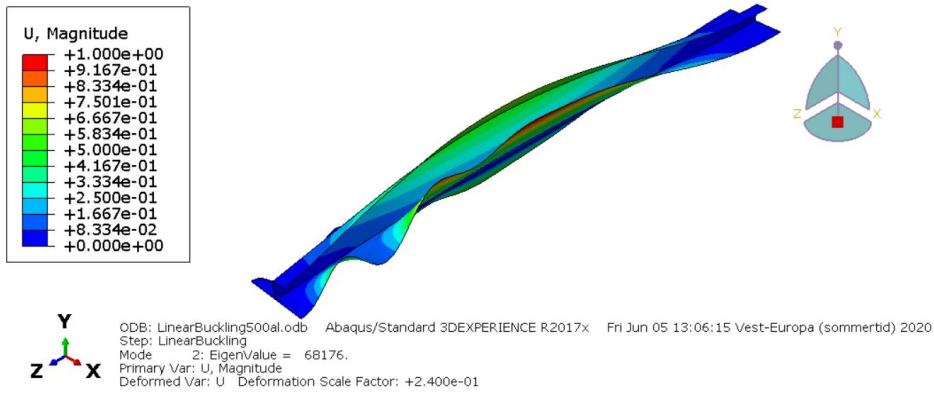

(b) Mode 2

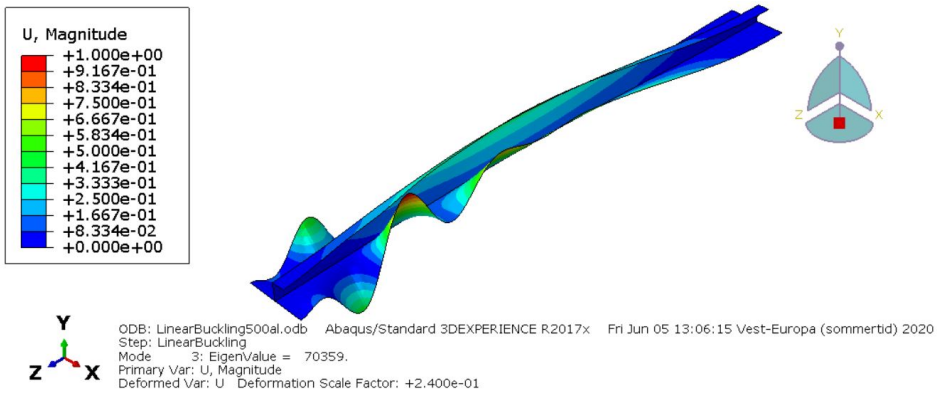

(c) Mode 3

E.3 Uninsulated aluminium stiffener with fire on stiffener side at 500°C

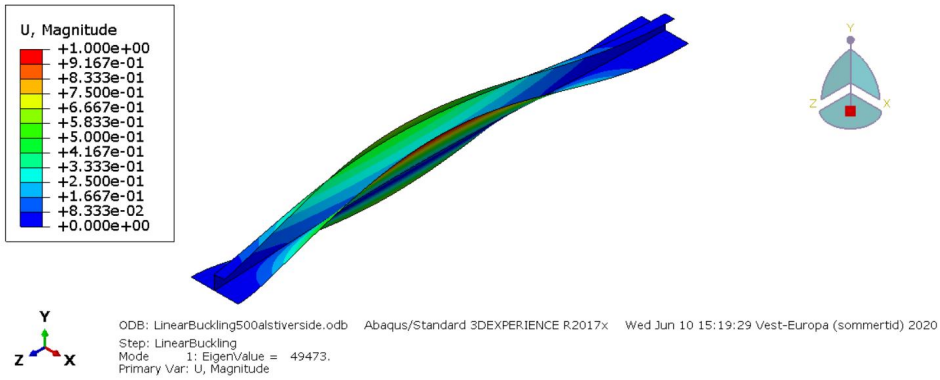

(a) Mode 1

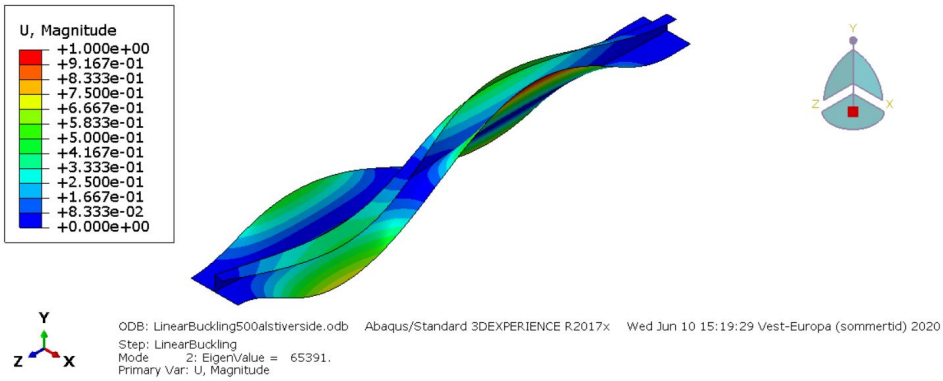

(b) Mode 2

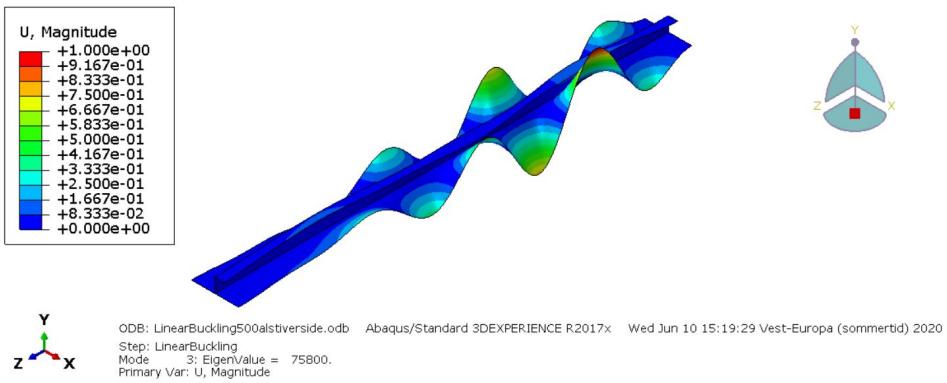

(c) Mode 3

E.4 Insulated aluminium stiffener with fire on plate side after 60 minutes

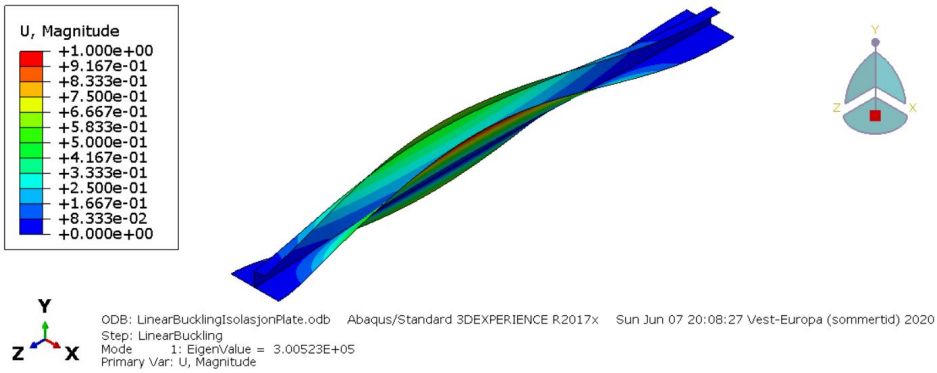

(a) Mode 1

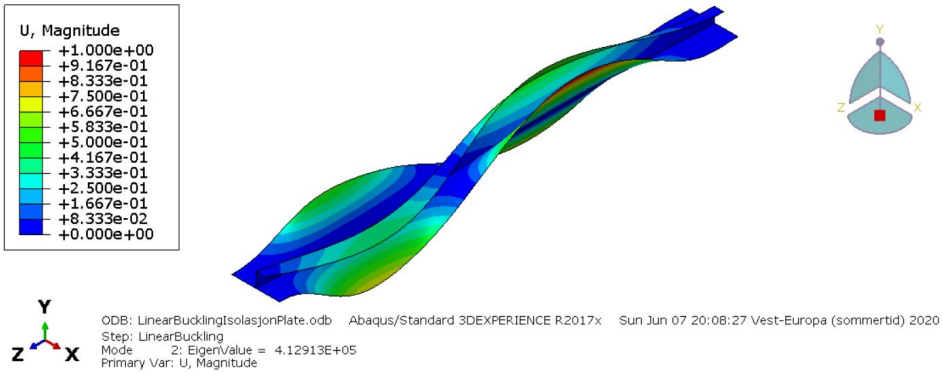

(b) Mode 2

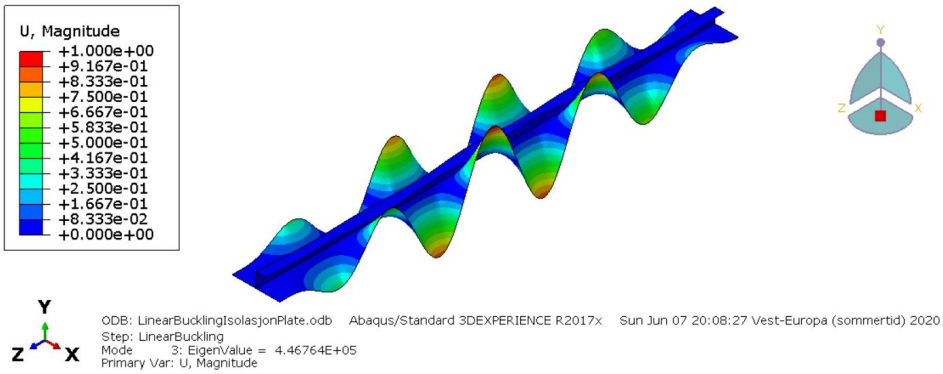

(c) Mode 3

E.5 Insulated aluminium stiffener with fire on stiffener side after 60 minutes

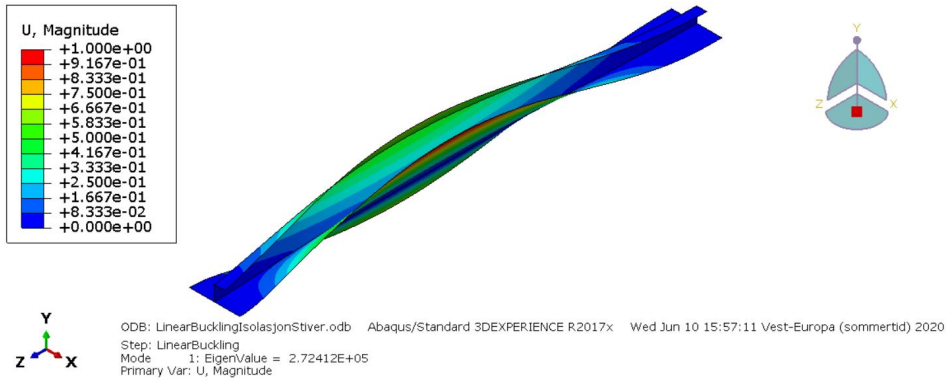

(a) Mode 1

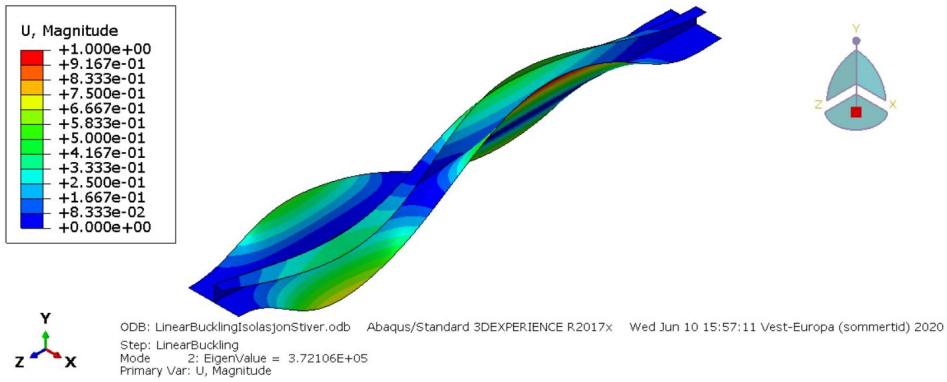

(b) Mode 2

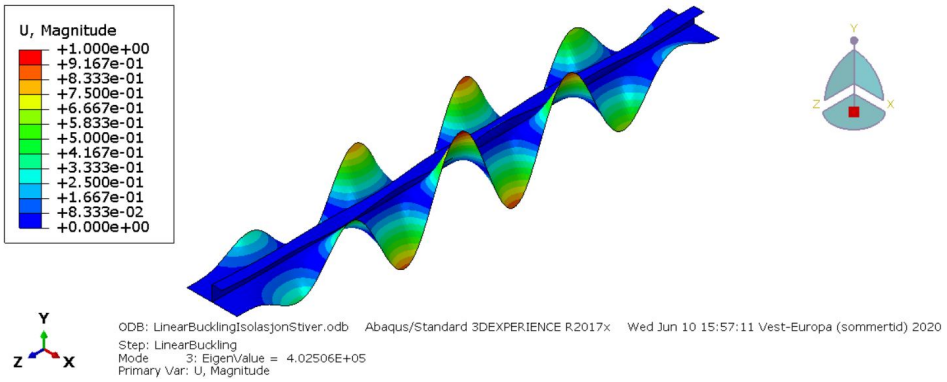

(c) Mode 3

E.6 Steel stiffener in room temperature

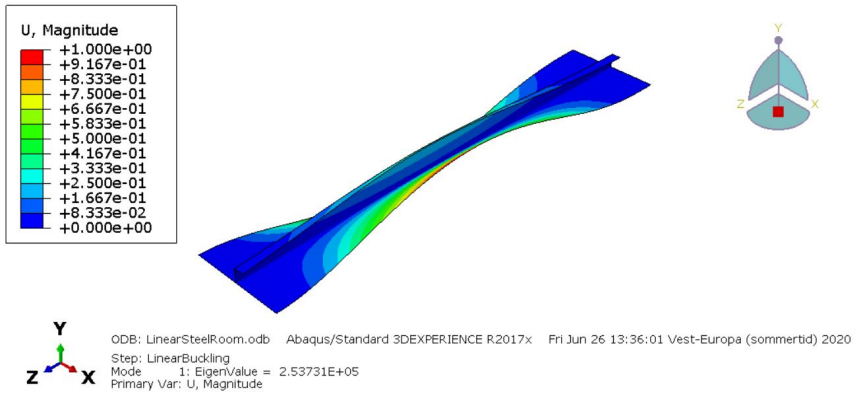

(a) Mode 1

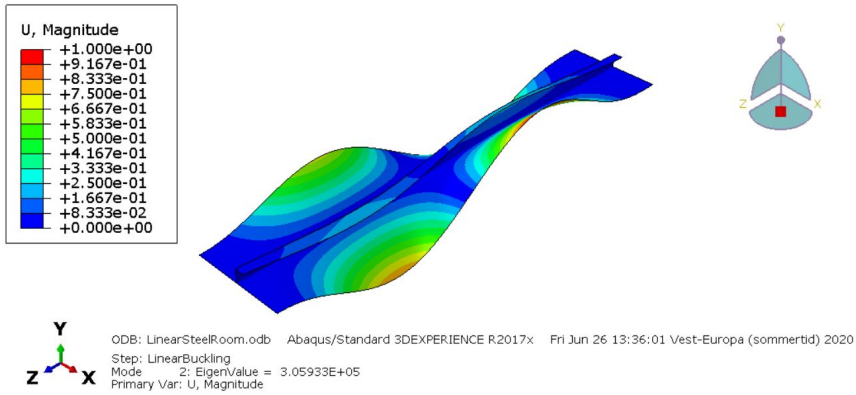

(b) Mode 2

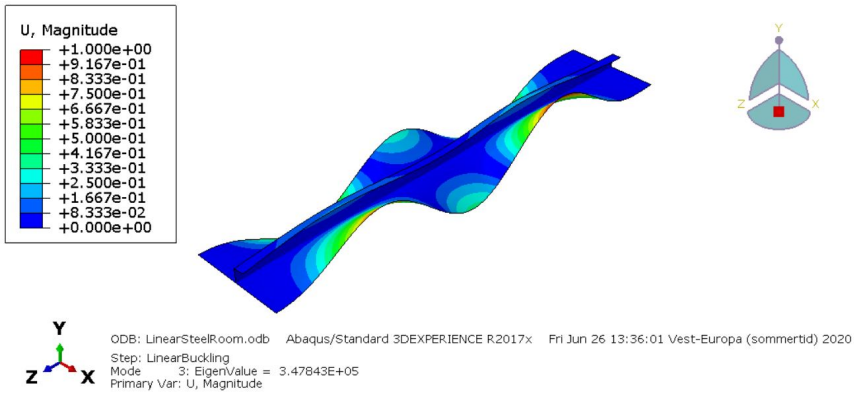

(c) Mode 3

E.7 Uninsulated steel stiffener with fire on plate side after 60 minutes

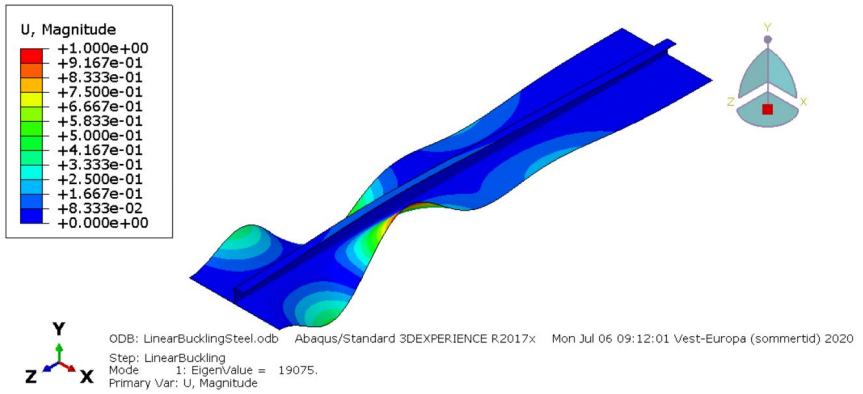

(a) Mode 1

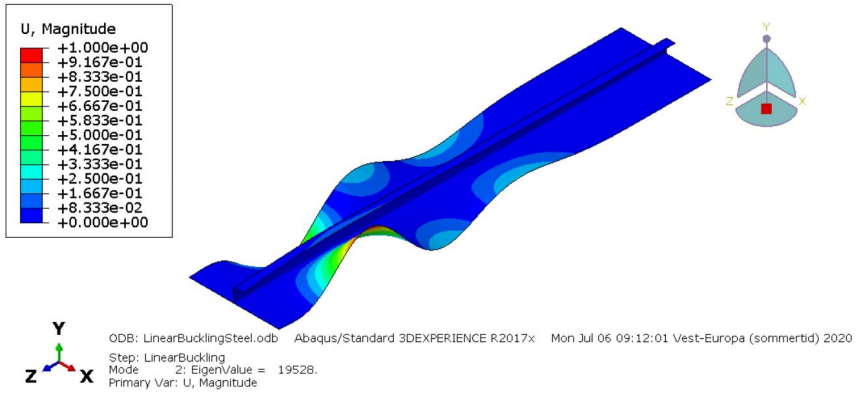

(b) Mode 2

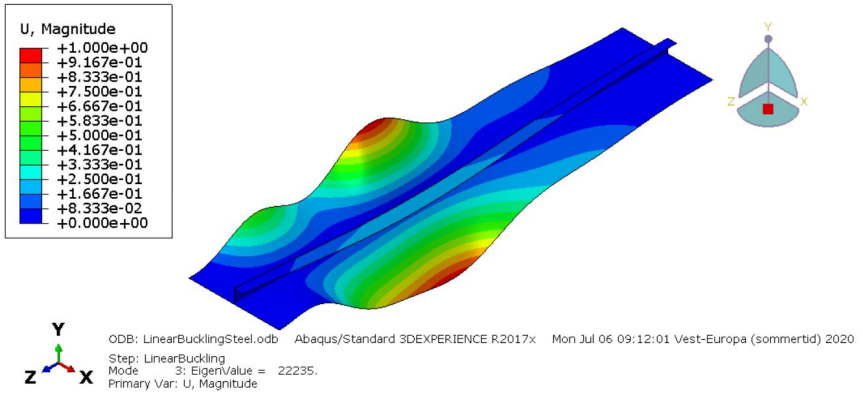

(c) Mode 3

E.8 Plate field

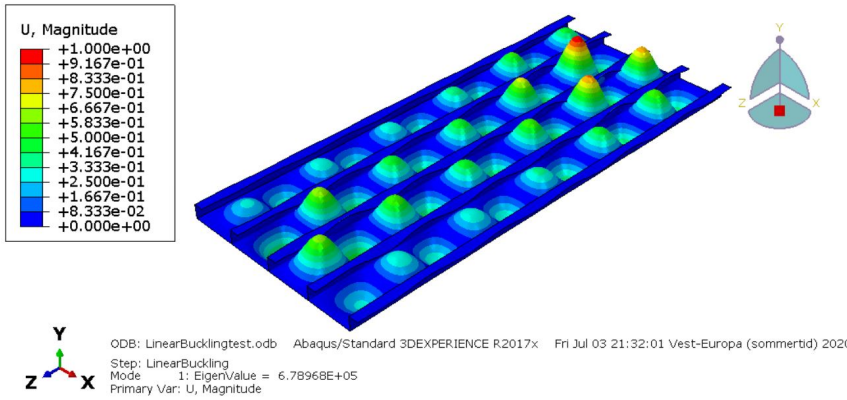

(a) Mode 1

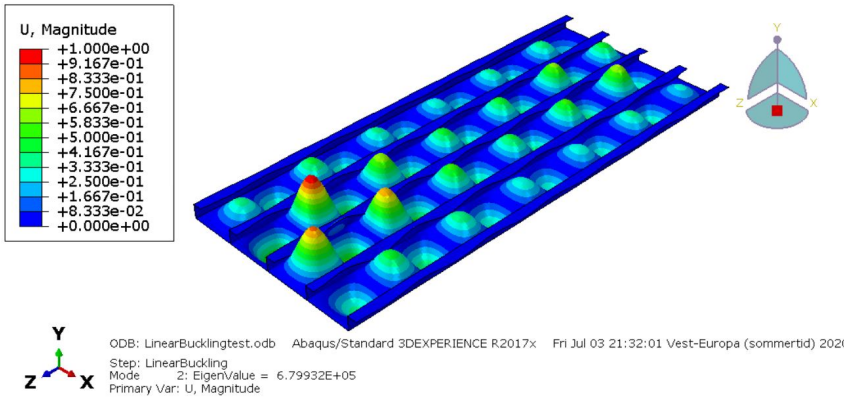

(b) Mode 2

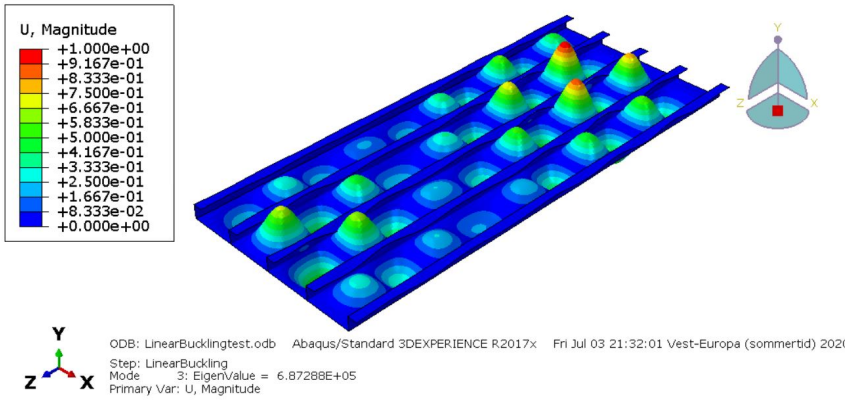

(c) Mode 3

F Nonlinear Buckling - Buckling shapes

F.1 Aluminium stiffener in room temperature

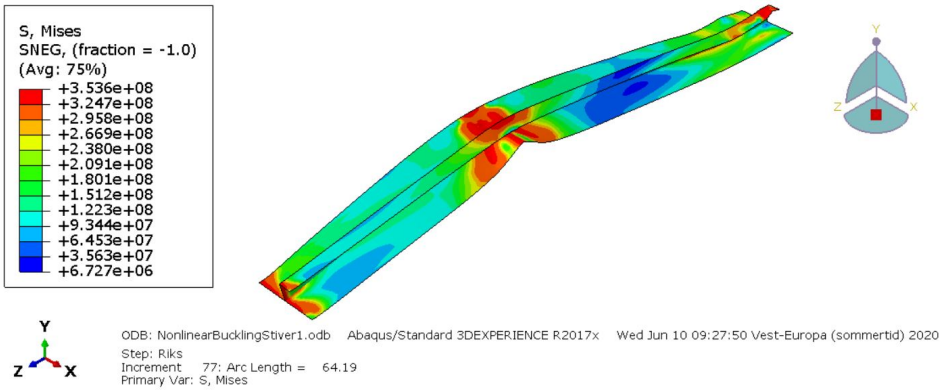

F.2 Uninsulated aluminium stiffener with fire on plate side at 500°C

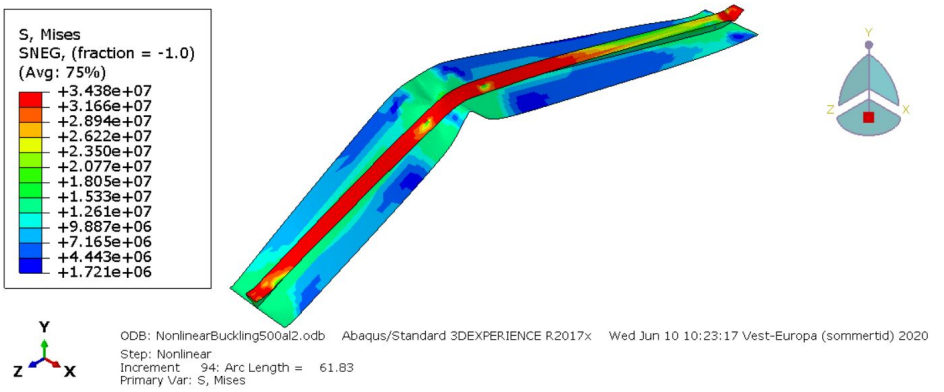

F.3 Uninsulated aluminium stiffener with fire on stiffener side at 500°C

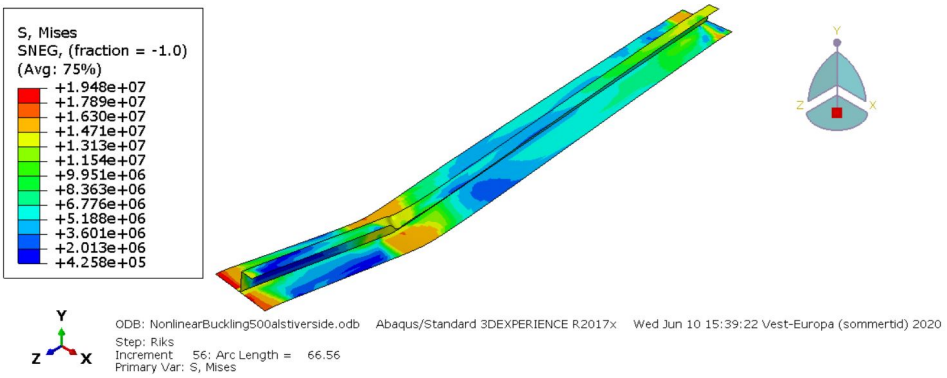

F.4 Insulated aluminium stiffener with fire on plate side after 60 minutes

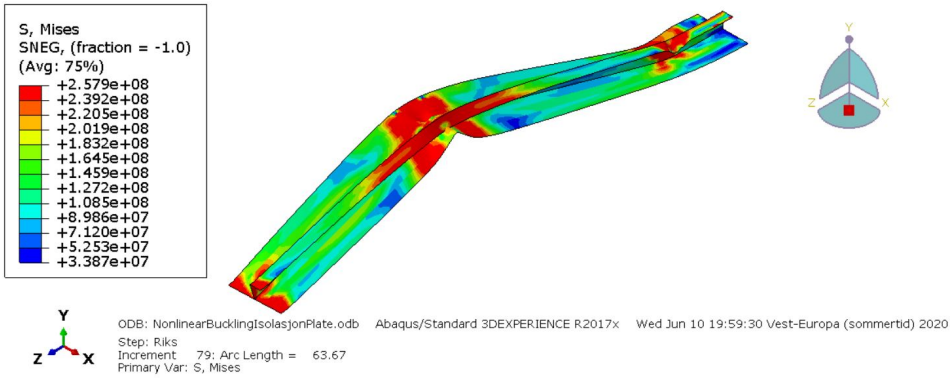

F.5 Insulated aluminium stiffener with fire on stiffener side after 60 minutes

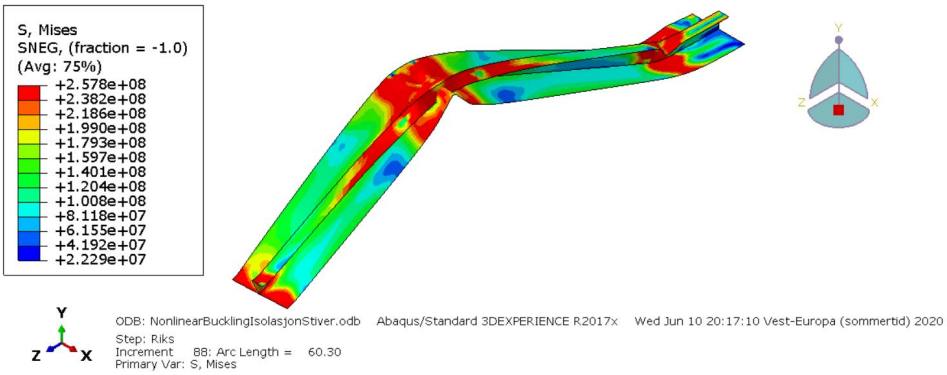

F.6 Steel stiffener in room temperature

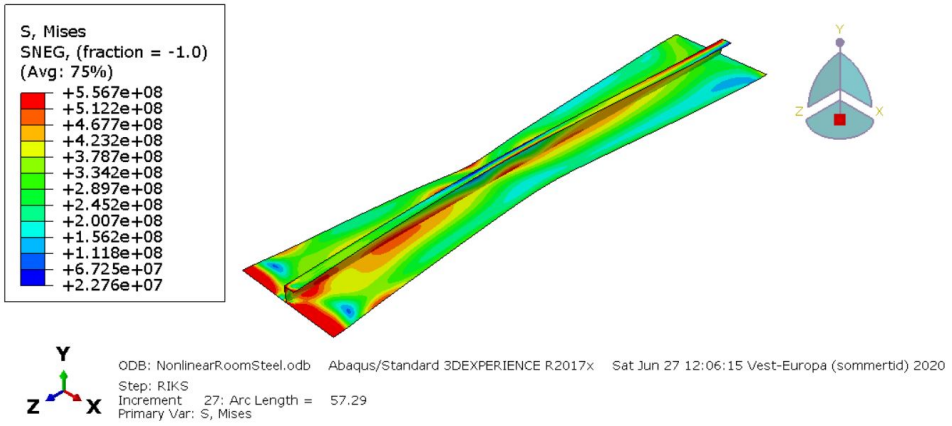

F.7 Uninsulated steel stiffener with fire on plate side after 60 minutes

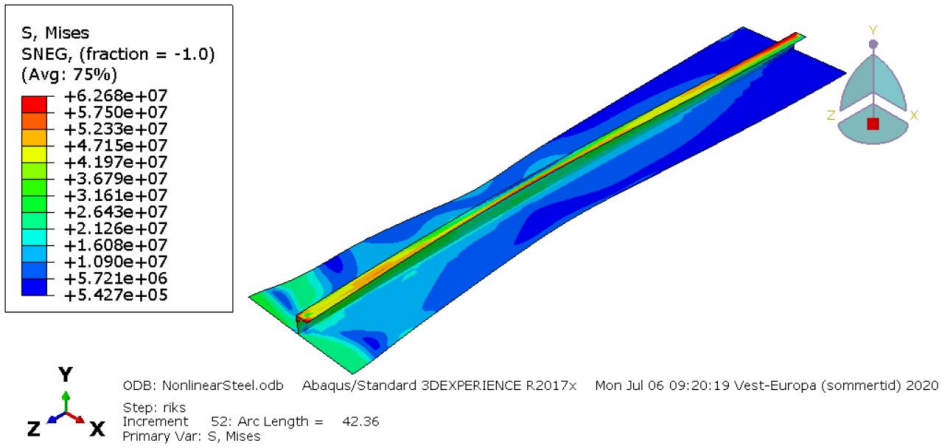

F.8 Plate field

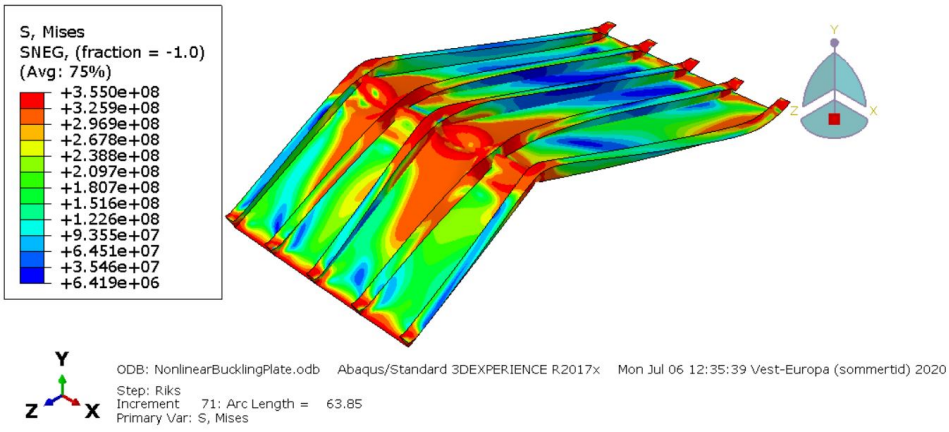

G Nonlinear Buckling - LPF, load-arclength curves

G.1 Aluminium stiffener in room temperature

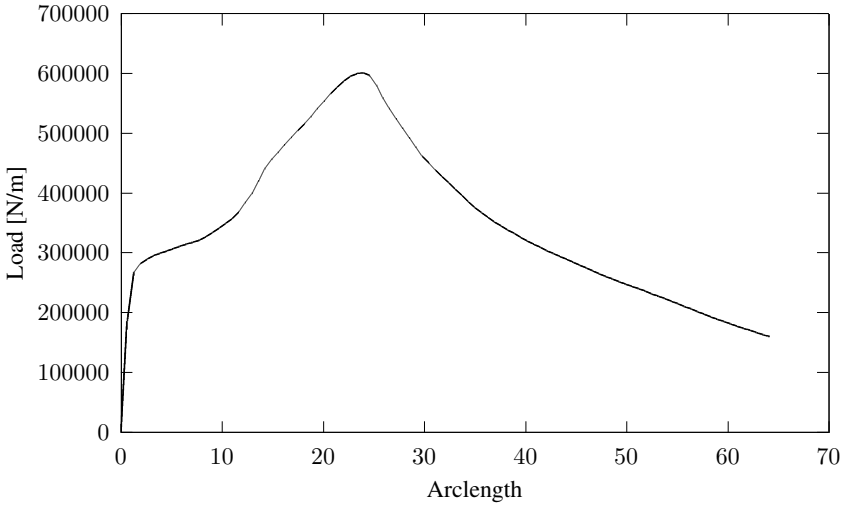

G.2 Uninsulated aluminium stiffener with fire on plate side at 500°C

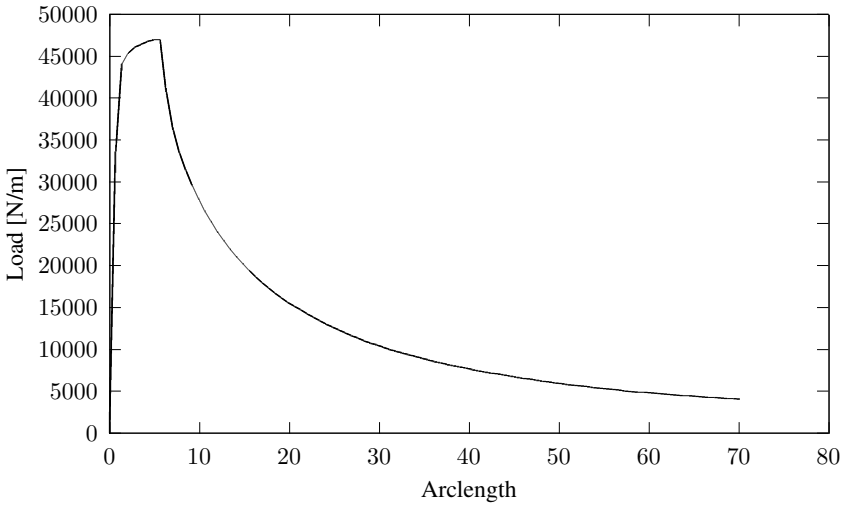

G.3 Uninsulated aluminium stiffener with fire on stiffener side at 500°C

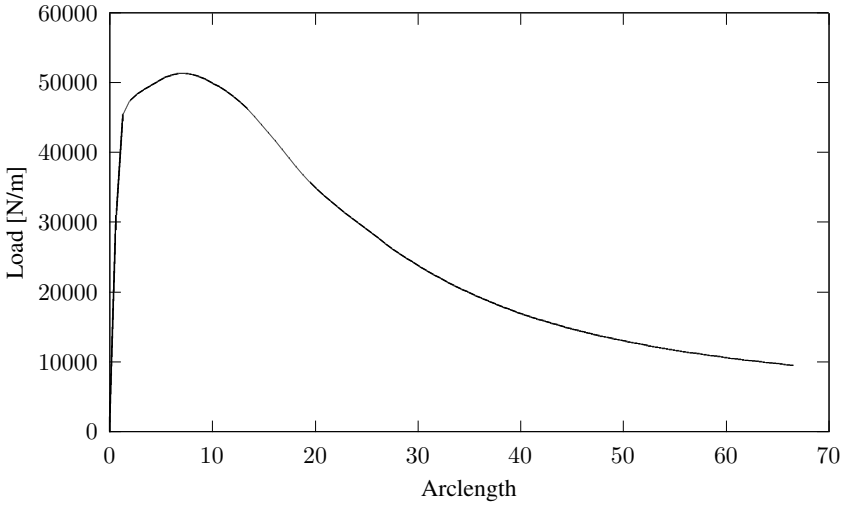

G.4 Insulated aluminium stiffener with fire on plate side after 60 minutes

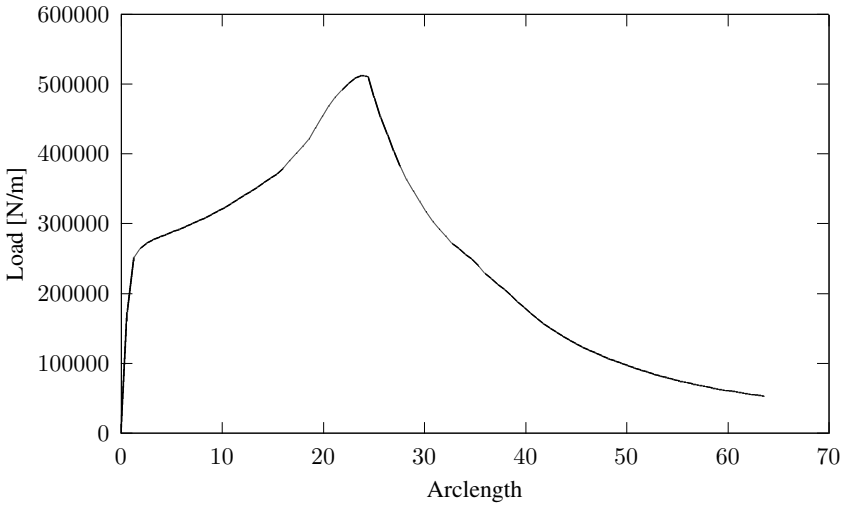

G.5 Insulated aluminium stiffener with fire on stiffener side after 60 minutes

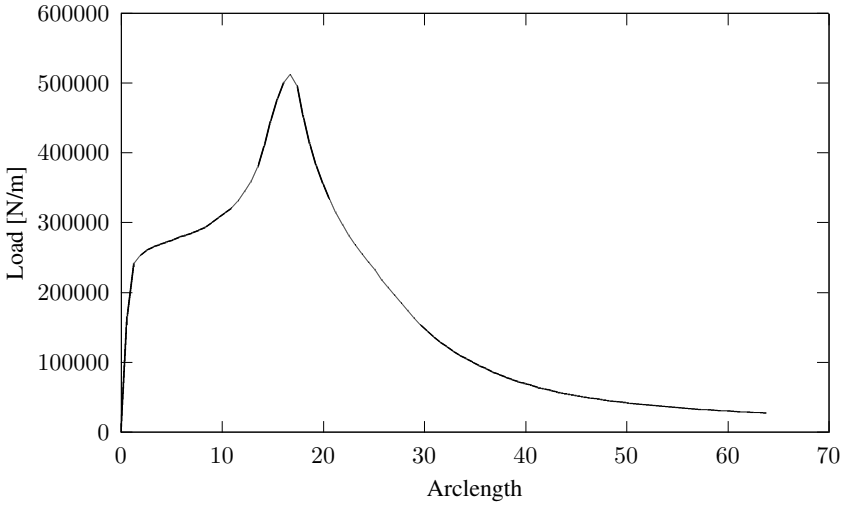

G.6 Steel stiffener in room temperature

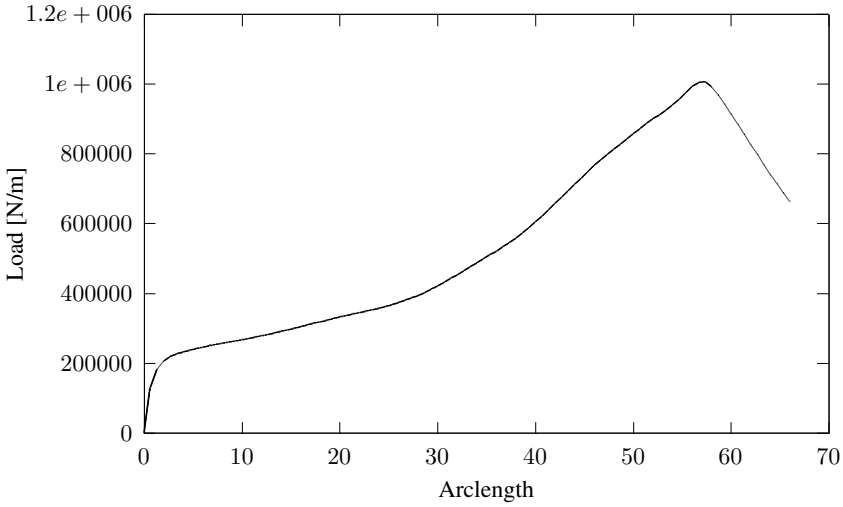

G.7 Uninsulated steel stiffener with fire on plate side after 60 minutes

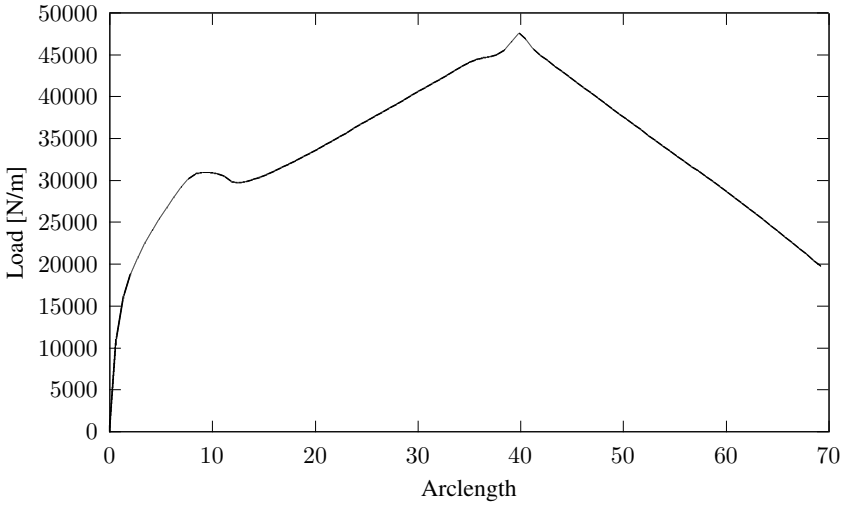

G.8 Plate field

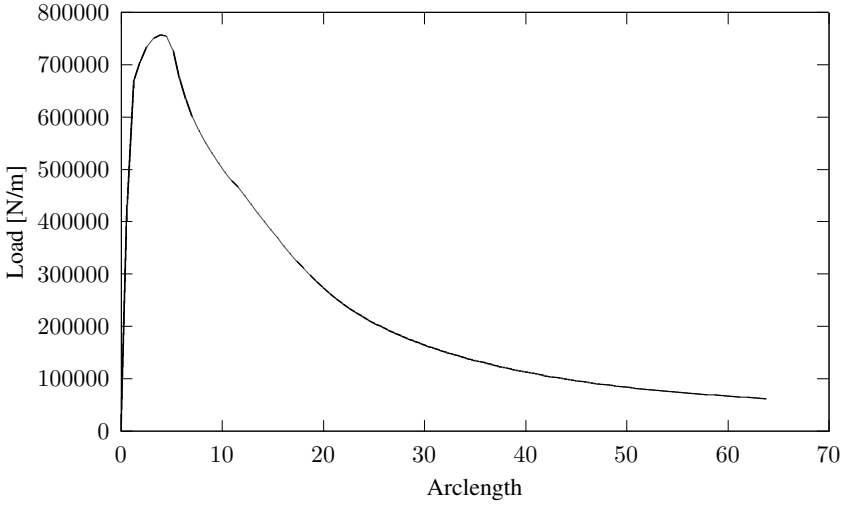

H Nonlinear Buckling - LPF, load-displacement curves

H.1 Aluminium stiffener in room temperature

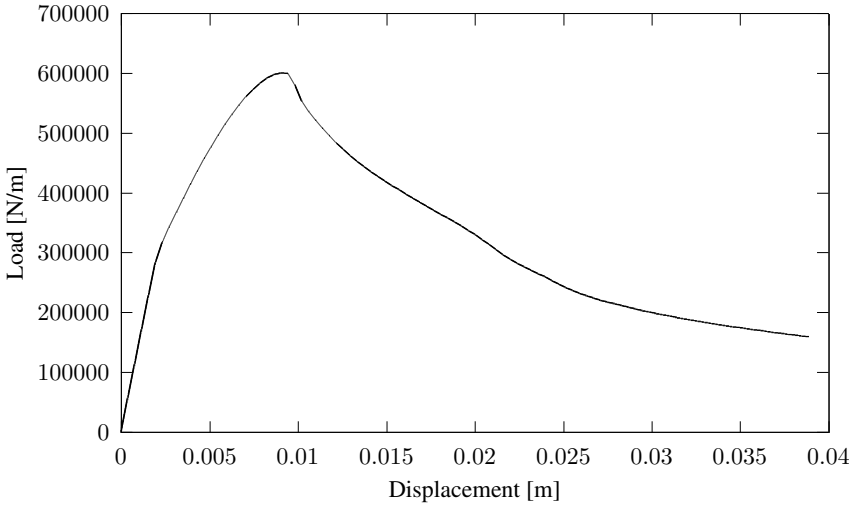

H.2 Uninsulated aluminium stiffener with fire on plate side at 500°C

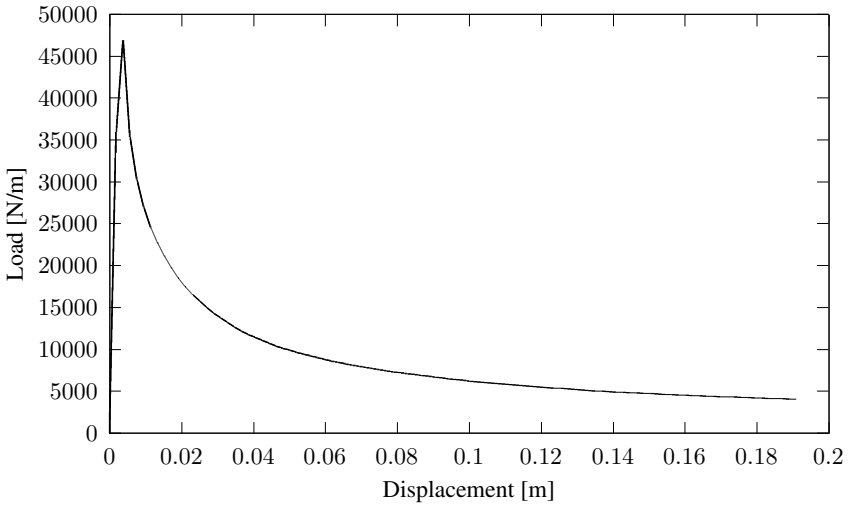

H.3 Uninsulated aluminium stiffener with fire on stiffener side at 500°C

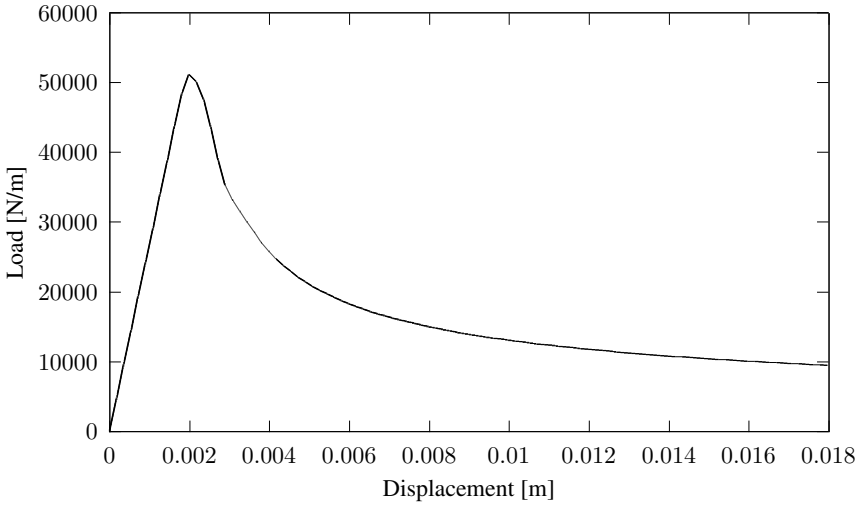

H.4 Insulated aluminium stiffener with fire on plate side after 60 minutes

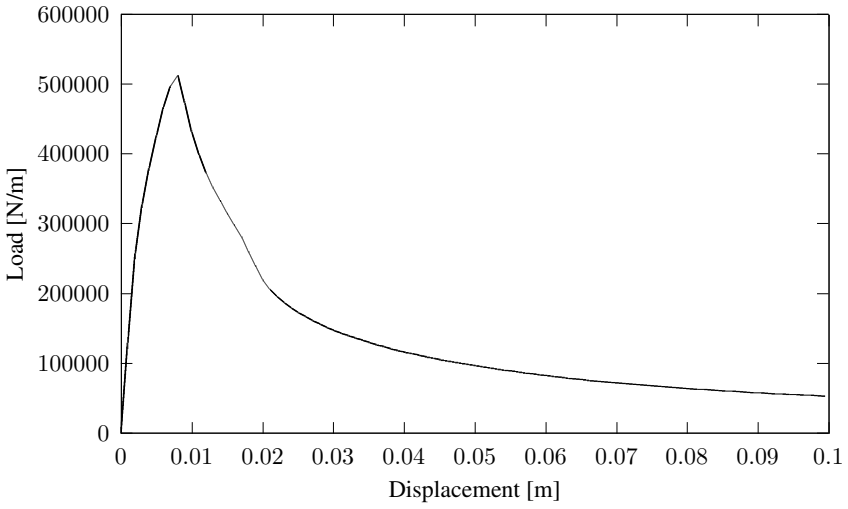

H.5 Insulated aluminium stiffener with fire on stiffener side after 60 minutes

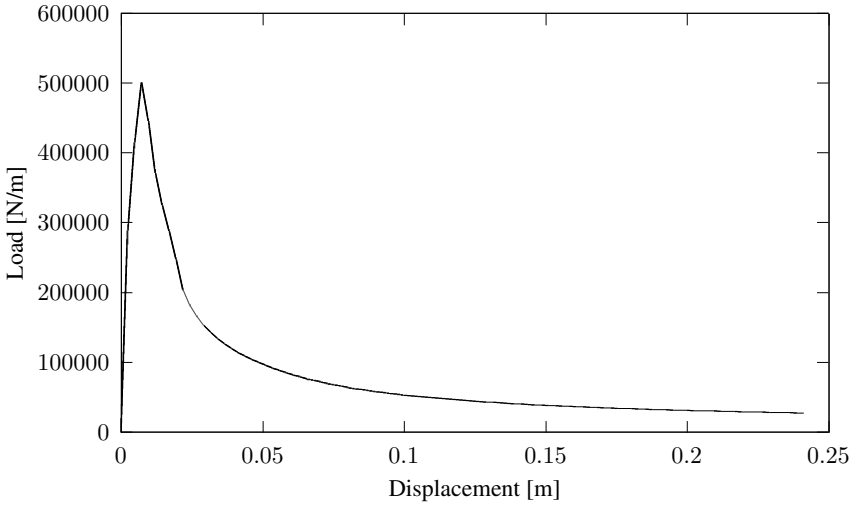

H.6 Steel stiffener in room temperature

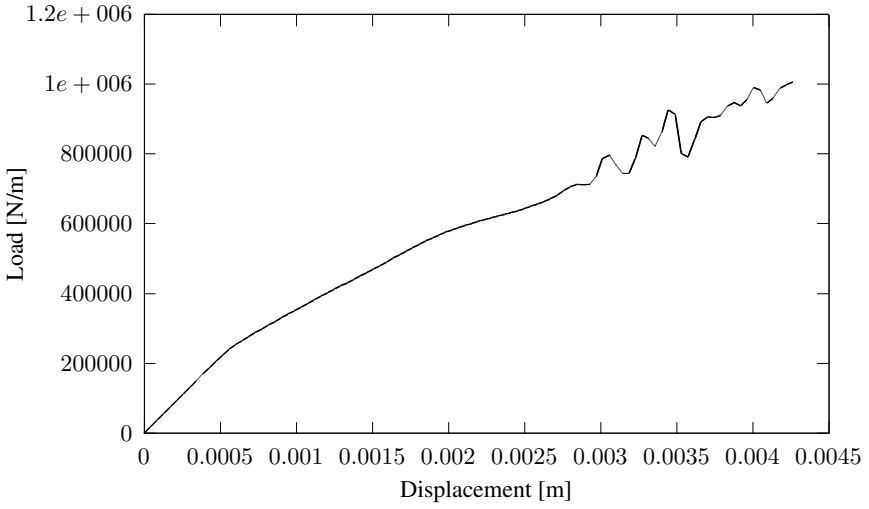

H.7 Uninsulated steel stiffener with fire on plate side after 60 minutes

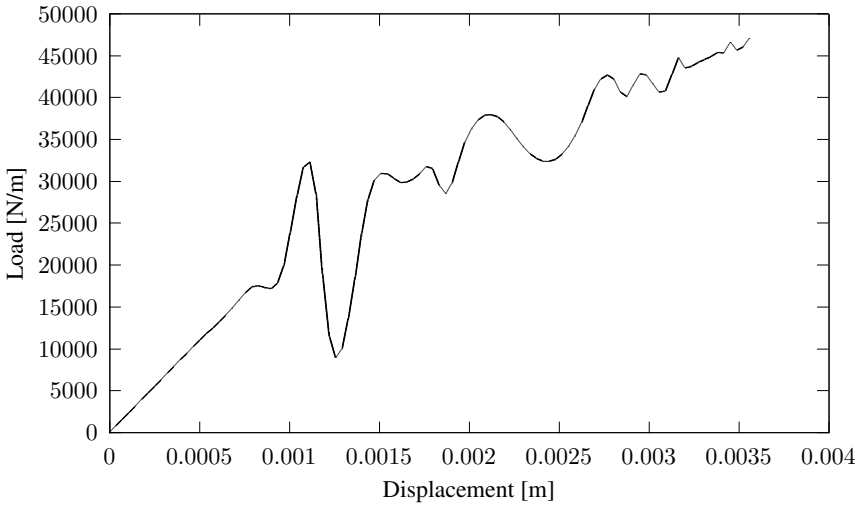

H.8 Plate field

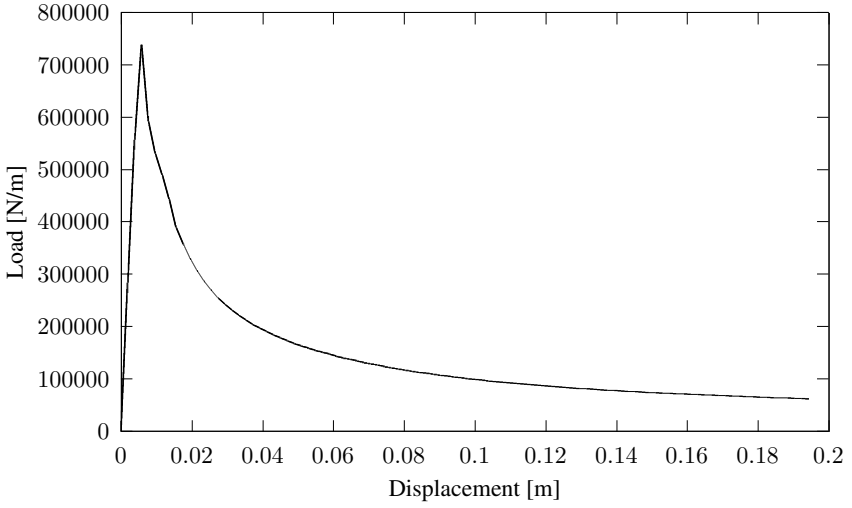

Aina Rindheim

NTNU
Norwegian University of
Science and Technology